Virtual Reality for Intracranial Brain Computer Interface Design and Human Neural Engineering

Courtnie Jean Paschall

A dissertation

submitted in partial fulfillment of the

requirements for the degree of

Doctor of Philosophy

University of Washington

2022

Reading Committee:

Rajesh P.N. Rao, Chair

Jeffrey G. Ojemann, Chair

Jeffrey Herron

Eric H. Chudler

Program Authorized to Offer Degree:
Bioengineering

University of Washington

Abstract

Virtual Reality for Intracranial Brain Computer Interface Design and Human Neural Engineering

Courtnie Jean Paschall

Co-Chairs of the Supervisory Committee:
Professor Rajesh P.N. Rao
Computer Science and Engineering

Professor Jeffrey G. Ojemann
Neurological Surgery

Implanted neural devices allow direct recording and stimulation of neural tissue. Immersive virtual reality (VR) offers a powerful new experimental venue, granting researchers unprecedented control over the visual and aural landscape to develop complex tasks with nuanced controls and otherwise impossible global variable access. Modern VR hardware also guarantees precise, continuous tracking in six dimensions (three linear and three rotational) of real-world objects, namely VR controllers, headset, and trackers. In my PhD research, I sought to leverage the advantages of VR to advance neuroscience research in a unique and valuable patient population. To do this, I built the first platform integrating immersive VR with awake, in-patient, invasive neural recording, aligning highly resolved neural signals to ongoing VR task variables and human behavior.[1] I then expanded this initial platform to enable direct electrical stimulation (DES) of the brain in response to behaviors and events tracked in the virtual environment. This capability allowed me to explore novel approaches to neurohaptic feedback and demonstrate the first bidirectional brain computer interface in virtual reality (VR-BCI).[2] By applying DES to the primary somatosensory cortex (S1), I enabled two human subjects to reach out, grasp, and *feel* a purely virtual object, and then to discriminate between visually identical virtual objects based only on their neurohaptic S1-DES profile. This represented the first time that humans used a neurohaptic cortical interface that was responsive to their volitional, active engagement to explore the feel of an immersive virtual environment. Then, incorporating online digital signals processing, I demonstrated a real-time bidirectional VR-BCI that enabled the first human "cerebronaut" (so coined by our research subject) to use gaze to select an object, a neural trigger to initiate animated grasp of that object,[3] and S1-DES to feel the contact between animated virtual hand and virtual object.

TABLE OF CONTENTS

Contents

LIST OF FIGURES

LIST OF TABLES

ACKNOWLEDGEMENTS

A Dios, Todo Poderoso

Thank you to my family, who supported my steps, faltering or strong, and championed my vision, blurry-eyed or clear. These were mostly nighttime years, many stars offset the dark:

Thank you to Bailey Wynn[1] and Enrique Francisco and Ellie for keeping me alive, healthy, and sane. I love you, Mom, Dad, Grandma. <3 Thank you to Jing and Liz and Braelyn and Kim and Sayeh and Lynn and Cavosie, David and Zach and Michael and Asad and Luke – for your time and energy and humor, support and hugs and faith and love. Thank you to Greg for keeping me on this path. Thank you to Retreat and Santo and Modo and Discovery Park for being havens.

Thank you to my friend and sponsor, Jean B. Viereck, for supporting my work and easing my out-of-placeness in Seattle.

Thank you to my senior PIs Prof. Rajesh P.N. Rao and Dr. Jeffrey Ojemann for trusting me enough to let me build something very new. Thank you to my academic mentor, Prof. Jeffrey Herron, for helping me achieve a significant amount of all I set out to do, and for digging out a pernicious error that allowed the VR-BCI research to continue. Thank you to Prof. Kurt Weaver and Dr. Jason Hauptman and Dr. Andrew Ko and Dr. Ben Grannan for your encouragement and advice. Thank you to Nick Allar and the EEG techs at HMC, and Mark Hanus at TDT, and Kalei Combs and Lori Jacobs for your availability and kindness. Thank you to Prof. Nathan Kutz for your patience and mastery as an educator, and Prof. Eric Chudler for your sense of adventure about the nature of neuroscience research and repeated reviews of this document. Thank you to Prof. Larry Sorensen for making me feel like I hadn't been completely abandoned by the most beautiful of sciences. Thank you to Prof. Francois Meyer for helping me find my first steps along this journey. Thank you to my mentees who let me be a part of their first steps along their journeys: Iman Tanumiharja, Sophia Lowe-Hones, Pranati Dani, Claris Winston, Cleah Winston, Kathryn Stangret, Warren Han, and Lukas Lark. I believe in you all with my whole heart.

Thank you to the graduate students of generations before on whose work I built my best ideas and in whose spirit the lab continues. Thank you to Samantha Sun and Lila Levinson who made up the whole of our small gradkid team for a while and in doing so, kept the lab progressing.

And always, thank you to the patients who chose to work with me in these and many other research efforts. May our work together benefit many.

To the next-gen grads, good luck! I offer you my best advice in earnest dedication:

[1] Again and especially, as sister and friend.

DEDICATION

To the Minimum Viable Product

& Maximum Effort

Chapter 1. Introduction

1.1 Virtual Reality

1.1.1 *Introduction*

Virtual reality (VR) offers a robust platform for human behavioral neuroscience, granting unprecedented experimental control over every aspect of an immersive and interactive visual environment. The flexibility and controllability of immersive VR have been exploited in animal model research for decades, though such studies often relied on animal-sized compartments to create a visual surround.[4,5] These immersive visual environments have been used to study things like maze-based spatial learning, visual sensory processing, goal-directed behavior, and other phenomena while the animal remained movement constrained, and have been developed for moths, flies, monkeys, sea slugs, and other animals – including humans. Of course, the larger the animal, the more expensive and difficult this "room scale" immersion becomes. While VR has been key in many animal-model studies, the technology required to create world-scale immersive environments has only recently become accessible by headset for both human and large animal studies.[6–8]

Headset immersive VR requires precise headset tracking and updated visual display to create a 2D world which moves and reacts around you so seamlessly and with such continuity that it creates the perceptual illusion of looking or moving around in an alternate reality. Using binocular image presentation, camera-and other sensor-based tracking, new VR head mounted displays (HMDs or headsets) can provide a complete three-dimensional reality with which humans can naturally interact and over which experimenters have near complete control. Controllers are used to translate hand movement and actions in the real world into rendered movement and interactions with objects

in this new, artificial world. Modern VR hardware now also integrates onboard eye tracking and face tracking to enable increasingly complex avatar rendering and can accommodate increasing counts of additional "tracker" components to link and render more aspects of the physical world in the virtual space. The precision, flexibility, and multimodal integration of VR makes it a profoundly important and an exciting new behavioral experimentation platform for research with human subjects.

With the advent of high-resolution and portable immersive virtual reality headsets, human VR-based research became feasible and accessible to the broader neuroscience community. As headset, immersive VR became more accessible, it was quickly integrated with non-invasive human neural recording modalities such as electroencephalography (EEG) and functional MRI (fMRI) to explore the neural correlates of human behavior and non-invasive brain computer interface (BCI).[8,9] This led to an explosion of VR-based behavioral and non-invasive neural recording research in humans. A Google Scholar search for papers published in the past four years with the key words "virtual reality" and "EEG," for example, yields over 16,000 results. Among these, VR has been used to study altered representations of self, attention, cognitive workload, the effect of embodiment on memory, social engagement, extra-human sensory perception (like seeing UV), motor planning with extra-human appendages (like moving a third arm or four legs), and the emotional impact of dying.[8,10–12] It is a profoundly flexible and functional research platform.

Medically, VR has been shown to be effective for pain and anxiety management and therapeutic VR experiences have helped people overcome severe phobias. The VR environment has also been a boon for non-invasive brain computer interface design: for example, using neural signals recorded by EEG to control a virtual prosthetic without having to build an actual interactive robotic

arm. Near immediately, portable and immersive VR enabled new approaches to behavioral and cognitive neuroscience experiments and non-invasive EEG research in humans.[13]

1.1.2 *Opportunity*

Despite the great promise and allure of VR, very few studies integrating VR hardware and intracranial neural recording have been completed. Human research with intracranial implants grants incredible insight into the dynamic, real-time activities and connections across the brain. Recently, chronic neural implants such as deep brain stimulators (DBS) and the RNS® System (NeuroPace, Inc., Mountain View) have enabled out-patient integration of intracranial neural signals and commercial VR hardware, though with a limited channel number.[14,15] In 2019, a research subject newly implanted with a penetrating Utah array learned to use their onboard BCI decoder by donning a VR headset and moving a virtual robotic arm on a virtual table across a virtual room before transitioning to the real robotic arm waiting for them in the labspace.[8]

In-patient invasive neural recording offers even greater access to human neural data through high-count electrocorticography (ECoG) and stereo-electroencephalography (sEEG) electrodes that are implanted in children and adults for clinical evaluation of epilepsy. This in-patient clinical setting, however, also presents unique challenges that have traditionally precluded VR integration. Overcoming these challenges to combine the advantages of both intracranial in-patient neural recording and VR task design is an important next step for human neuroscience research. It was necessary and important, and a significant output of my thesis work, to design an immersive VR platform for invasive human neural engineering and cognitive neuroscience research– to unite the experimental control and flexibility of VR with the spatiotemporal resolution and neuromodulation opportunities of implanted electrodes in a clinical environment.

In this thesis, I present a first demonstration and critical assessment of a VR task platform in human patients (Figure 1.1) with invasive electrode recordings from both ECoG and sEEG.[1] I detail novel BCI developments enabled by this platform as well as recreation and expansion of a canonical neuroscience task. I present yet unpublished results from the first fully bidirectional BCI in virtual reality and discuss, throughout this thesis, the training and iterative advances that led me to such a rewarding culmination of my time as a graduate student.

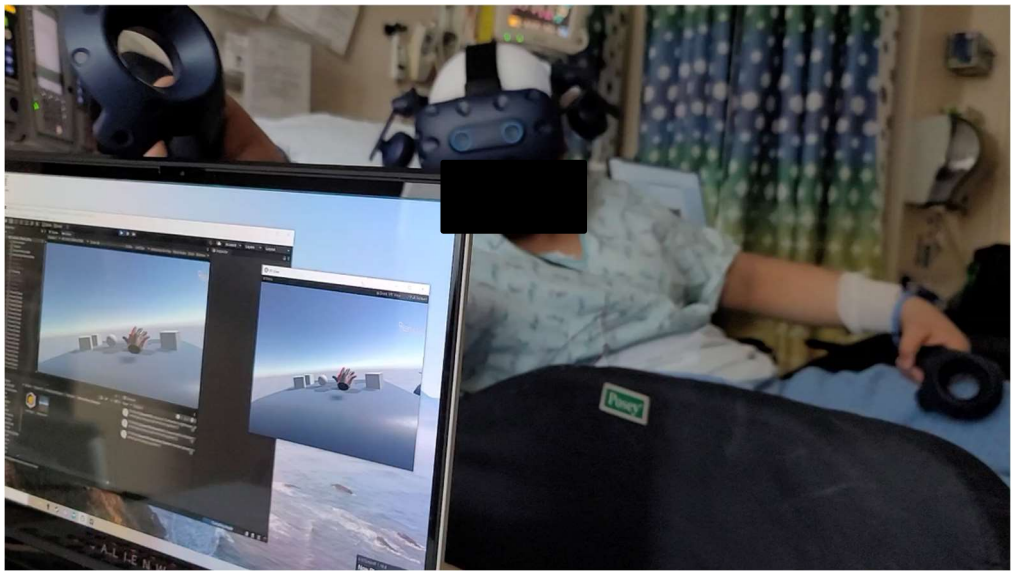

Figure 1.1 *in vivo* Virtual Reality. An invasive neural recording patient engaging with virtual objects in an immersive virtual reality task -- reaching out beyond the confines of the hospital bed, to grasp and interact with objects, and (unpictured) to next toss and throw then towards a game target object.

1.2 NEUROELECTROPHYSIOLOGY

1.2.1 *Neural Recording*

After a 40-year hunt for the physical basis of mind, German physician Hans Berger demonstrated conclusively and singularly[16] that continuous electrical fluctuations recorded from the scalp (or, in his case, post-trepanation exposed dura) reflected underlying neurological activity (1929).[17] He termed the process of using electrodes to record or "map" [*-graphy*] the neural activity of the

cortex, Electroencephalography (EEG). Berger was also the first to apply Fourier spectral features analysis in EEG data and the first to associate "exacting intellectual work, even [just] a high level of attention" with changes in the neural spectral power distribution.[16,17] In Berger's own words (1938, translated from German):

> *When mental work is performed or when the type of activity designated as **active conscious activity** becomes manifest in any way as, e.g., upon the transition from the passive to the active E.E.G., a considerable **decrease** in the amplitude of the potential oscillations of the human brain occurs in association with this shift in cortical activity.*[18]

While intracranial electrical activity had been recorded previously, it was Berger's work that confirmed that ongoing neural activity – and the frequency content of that activity, in particular – was directly correlated with cognitive processes. The study of relationships between cognitive functions, including perception, memory, language, emotions, and social cognition, and this oscillatory electrical activity of the brain is called cognitive neuro-electrophysiology.[19] Frequency-based analysis continues to offer a powerful approach to understanding human behavior and cognition, and is supported by research demonstrating the biological basis of oscillatory neural activity. Prior studies have now modeled at least three neurobiological mechanisms that produce oscillatory neural behavior, characterized by varying amounts of interneuron inhibitory balance in a particular biological neural network.[20] In general, research has concluded that oscillatory dynamics "constitute a ubiquitous and fundamental neural mechanism that supports myriad aspects of synaptic, cellular, and systems-level brain function across multiple spatial and temporal scales."[21]

In EEG recordings, the rhythmic activity of neural signal reflects the coherent fluctuations in the excitation of populations of (mostly cortical) neurons – "hundreds to hundreds of thousands of neurons," in fact. This aggregate activity is called a Local Field Potential (LFP) recording. In EEG, recorded LFP predominately consists of activity from cortical pyramidal neurons in the human cortex.[19,22] With implanted microwire arrays, the tiny electrical fields generated by just one neuron's activity may be recorded. Such recordings are called single unit activity (SU) and capture the individual action potentials of one little brain cell. With implanted "macro" electrodes such as ECoG and sEEG (Figure 1.2), synchronous excitation from thousands to tens of thousands of neurons may be recorded.[23,24] This activity is recorded extracellularly and represents the aggregate electric field, and it is also referred to as LFP.

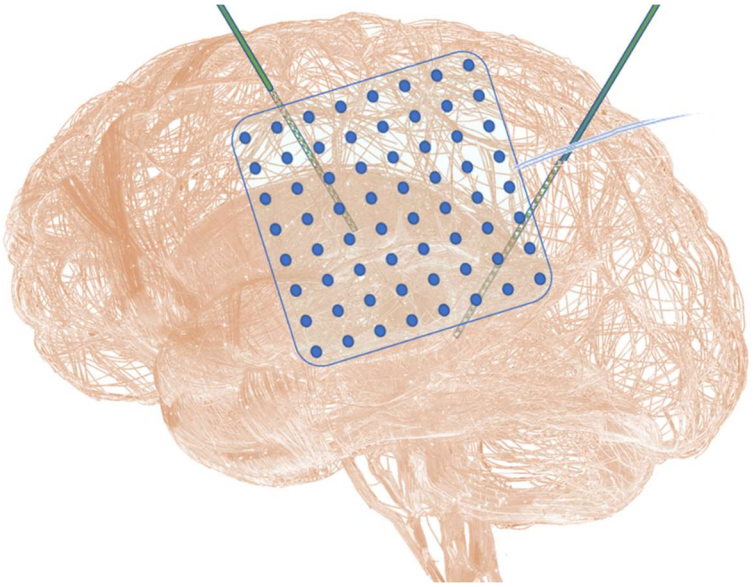

Figure 1.2 Graphic of Intracortical Arrays. Electrocorticography (ECoG) are circular electrodes in grids or strips implanted subdurally or epidurally to record from the cortex. Stereo-EEG are cylindrical electrodes along depth probes implanted stereotactically to record from subcortical structures. Often, superficial sEEG contacts record from cortex, as well.

ECoG are flat, circular electrodes embedded in strip or grid arrays that are implanted subdurally or epidurally to record neural activity directly from the cortical surface of the brain. Clinical ECoG commonly uses 2.3-3mm exposed electrode diameter (10mm^2 surface area) with 10mm spacing and 2kΩ target impedance.[25,26] Stereo-electroencephalography (sEEG) and deep brain stimulation (DBS) electrodes are vertical depth probes with embedded cylindrical electrodes, stereotactically

implanted down to subcortical neural structures. Stereo-EEG probes typically host up to 16 cylindrical electrodes at 5mm of electrode spacing down the length of the probe, each contact having 1.1mm diameter and 2.3mm of exposed length (16mm^2 surface area) for about 2kΩ of target impedance.[25] As sEEG have cylindrical electrodes evenly spaced along the implant depth of the probe, these implants can offer both cortical and subcortical neural recording and stimulation. In contrast to scalp EEG, intracranial electrodes offer a significant improvement in spatiotemporal signal resolution and enable direct electrical stimulation (DES) of the human brain. Implanted intracranial electrodes enable higher-impedance recordings of neural activity directly from surrounding cortical and subcortical neural tissue.

1.2.1.1 The Epilepsy Monitoring Unit (EMU)

In-patient invasive neural recording offers high-count ECoG and sEEG montages (multiple implants at once) implanted in children and adults for clinical evaluation of epilepsy. In this patient population, intracranial electrodes are temporarily implanted for a week to two weeks to precisely map epileptogenic neural tissue and characterize seizure progression. This information is used to evaluate treatment options for refractory epilepsy, including chronic ECoG implantation and resection of seizure foci. Invasive neural recording with ECOG and sEEG usually occurs in an in-patient hospital wing called the Epilepsy Monitoring Unit (EMU). These clinical mapping studies usually incorporate 100 to 200 or so electrodes from which simultaneous local field potentials (LFPs) can be recorded and precise electrical stimulation can be delivered.

1.2.1.2 Other Neural Recording Modalities

Other neural recording modalities target different types of on-going physiological representations of neural activity (e.g., electrical, hemodynamic, chemical). For example, functional near-infrared spectroscopy (fNIRS) and functional Magnetic Resonance Imaging (fMRI) map hemodynamic

changes and correlates of energy utilization to reflect increases and decreases in neural activity, and magnetoencephalography (MEG) leverages electromagnetic interaction to non-invasively record electrical currents in the brain.[27] MEG offers greater spatial resolution and localizability compared to EEG. Novel intracranial recording technologies, including cranial venous delivery of a stent-like[24] electrode array and direct radio-transmitting injectibles[25], are being actively developed.

1.2.2 *Neural Stimulation*

Direct electrical stimulation (DES) of the brain was known to produce movement[28,29] more than 40 years before continuous neuroelectric recordings of the brain demonstrated the electrical nature of neural activity.[17] In the early 1900s, intraoperative DES was used to map brain regions and localize epileptic foci.[30] In fact, since its first use in the late nineteenth century, intraoperative DES has been standard technique for evaluating eloquent neural tissue prior to resection in the treatment of tumors or epilepsy. In this evaluation, a patient is awakened during surgery and asked to perform motor, language, and cognitive tasks while receiving or not receiving DES. Performance on these tasks during DES is used to determine the functionality the neural tissue and help determine whether neural tissue may be resected (or at what cost). DES continues to be used to support medical decision-making[31–33] alongside research aims.

In 1909, Krause used intraoperative DES to detail the first organizational map of the human motor cortex.[34,35] In 1912, Cushing characterized the sensory responses DES of the postcentral gyrus, now called the primary somatosensory cortex (S1).[30] In 1934, intraoperative ECoG became available, enabling surgeons and researchers to both stimulate and record from neural tissue.[36] Such studies highlighted, for example, that DES could either have an inhibitory or excitatory effect on neural activity, depending on DES parameters and the location of stimulation (Figure 1.3). The

ability to stimulate and record greatly expanded early intracranial research opportunities (Figure 1.3), but such studies were still restricted to the operating room until modern neural implants were designed. With the development of the transistor in the mid-1950s, stimulators could now be implanted inside the body, which led to a "remarkable burst of innovation and experimentation."[37] In addition to the development of cardiac pacemakers (implanted stimulators), the last decades of the millennia also saw the advance of phrenic nerve and diaphragm pacers, cochlear implants, spinal cord epidural stimulators, intraspinal stimulators, and finally the first chronically implanted brain neuromodulator: the Deep Brain Stimulator (DBS).[37–44] Most recently, sEEG and ECoG, among other electrode architectures, may be implanted for longer durations (see Section 1.2.1.1 - The Epilepsy Monitoring Unit) in the human brain for medical evaluation and may provide DES for medical intervention and human experimentation, post-operatively.[26,45]

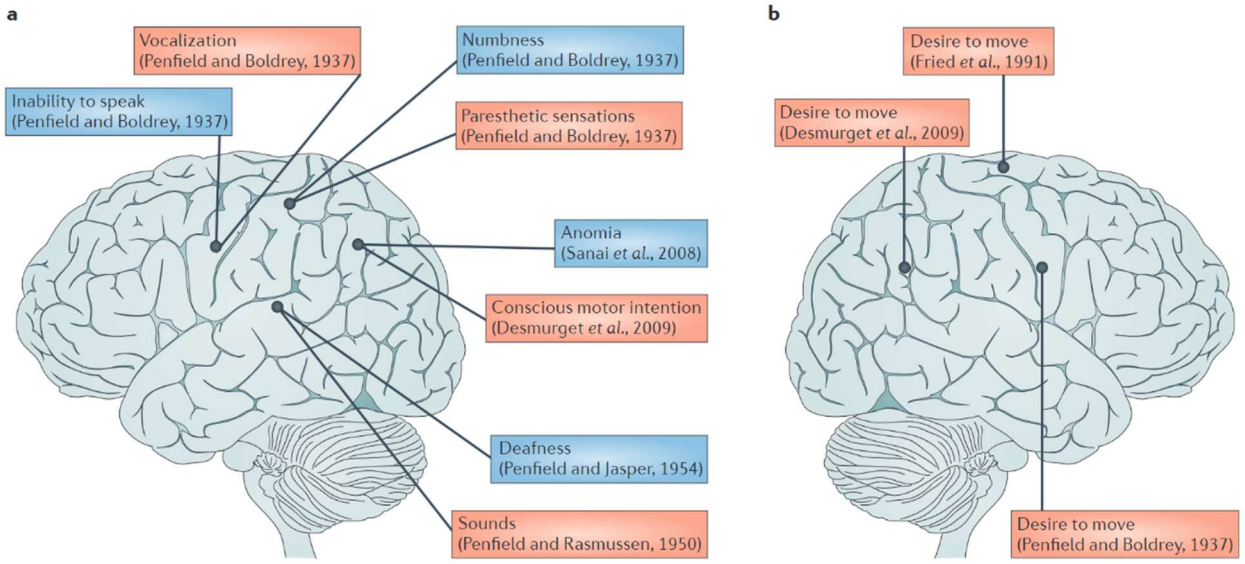

Figure 1.3 Studies and effects of cortical DES in humans. This figure is reproduced from Orchers et al. 2012 review of DES and visualizes the various studies and their observations in evaluating DES of (a) left and (b) right cortical hemispheres. DES was shown to evoke inhibitory or excitatory effects depending on DES parameters.

As a quick note about the cellular effects of DES: when applied to grey matter (non-myelinated, cell-body dense neural tissue), extracellular stimulation primarily excites *axons* rather than cell bodies, eliciting both antidromic and orthodromic activity that can evoke neural activity at a remote location relative to the site of stimulation.[46–48] Remote cortical activity elicited by DES is called a cortical evoked potential (CEP).[49–52]

1.2.2.1 Therapeutic Deep Brain Stimulation (DBS)

Deep Brain Stimulation (DBS) is a therapy used to restore controlled movement in those with neurodegenerative motor disease, specifically Parkinson's disease (PD) and essential tremor (ET)[2]. The Food & Drug Administration (FDA) approved DBS to treat essential and advanced parkinsonian tremor in 1997, revised to include earlier-stage PD in 2016.[54,55] First described by James Parkinson in 1817, Parkinson's disease is the second most common neurodegenerative disorder after Alzheimer's disease and affects millions of people worldwide.[56,57] In PD, idiopathic loss of dopaminergic neurons in the substantia nigra pars compacta produces an imbalance between the direct and indirect ganglia-thalamocortical motor control pathways, leading to overdominance of the indirect pathway and the pathognomonic features of the disease: akinesia, bradykinesia, rigidity, and resting tremor[3]. Rapid and dramatic improvements in parkinsonian motor symptoms are seen with direct electrical stimulation of subcortical structures along this motor control pathway; subcortical targets for PD include the subthalamic nucleus (STN), globus pallidus internus (GPi), and ventral intermediate nucleus of the thalamus (ViM).[26,54,55] Since their

[2] Essential tremor is an idiopathic disease characterized by a 4-11Hz tremor during volitional movement that may involve dysregulation of cerebellothalamocortical motor control circuits.[53]

[3] PD is also micrographia (small handwriting), shuffling gait, fixed posture, masked faces, and reduced blinking. Non-motor features often include depression and anxiety, sleep disturbances, cognitive impairment, and autonomic dysfunction. While motor function may be largely restored with dopamine replacement or DBS neuromodulation, the cognitive symptoms of PD rarely respond to treatment.

initial FDA approval, DBS implants have been used to treat over 40,000 people with PD and ET neurodegenerative disorders.[58]

While DBS has proven a reliable and profoundly beneficial PD therapy, its precise mechanism of action has not yet been elucidated and DBS stimulation is associated with both motor and cognitive side effects that include dysarthria, depression, and impulsivity, among others.[59,60] Ongoing research seeks to clearly define the neurophysiological mechanism of DBS therapy and to improve DBS efficacy and reduce side effects. These latter goals, in particular, have motivated the development of adaptive DBS[15,59–64] therapy in which subcortical stimulation is modulated in response to neuro-electrophysiology and/or kinematic-behavioral biomarkers. LFP analyses from the cortex, STN, and other subcortical targets of PD patients have suggested distinct types of PD separable by neural activity[65] and specific neural signals features (i.e., increased β-bandpower, 10-30Hz in STN) associated with parkinsonian motor dysfunction.[59,60] These neural features may someday support customized and targeted DBS intervention and new neural signals targets by which to regulate online, adaptive neuromodulation are being actively explored. My contributions to this hunt are described in Chapter 3.

The demonstrated success and safety of DBS for PD has encouraged adoption of DBS protocols for other neurological disorders, including clinical depression, chronic pain, post-traumatic stress disorder, obsessive compulsive disorder, epilepsy, and Tourette's syndrome.[66–69]

1.2.2.2 Non-invasive Neural Stimulation

Noninvasive neural stimulation technologies include transcranial Direct Current Stimulation (tDCS), Transcranial Magnetic Stimulation (TMS), and Transcranial Focused Ultrasound (tUS). Transcranial tDCS applies weak electrical current to modulate brain activity – strong current directly applied would damage superficial tissue (like skin).[70] The response to tDCS is highly

influenced by stimulation parameters.[70] TMS uses a primary coil placed near the skull which produces a rapidly changing magnetic field to induce an electrical current in the underlying cortical surface.[71] Single-pulse TMS briefly depolarizes cortical tissue and may produce perceptual effects.[72] Non-invasive stimulation by tUS uses short bursts of low-intensity ultrasound to modulate neuronal activity.[73] It is an emerging modality that offers greater stimulation precision and depth compared to tDCS and TMS.[74]

1.2.3 *Neural Engineering*

Neural engineering (or neuroengineering) leverages neural interface devices to specifically modify neural circuits or neural behavior – "to understand, repair, replace, enhance, or otherwise exploit the properties and functions of neural systems."[37] From this vantage point, neural engineering currently includes sensorineural engineering (replace, enhance), directed neuroplasticity (repair, enhance, exploit), and closed-loop neuromodulation (all of the above).

Sensorineural engineering seeks to simulate natural or supranatural sensory information by direct electrical stimulation of neural tissue. The cochlear implant, for example, is the most successful and iconic sensorineural engineering device to-date, having restored functional audition to over 740,000 people with severe sensorineural hearing loss.[75] Retinal implants have received regulatory approval[76–78] for the treatment of retinal degeneration, neurohaptic feedback[79–81] by DES is being actively characterized and integrated within neuroprosthetics[82,83] research and design, as well as neural interfaces for the vestibular system[84] and olfaction.[85] My work contributing to the advanced design of synthetic touch integrated with natural behaviors (neurohaptics) and virtual reality for neurohaptic interface design is discussed in Chapter 5 - Designer Touch: Neurohaptic Engineering.

Directed neuroplasticity[86,87] refers to physiologic, neuronal circuit manipulation by means of local activity-dependent stimulation[88–91] or local paired-pulse stimulation[92,93] to encourage (or

theoretically, to intentionally discourage) activity-dependent biological connectivity between neuronal populations in the brain. Both activity-dependent and paired-pulse approaches to directed neuroplasticity harness Hebbian plasticity[56] – colloquially, neurons which "fire together, wire together" – to guide connectivity. This has been proposed as a means of cortical repair following injury or stroke.[86,94–96]

Closed-loop refers to the use of a neural or behavioral cue to determine either the presence or parameters of stimulation. Discussed previously in the context of adaptive DBS[62] (Section 1.2.2.1), closed-loop neuromodulation umbrellas the remaining forms of neural engineering that encode task-dependent, behavior-dependent, and neural state-dependent stimulation to achieve an equivalently broad (task, behavior, or neural) outcome state. Examples include event-dependent stimulation to enhance episodic memory and recall,[97] intention-dependent stimulation to facilitate motor rehabilitation in stroke,[94] and feedback-dependent stimulation in a bidirectional brain computer interface (see Section 0).

1.3 Brain Computer Interface

1.3.1 *Introduction*

In 1973, Jacques Vidal proposed an EEG-based neural signals interface between a human and a machine.[98] In this proposal, he called for the development of a neural language by which one could "query" the state of the brain and efficiently interpret the brain's reply. This image of an input-output interface directly between the world and the brain he termed a Brain Computer Interface (BCI). Two years prior, in a landmark study, Fetz and Finocchio had demonstrated operant conditioning of cortical neuron activity.[99,100] By having a monkey modulate the activity of individual neurons for a reward, they had shown that the brain can volitionally control the firing rate of individual neurons. This amounts to a one-dimensional (1D) neuronal control signal: firing

rate up or down. With this, the brain can control the output of a simple effector –the movement of a cursor across a computer screen, for example. This study proved that the output side of a BCI was possible.

A little over thirty years later and with improved intracortical electrodes, non-human primate researchers implemented real-time volitional BCI control over a 3D cursor[101] and then quickly followed up with control over a robotic arm.[102] Human BCI with implanted electrodes soon followed, yielding BCI-controlled desktop screens, wheelchairs, and robotic arms.[103–105] Early BCI implementations relied on single unit activity from microelectrodes, as had been used in animal models, but soon BCI using local field potentials recorded from ECoG and sEEG macroelectrodes were built.[106–108] While BCI has focused on decoding neural activity from the motor cortex, other control channels have been explored, including imagined speech[109], auditory imagery[110], and hippocampal ERP.[111]

1.3.2 *Impact & Opportunity*

BCI to augment, replace, or repair motor and sensory function holds tremendous promise to restore independence and quality of life to those with sensorimotor deficit due to neurological disease, disorder, or injury.[105,112–114] Over 5 million people in the United States alone live with some form of paralysis from stroke, spinal cord injury, or neurological disease.[115] Those with tetraplegia (loss of upper and lower extremity control) rank the restoration of hand and arm function as the highest priority[116] for independence and well-being[4].

Traditionally, leading BCI research teams work with tetraplegic patient populations who receive implanted, research-only micro-arrays for chronic neural decoding of single unit activity to drive

[4] Paraplegics (loss of only lower extremity control) rank continence and sexual function as their highest priority.

large robotic arms with increasing axes of volitional control. The cost of these robots and the engineering work required is prohibitive and inflexible. This poses a critical problem for the scientific community during exploding interest in the field of BCI. Virtual reality presents a new opportunity for BCI development in which neural control can be expressed over visually realistic, fully responsive, and first-person virtual avatars. Virtual reality offers a compact system and includes ocular movement recording, 3D kinematic tracking of any number of joints, and immersive visual feedback. In addition, decoded motor actions can be mapped to a completely customizable personal avatar that can be readily modified to the user's or the experimenter's needs. A strong motivation for my research was to leverage the intracranial patient population to whom I had access, to advance BCI for neuroprosthetics and functional restoration. ECoG and sEEG are already approved for medical implant in various patient populations, granting access to more patients and opportunity for design iteration.

1.3.3 *Neurohaptics*

Touch sensation offers complex and innate biological feedback that enables natural interaction with the world around us. Restoring this feedback is an important component of functional, closed-loop brain-computer interface (BCI). While multiple technologies promising sensory restoration exist, S1-DES plays a central role as it can be leveraged to elicit artificial somatosensory percepts independent of peripheral sensory channels.[4,79,117–119]

Intracranial electrodes can also deliver direct electrical stimulation (DES) to neural tissue, which may be used as neurohaptic feedback during behavioral tasks or in the development of bidirectional BCIs.[26,79] DES to the somatosensory cortex (S1) has been reported to evoke perceivable sensations[120], called percepts, that are characterized by the function of the neural tissue being stimulated.[121] For example, suprathreshold stimulation of the hand region of the

somatosensory cortex can reliably elicit a percept in the contralateral hand. Although percepts elicited by DES are reliably localizable[81,121], the subjective descriptions of these somatic percepts tend to emphasize the artificial, strange, and unfamiliar nature of the evoked sensation.[80,122] DES percepts in humans are distinct from co-located tactile sensation.[123,124] These distinct, localizable DES sensations have been exploited as neurohaptic feedback to guide movement behavior in humans[79] and to guide virtual object selection in non-human primates.[4] By providing functional feedback to guide behavior, DES can improve BCI performance.[125] A review of DES for BCI can be found here[26,126].

The capability of using DES to create controlled percepts has led to an emerging field of "neurohaptics" which focuses on delivering synthetic tactile feedback to improve BCIs performance. Neurohaptic feedback refers to the use of a direct neural interface to evoke somatic sensations to produce a synthetic sense of touch or represent state and object variables. As DES percepts are not particularly sensorimimetic (i.e. the feelings are different from natural sensations), much of the neurohaptic literature has sought to instead characterize the utility of these percepts.[80] For example, researchers have characterized the perceptual separability or just-noticeable difference of DES parameters such as amplitude and pulse frequency. [80,122] A psychophysics evaluation of DES often employs 1-back or two-alternative forced choice (2AFC) task designs in which subjects are asked to either identify the stronger of two sequential percepts or indicate whether two percepts are distinct. Strength of the evoked percept has been shown modulate with stimulation pulse-width, frequency, and amplitude[23,120,122,127,128]. From such studies, discriminability of pulse train duration, pulse amplitude, and pulse frequency have been quantified and this information later utilized to guide motor behavior in humans in a guided grip aperture task. It was shown that humans could quickly reach the target grip aperture by moving their hand

in accordance with the DES feedback and could even be led to follow a constantly changing target aperture.[23] Similarly, in non-human primates, stimulation sequences of different burst frequencies were shown to be discriminable and could be used to guide selection in a self-directed virtual object interaction task.[4] These prior results support the use of behavioral experiments for neurohaptic evaluation and highlight the fact that while static parameter manipulations have been shown to be discriminable, the utility of continuous parameter variation has yet to be explored.

1.3.4 *Terminology: Bidirectional, Adaptive, Closed-Loop*

A quick note on terminology, the terms closed-loop, adaptive, and bidirectional are closely related but used by slightly different research communities in slightly different ways. As discussed, closed-loop frameworks commonly include components that monitor ongoing brain activity; process and classify cognitive state and predict performance; deliver targeted neuromodulation; and evaluate physiological and performance changes to titrate stimulation. Adaptive tends to refer to closed-loop technologies which specifically update stimulation parameters in response to decoded neural activity. Bidirectional brain-computer interface (bidirectional BCI) refers to BCI architectures that both use neural signals to control a downstream effector and deliver return information from the effector by electrical stimulation (e.g., DES or peripheral nerve stimulation).

Chapter 2. General Methods

2.1 Human Subjects

2.1.1 *IRB Approval & Protocols*

Clinical data were recorded under an approved Institutional Review Board (IRB) protocol following formal consent of the subject and their legal guardian if under 18 years of age. All studies were conducted in accordance with approved Institutional Review Board (IRB) protocols, reviewed by the University of Washington and, if involved, Seattle Children's Hospital. The recruitable populations include (1) patients to be implanted with sEEG and ECOG intracranial electrodes for epileptic seizure localization, and (2) patients to be implanted with DBS for chronic neuromodulation therapy of Parkinson's Disease (PD) and Essential Tremor (ET) and intraoperative recording from temporarily implanted ECOG intracranial electrodes. Only in intraoperative studies were cortical electrodes placed to accommodate research aims. In every other case, surgical planning dictate electrode coverage and approach.

During VR studies at Seattle Children's Hospital, recorded clinical data included continuous intracranial ECOG and sEEG neural signals, in-room video from two wall-mounted cameras, in-room sound, two DC input channels recording a stereo audio synchronization signal from the task VR laptop and behavioral time series including kinematic vectors and object interaction flags from within the VR task. In-room video was captured at 30fps from two orthogonal views of the patient. Clinically, this is done to capture seizure, pre-ictal, and post-ictal behavior. Research analysis used the video capture for initial approximate behavioral alignment and labelling of patient behavior outside of the recorded task variables (e.g., verbal responses). Subjective responses to some tasks were also acquired by questionnaire and recorded free response. During VR studies at Harborview

Medical Center, in-room audio and video was not accessible. Data collected during intraoperative studies at the University of Washington Medical Center included only neural signals.

Whenever performed, direct stimulation of neural tissue was approved within known standards of charge density safety[129] and at electrical current magnitudes below 15mA, the maximum used by clinical stimulators.

2.2 Research Hardware & Software

2.2.1 *Tucker Davis Technologies Suite*

A Tucker Davis Technologies (TDT) system was used for research-grade neural recording and control of direct neural stimulation. This system included an RZ2-2 Digital Signal Processor, PZ5-96 Neuro-digitizing Preamplifier, and IZ-2 Subject Interface Module for neural stimulation. Neural signals were be collected at 12.2kHz, DC-coupled. The IZ-2 delivered constant current, stimulation pulses as biphasic, charge-matched, square waves. The leading phase may be positive or negative, depending on the sign of the programmed stimulation amplitude. Pulse amplitude indicates the current magnitude across the electrode surface and is the same in magnitude during both phases of a single, biphasic pulse. The magnitude of constant-current stimulations was voltage-limited for safety, making the set of stimulation magnitudes dependent on individual impedance measurements per electrode and per patient.

Custom control circuit to manage recording, stimulation, and rapid switching between recording and stimulation hardware states were designed for each experiment.

2.2.1.1 Synapse

Synapse the proprietary software and user-interface for TDT systems, enables real-time control of TDT hardware during an experiment, allowing query and update of signals processing, pulse

generation, and stimulation parameters.[130] Synapse is a graphical interface that facilitates the design, management, collection, and storage of data from neurophysiology experiments using System 3 hardware. Synapse also enables auto-detection of connected hardware and a hardware abstraction layer (HAL) to facilitate the workflow and implementation of real-time digital signals processing, logic circuits, neural stimulation control, and data recording, monitoring and display.

> *With Synapse's advanced automation, underlying relational database, and sophisticated hardware interface; the power and flexibility of TDT's proven multi-DSP hardware platform is never more than a few clicks away.*[131]

Synapse also provides a customizable run-time interface to enable within-experimental updates. Access by external APIs to components, called Gizmos, within Synapse can be toggled during circuit development. Throughout this document, when necessary, Synapse system communication flow diagrams or snapshots of the run-time interface will be provided.

2.2.2 *Natus Clinical Recording System*

In parallel with the TDT neural recording system for research neural signal acquisition, clinical neural signals from all implanted electrodes were recorded by a Natus Quantum biosignal system (Natus Medical Incorporated, San Carlos, Ca) at a 1024Hz sampling rate. By hospital protocols, individual contacts were referenced to a scalp needle electrode and grounded to a screw that physically anchored an ECoG or sEEG implant. Synchronized in-room video was captured at 30fps from two orthogonal views of the patient bed, and audio from a wall-mounted microphone. These data were recorded for clinical evaluation of seizure activity: to record preictal, during seizure, and postictal behavior. In our research, video was used to confirm alignment between data streams and label patient behavior outside of recorded task variables. For research, an additional audio synchronization input was used to align research data with clinical neural data. The audio input was recorded across bipolar DC inputs (channels 1 and 7) accessible at the bedside Natus

amplifier. Audio voltage was recorded with no low-pass or high-pass filter at the system sampling frequency (either 1024Hz or 2048Hz, determined by clinical need). The two DC input channels were, referenced to electrical ground at recording, and later bipolar referenced to remove DC bias in the clinically recorded audio signal.

2.3 Electrode Localization

Electrode localization was accomplished using preoperative Magnetic Resonance Imaging (MRI) data acquired on a clinical Philips 3T Achieva scanner with a standard 8 channel SENSE head coil. Postoperative computerized tomography (CT) scans were acquired on a CereTom scanner (512x512x88 matrix resulting in an in-plane resolution of .5x.5 mm / 1.25 slice thickness). The post-operative CT scans were co-registered with preoperative T1 MRI using an affine registration through the Statistical Parametric Mapping (SPM) software package. Three dimensional reconstructions of the pial surface were generated using FreeSurfer. Electrode channel positions were estimated from postoperative CT and then either projected onto the reconstructed pial surface ECoG or localized subcortically sEEG. A secondary registration into MNI152 1mm space[132] enabled automated atlas identification of each electrode used to identify electrodes implanted on, in, or near the primary somatosensory cortex.

2.4 A Primer on Neural Signals Analysis

Oscillations are described by four pieces of information: frequency, power, phase, and temporality (timing and duration). Frequency is the speed of the oscillations and has units of cycles per seconds or hertz (Hz). Power is the amount of energy in a frequency band and is the squared amplitude of the oscillation. Phase describes the progression of a function or waveform along its oscillatory "loop" – as the definition of any oscillatory function is that it returns to its starting place before

beginning again – and is measured in radians or degrees. Lastly, timing and duration refer to the relationship between the onset and continuity of any oscillatory feature and some other event of interest, e.g., neural activity in relation to a particular cognitive or behavioral task performed by a subject. In a broad sense, oscillatory neural activity may be ongoing or temporary (stable or dynamic), and may reflect behavioral, cognitive, perceptual, or somatic processes.

Fourier theory states that any continuous signal may be represented by a series of simple, stable oscillating sines and cosines with weights determined by the Fourier Transform (FT).[133–135] The mathematical process of representing a complex function as the summation of simpler functions is called a decomposition. A discrete Fourier transform (DFT) decomposition assigns weights to the frequency components[5] of the decomposition based on the dot product between the given signal and sine waves of different frequencies (the kernels), although there is a lot of computational redundancy in this approach. The Fast Fourier Transform (FFT) refines the implementation of the DFT.

An assumption of the Fourier Transform is that your data are stationary or "well behaved." Another way of saying this is that the DFT decomposes a time series into a summation of infinite oscillating functions, so "time" is abstracted from the data. Of course, the lack of stationarity in neural data is exactly what we want to study as it reflects dynamic properties of the brain.[136] To understand the temporal structure of non-stationary data, time-frequency estimates must be calculated. One way to do this is with a Short-Time Fourier Transform (STFT) in which data are windowed in time and then FFT is applied. Windowed FFT or STFT accomplishes a time-frequency decomposition

[5] The number of unique frequencies extractable by DFT is half of the number of data points (N) in the time series, plus the zero frequency: N/2+1. By the Nyquist theorem, at least two points per cycle are needed to estimate the FT coefficient (power), so the maximum frequency resolvable by sampling rate f_s is $f_s/2$. A time series of length N, then, can be decomposed into N/2+1 component frequencies at a max frequency resolution of N/2+1. Frequencies $\propto$ [0 : N/2+1 : $f_s/2$]

but presents a tradeoff between temporal and frequency precision and resolution[6]. As window length determines both frequency resolution and temporal *im*precision: longer windows of data provide better frequency precision and resolution, at the expense of temporal precision, and shorter windows provide better temporal precision at the expense of frequency precision and resolution. Temporal precision may be improved, though, by carefully selecting windowing and overlap parameters.

Windowing data is a convolution process[7], equivalent to the application of a nonlinear filter that smoothly attenuate neural signal around a center time point. The data loss from windowing can be mitigated by overlapping windows in time. Temporal overlap between successive time segments (1) improves the temporal precision, (2) mitigates the loss of signal due to windowing, and (3) smooths the time-frequency plots for easier visualization and analysis of relationships between time-frequency and continuous behavioral variables. The Hann or Hanning window is the most common and reliable window applied in neural signals STFT. It is advantageous because it tapers the data fully to zero at the beginning and end of the segment.

Another method for time-frequency decomposition is to apply a band-pass filter and then Hilbert transform the filtered signal, called the filter-Hilbert method. This method offers more control over the frequency characteristics of the filter and returns both bandpower and band-phase estimates by

[6] Frequency resolution is the smallest distinguishable frequency step and is set by the length of your window (N). Frequency precision is the accuracy of your estimate of frequency content and is a function of both frequency and window length. Essentially, the more wavelengths of a given frequency that can fit into your data window, the better you can estimate that frequencies strength in your signal. Temporal resolution is the smallest observable time step and is defined by the sampling rate (f_s). Temporal precision is the smallest time step your transformation can accurately represent and is determined by window length and window overlap parameters.

[7] By the convolution theorem, convolution in the time domain is equivalent to element multiplication in the frequency domain (frequency-by-frequency multiplication). Convolution can therefore be conceptualized as a frequency-domain filter, in which the frequency profile of the signal is passed through the frequency profile of the kernel. This is the basis of the wavelet convolution. A (complex) sine wave windowed with a Gaussian is a (complex) Morlet wavelet. Morlet wavelets are well suited for localizing frequency information in time.

creating and adding the "phase quadrature" component[8] of the real oscillatory signal.[137] The result of the Hilbert function, like the result of complex wavelet convolution, is called the analytic signal as it expresses rotational dynamics in the complex plane (complex dynamics that can be extracted as linear power and discontinuous phase for traditional signals analysis).

Finally, neural signals demonstrate – as do most all biological signals – strong 1/f power scaling. This means the power spectral density exponentially decays as frequency increases, concentrating the greatest signal power in low frequencies with a long, shallow tail of high-frequency content. This can shrink the signal-to noise-ratio (SNR) at higher frequencies in ECoG and sEEG data, making meaningful signal metrics difficult to assess. Taking the average of the coefficients of several frequency bins surrounding each frequency of interest at higher frequencies can increase the SNR.[135]

[8] The Hilbert transform returns the complex signal of a real oscillatory function by rotating the positive and negative components of the FT one "quarter turn" counterclockwise in the complex plane and adding the result to the original signal. Effectively, this doubles the positive frequency coefficients and zeroes the negative frequency coefficients.

Chapter 3. Intraoperative Neural Engineering

3.1 Introduction

Directional Deep Brain Stimulation (directional DBS or dDBS) utilizes a novel probe design that replaces traditional cylindrical electrodes with radially segmented or "directional" electrodes. Directional DBS was designed to maximize the stimulation of pathological regions of interest while minimizing the off-target stimulation believed to be responsible for most DBS therapy side effects[138,139]. Directional DBS probes may be useful as directional sensing devices as well as directional stimulators. This chapter presents an evaluation of the directional sensing capability of the dDBS probe architecture that may suggest new opportunities for biomarker detection and an evaluation of the effect of directional dDBS stimulation on cortical activity.

3.2 Resting State Analysis

3.2.1 *Introduction*

In previous studies of dDBS local field potential (LFP), predefined frequency bands, like the beta band (8-35Hz), have shown disease-relevant modulation specific to the contacts facing the therapeutic target, either the globus pallidus internus[140,141] or subthalamic nucleus (STN).[142] These results suggest that the spatial and directional specificity of dDBS may help in the identification of anatomy-specific signal features that could serve as a biomarker of disease pathology, a guide to assist clinical dDBS programming, or a target for adaptive neuromodulation.[62,139] In this chapter, I discuss a novel and exploratory data-driven analyses of resting state neural signals from patients undergoing dDBS implantation. I leverage methods of broadband time-amplitude correlation and spectral power comparison to demonstrate unique directional sensing and anatomy-specific spectral characteristics within each subject's neural recordings. Using precise whole-brain

reconstruction, spectral features were associated with specific subcortical structures across six patients implanted for treatment of neurological movement disorders, supporting these methods and directional leads as tools for biomarker sensing and discovery.

3.2.2 *Methods*

3.2.2.1 Data Collection

Neural data were collected intraoperatively from six anesthetized human patients undergoing dDBS lead implantation for the treatment of neurological movement disorders. Four patients with Parkinson's disease (Subjects 1 – 4) received bilateral dDBS implants to subthalamic nucleus (STN) targets (n=4 patients, 8 probes), and two patients with Essential Tremor (Subjects 5 & 6) that received unilateral dDBS implants to left-sided ventral intermediate thalamic nucleus (ViM) targets (n=2 patients, 2 probes). All patients received the Boston Scientific Vericise directional DBS lead, segmented in a 1-3- 3-1 configuration (Figure 3.1).

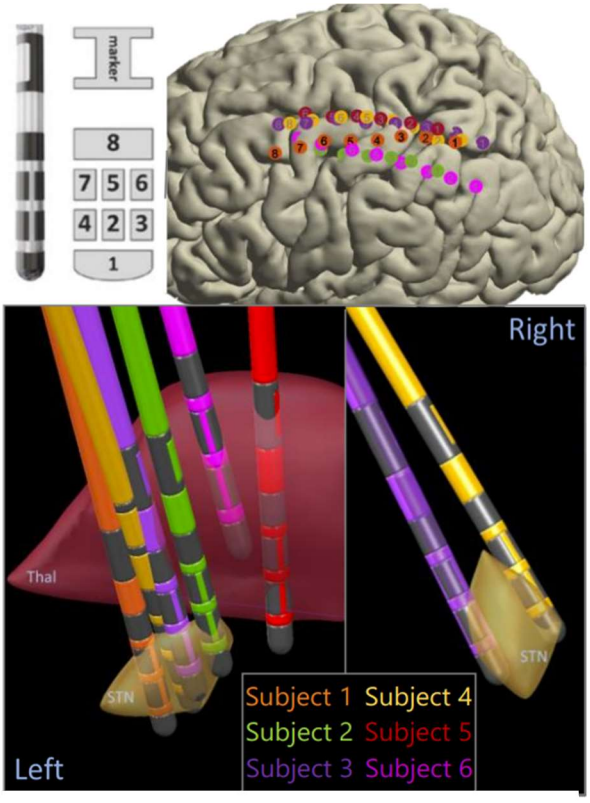

Figure 3.1 Electrode diagram and localization. (top left); Electrode configuration on the Boston Scientific directional DBS electrodes, 1-3-3-1. (top right) Cortical electrode localization for each subject. Note that cortical electrodes run posterior to anterior, with the first contact (labelled 1) over the parietal cortex. (bottom) dDBS electrode placement with targets in the STM or ViM. No imaging data exist for the right dDBS leads of Subjects 1 and 2.

Patients consenting to intraoperative research were also implanted for the duration of the surgery with a 6- or 8-contact ECoG strip, placed subdurally over the left central sulcus, parallel

to the longitudinal fissure, and approximately spanning the hand primary motor and primary somatosensory cortices (Figure 3.1).

Preoperative 3T MRI and intraoperative CT were coregistered with Freesurfer for manual cortical electrode localization, and LEAD-DBS software was used for dDBS localization and orientation.[143–145] Cortical and subcortical electrodes were localized in patient space and projected onto an MNI-ICBM[146] Brain Atlas. The right dDBS electrodes for Subjects 1 and 2 are not localized or in this study as the intraoperative CT scans for these probes were not available. Data for resting state LFP analysis were collected for a minimum of two minutes (average duration 5.56 minutes) in each patient, during which no stimulation or surgical activities occurred. Neural recordings were collected at 12.1kHz, DC-coupled using a Tucker Davis Technologies system.

3.2.2.2 Data Preprocessing

Directional DBS data were rereferenced from scalp electrode to the common average of the directional contacts (contacts 2-7), and cortical ECOG data were rereferenced to the common average of the full 6- or 8-contact strip. Both dDBS and ECoG signals were band passed between 1-300Hz and decimated to a 1220Hz sampling frequency. Line noise (60Hz and harmonics) was removed using EEGlab's cleanline spectral power algorithm.[147] This method interpolates across noise peaks centered at 60Hz and harmonics in the spectral power density estimate, minimizing distortion from a steep notch filter or narrowband The time-frequency content of each recording was determined by windowed Fourier analysis with 1.68 second Hamming windows (2048 samples with 50% overlap) for 1Hz frequency bins from 2-140Hz.

3.2.2.3 Spectral distribution analysis

The distributions of spectral powers were pairwise compared between directional contacts for all 1Hz frequency bins. The statistical significance of dissimilarity was determined using the

agreement between Wilcoxon rank sum, Kolmogorov-Smirnov, and Kruskal Wallis distribution comparison methods for each pairwise comparison. The null hypothesis of the Wilcoxon rank sum assumes equal medians, that of the Kolmogorov-Smirnov assumes equal cumulative distributions, and that of the Kruskal-Wallace assumes equal rank means (approximated as medians).

Each of these are nonparametric methods, appropriate as the spectral power distributions were very non-normal by visual inspection, Anderson-Darling, and Lilliefors tests for normality. Constructing a significance test based on the agreement of these three methods was implemented as a way of additionally controlling for Type 1 error.

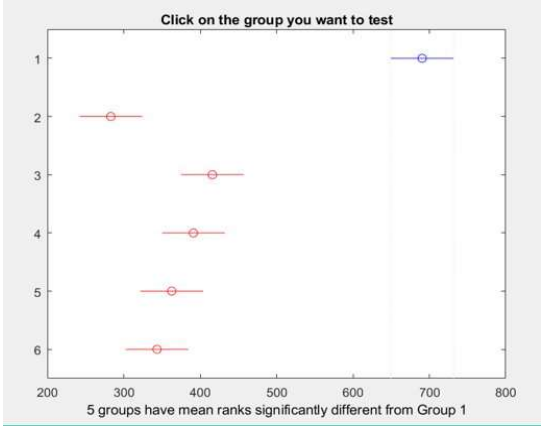

Figure 3.2 Exemplar significant result. Following multiple comparisons correction, spectral power at 24-25Hz was found to be significantly higher on dDBS channel 2, for Subject 1, than any other channel (3-7). Importantly, spectral power between vertically stacked electrodes 2 and 5 was also significantly different individual pairwise comparison.

The threshold of significance within each test was also Bonferroni corrected to $\alpha < 0.003$, to account for the multiple pairwise electrode comparisons ($_6C_2 = 15$) within each frequency bin. A significant result of this method indicates that within the frequency bin being evaluated, there exists a significant difference in the distribution of frequency power in at least one of the 15 pairwise comparisons (Figure 3.2).

3.2.2.4 Correlation Analysis

Time-amplitude correlation was used to evaluate signal similarity between dDBS electrodes within a probe, and between dDBS electrodes and cortical strip electrodes. For time-amplitude analysis, neural signals were additionally smoothed (Figure 3.3) using a custom low-pass, FIR Kaiser window filter with a 40Hz cut-off frequency (74.8Hz stopband, 10Hz passband with 0.1 ripple and

60dB stopband attenuation) to preserve the high-power lower frequency content while avoiding effects of intraoperative equipment (~46Hz) and line noise (60Hz).

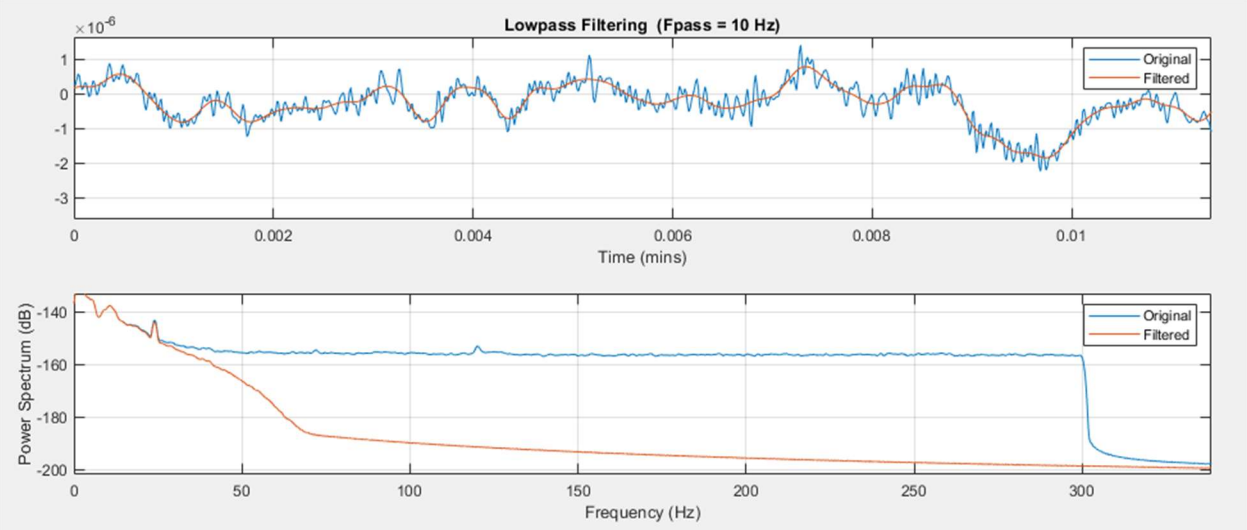

Figure 3.3 Time series smoothing using low-pass causal FIR. (top) An exemplar dDBS, preprocessed local field potential recording in blue, overlayed with the same signal following low pass filtering in orange. (bottom) The spectral information of each signal before (blue) and after (orange) low-pass filtering. This plot visualizes the spectral power shaping of the FIR Kaiser window low-pass filter.

From this, a scaled Pearson's correlation metric with a 3 second window length was used to pairwise compare dDBS contacts within a probe, as well as dDBS contacts to cortical ECoG contacts (Figure 3.4). Autocorrelation of individual dDBS recorded signals revealed modest sinusoidal and series dependence in our data. Series dependence refers the time time-constant of the autocorrelation function, or how quickly self-correlation decays (how sensitive autocorrelation is to offset). Sinusoidal dependence is seen as periodic rises in autocorrelation over time.

To control for series dependence, a scaled cross-correlation analysis was applied in which every 3 second window in one electrode's recording was compared to every other non-contemporaneous 3 second window in a paired electrode's recording. The p-value of the scaled Pearson's rho was then determined from the distribution of cross-correlated rhos.

3.2.2.5 Stability Metrics: Ratio & Variance

To evaluate the reliability or stability of the correlation between two recorded signals over time, a stability metric was defined and calculated. Here, "stability ratio" is defined as the ratio of the whole-signal rho to the scaled rho, and "stability variance" is the standard deviation of the windowed rhos.

3.2.3 *Results*

3.2.3.1 Spectral Distribution Results

	Significant Frequencies (L)	Significant Frequencies (R)
Subject 1	**(6)** 2-6, **(2)** 16-20, **(3)** 44-45, **(5)** 46-47, **(3)** 49-140	**(2)** 2-13, **(6)** 59-72, 85-89, 117-120, 131-138
Subject 2	**(3)** 10-13, **(4)** 14-15, **(3)** 47-48, 127-128	**(7)** 2-9, **(5)** 11-12, **(7)** 32-48, **(5)** 49-51, **(2)** 58-61, **(5)** 62-64, **(2)** 65-74, **(5)** 75-76, **(2)** 80-93, **(5)** 94-96, **(2)** 97-99, **(5)** 100-104, **(2)** 105-122, 124-133, 135-140
Subject 3	**(4)** 3-19, **(2)** 70-71	**(3)** 3-10, 12-31, **(2)** 50-62, **(4)** 65-70, 77-82, **(2)** 83- 89, **(4)** 90-95, **(2)** 96-97, 103-110, 112-115, **(4)** 116-121, **(2)** 122-123, **(4)** 126-129, **(2)** 130-140
Subject 4	**(3)** 3-23, **(5)** 24-25, **(3)** 26-46, 48-58, 62-71, 73-140	**(2)** 2-12, 24-25, 46-47
Subject 5	**(6)** 10-11, **(4)** 12-19, **(2)** 27-30	-
Subject 6	**(2)** 43-44, 77-82, 101-103, 111-112, 127-140	-

Table 3.1 Spectral results for dDBS analysis. Significant frequencies between directional contacts per subject, as found by agreement between three nonparametric statistical tests. Bolded numbers in parenthesis identify the dDBS electrode of maximum power, followed by significant frequency bands on that electrode. Underlined, bolded numbers indicate electrodes that anatomically face or are embedded in the target structure, either STN (Subjects 1-4) or ViM (Subjects 5-6). Results above are from the left and right dDBS probes from six human subjects. Note that the right probes for subjects 1 and 2 were not localized (gray).

The pairwise contrast of spectral power distributions revealed frequency bands that were significantly different in at least one of the pairwise comparisons. Table 1 reports these significant frequency bands by subject and the electrode on which the mean power in frequency was greatest (Table 3.1). A frequency band was defined as two or more consecutive 1Hz frequency bins that were both statistically significant and dominant on the same electrode. In the table, significant bands of frequencies are listed after the electrode number, in bold, on which they are dominant. Bolded and underlined numbers indicate the electrode of dominance is one facing or embedded in the anatomical target. As an example, in the

left dDBS probe of subject 2, spectral bands 10-13 Hz, 14-15 Hz, 47-48 Hz, and 127-128 Hz were found to be statistically distinguishable and of highest spectral density on directional contacts 3 and 4 (Table 3.1). The results of the electrode localization show that only these two directional electrodes are embedded within the STN, and no other directional contacts on the probe face or contact the target subcortical structure (Figure 3.1). Interestingly, these emergent frequency bands mimic standard alpha, beta, low-gamma, and high-gamma frequency divisions. The strength of dominance at each significant frequency was also characterized by percent increase over mean power and by z score based on mean and variance of power at that frequency across electrodes. This information may be included in future studies comparing spectral feature strength with orientation and distance from anatomical target.

3.2.3.2 Correlation Analysis

The time-series correlation analysis results are presented visually in Figure 3.4 in a node-and-edge graphical plot in which line color reflects the direction and strength of signal correlation and line width reflects the significance of the correlation between pairs of electrodes (significance at $p<0.05$).

Each node in this figure represents an electrode, and their alignment in the graphs reflects their actual manufactured, stacked-ring geometry. The graphical plot facilitates visualization of the correlational relationships between dDBS contacts and seems to reflect underlying probe orientation relative to the therapeutic target. For example, the correlation graph of the left dDBS lead for Subject 3 demonstrates strong and significant negative or anticorrelations between the lower ring electrodes (2,3 and 4) and the upper ring electrodes (5,6, and 7), depicted as thick, red edges connecting electrodes 3-5, 3-7, 4-5, and 4-6, as well as significant but less negative correlations between electrode 2 and all other electrodes. This is consistent with the electrode

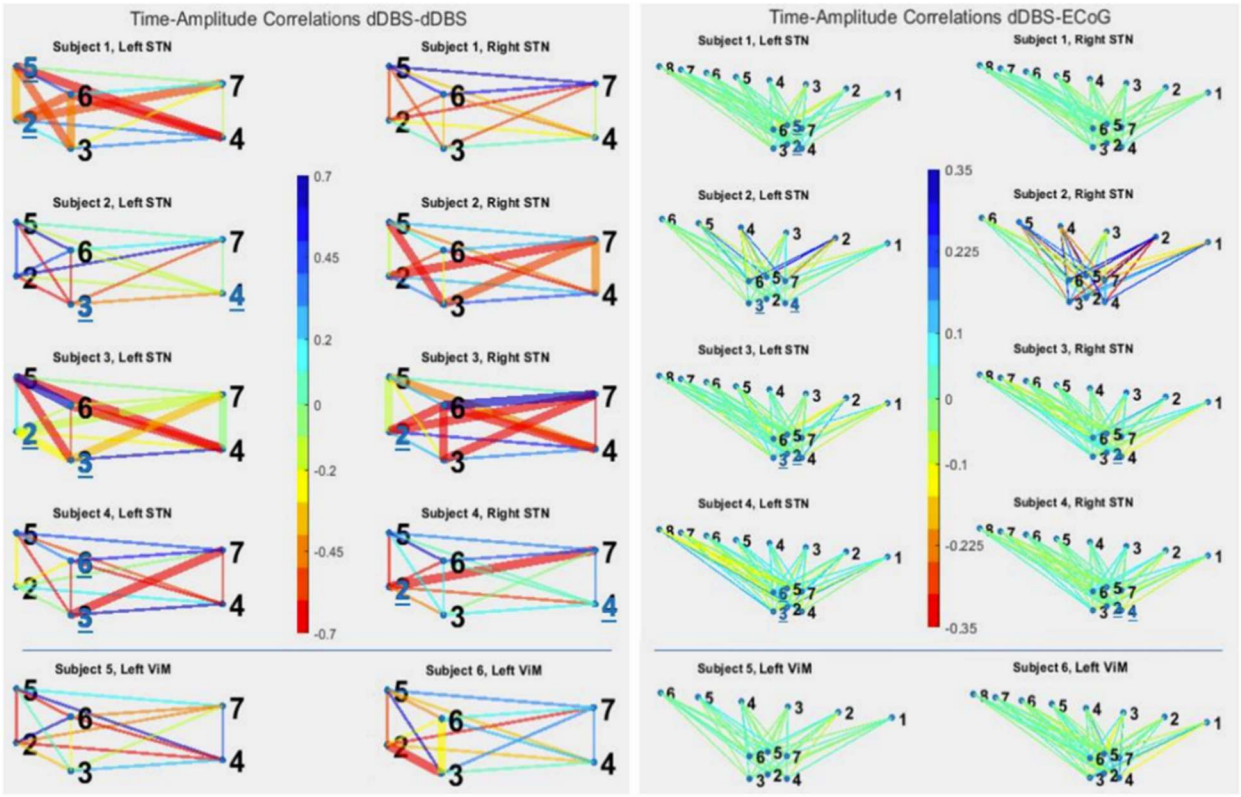

Figure 3.4 Strength and significance of dDBS-dDBS and dDBS-ECOG correlations. (left) Graphic depicting correlations between direction DBS contacts. The magnitude of the scaled Pearson's rho is encoded in the color of the edges between nodes, with strong negative correlations in red and strong positive correlations in blue. The statistical significance of the pairwise correlation is encoded in the width of the edge, wide indicating significance at $p<0.05$. (right) Graphic depicting the correlations between dDBS and left ECoG contacts which run posterior to anterior, numbered 1 to 8. Here, only correlation is reflected in the edge color between electrodes. Note that the color bar has different limits between (left) and (right), reflecting strong differences in mean correlation values. In both graphics, blue underlined nodes for subjects 1-4 are those that face or are embedded in the STN.

localization results, which demonstrate that only the lower ring directional electrode 2 was implanted in the medial surface of the STN (Figure 3.1).

The results of the correlational analysis between depth and cortical electrodes are depicted on the right in Figure 3.4. As seen, strong negative and positive correlations (red and blue, respectively) between depth and cortical electrodes are rare, with most rho values hovering around 0 (green). The presence of occasional strong correlations, however, demonstrates interesting geometry and may imply a useful and quickly calculated broad-band functional connectivity metric. For

example, between the left dDBS lead of subject 2 (STN) and the left cortical strip, strong positive correlations exist between depth contacts 6 and 5 and cortical contact 2, with moderate negative correlations between these depth electrodes and cortical contact 4. The opposite relationship is seen in depth contact 7, however, which demonstrates negative correlation with cortical contact 2 and positive correlation with 4. Referring to depth connectivity, electrodes 5 and 6 share strong positive correlation, and both share a weak correlation with contact 7. By anatomy, the upper ring (contacts 5, 6 and 7) is embedded within the thalamus while the lower ring is implanted below the thalamus and nearer the STN. Cortical contact 2 may overlay a sensory integration area of cortex and 4 is over the hand area of the primary somatosensory cortex. Future analyses may yet to explore the utility of resting signal correlations between depth and cortical electrodes and their relationship to the expression of evoked potentials at the cortex following directional depth stimulation.

3.2.3.3 Stability Metrics

The stability ratio revealed a mean value around one across all contacts (stability ratio = 1.067 ± 0.337), although the maximum ratio was just over 4 and the minimum ratio approximately 0.4. Similarly, the standard deviation (std) of rho values across contemporaneous signal epochs was shown to be small (mean std = 0.101 ± 0.111), though some pairwise comparisons demonstrated standard deviation values over four times this. These results suggest that specific dDBS pairs may be uniquely sensitive to dynamic changes in local activity. Interestingly, pairs demonstrating the greatest change in correlation over time are often pairs adjacent to the STN-facing electrodes. For example, in Subject 1, while electrodes 5 and 2 face the STN, the electrode pair 6-7 demonstrates a marked deviation of the stability metric from one, with a standard deviation of its over 5 times

that of other electrode pairs. The evaluation of correlation stability or variance as a useful metric is left for future studies.

3.2.4 *Discussion*

Overall, these results confirm that directional electrodes capture distinct neural signals data, demonstrated here as aggressively significant difference between spectral distributions, and suggest that dynamics of temporal correlation in minimally preprocessed, low-frequency broadband voltage signals may reflect important depth-depth and depth-cortex connectivity. Specifically, this work evaluated two data-driven time-amplitude and time-frequency approaches to uncovering useful signal features along dDBS probes, providing a pathway for future investigations.

A useful and immediate application of these directional sensing results emerged during electrode localization in this study. Currently, directional localization requires the fitting CT voxel brightness to the spatial frequency surrounding the orientation maker on the probe (Figure 3.1, the metal strip identifying the 2-5 electrode column), and the selection of the most-probable direction based on the CT artifact[148]. However, this process does not always yield certain results. The directional orientation result for the left dDBS lead in Subject 2, for example, yielded nearly equal probabilities for one orientation and its 180-degree opposite. The spectral distribution method, however, identified significant frequency banding on electrodes 3 and 4, and none on electrode 2. As demonstrated by the results from other subjects and a recent publication[149], electrodes facing the STN possess significant spectral power increases compared to electrodes not facing or embedded within the STN. Therefore, the orientation in which electrodes 3 and 4 faced the STN was a better solution than the orientation in which electrode 2 faced the STN.

The original mapping listed electrode 2 as the anterior or STN facing electrode simply because implantation technique often yields this orientation. Surgical notes also mention the visible, non-implanted left DBS marker facing medially and not anteriorly, further corroborating that the accurate depth orientation was, in fact, the one reflected in the significant spectral features.

A next step in the evaluation of these methods and metrics would be analysis of signals with awake, conscious movement and disease symptomology, as it remains to be seen whether these data-driven, resting state findings relate to symptom severity or therapeutic efficacy of stimulation. Additionally, in pursuit of signal features for adaptive DBS modulation, a future study may evaluate the change in spectral banding and time correlation following dDBS stimulation.

3.3 Evoked Potentials Analysis

3.3.1 *Introduction*

As mentioned, cortical evoked potentials (or CEPs) are changes in neuronal activity seen as stimulation-locked waveforms in recordings of cortical LFP. CEPs are thought to reflect functional connectivity between the site of neuromodulation and evoked potential, with stronger functional connectivity reflected in stronger cortical evoked potential strength. To quantify CEP magnitude, three methods supported by existing literature were applied. These include windowed root mean squared (rms), polynomial smoothing, and windowed high gamma (70-110Hz) bandpower.[61,150] In this preliminary analysis study, I evaluated the effect of directional DBS stimulation amplitude and orientation on evoked potentials at the ipsilateral cortex, processed using one of these methods. In the end, only quadripolar results for one patient were calculated and presented.

3.3.2 *Methods*

3.3.2.1 Simulation Trials – Data Collection

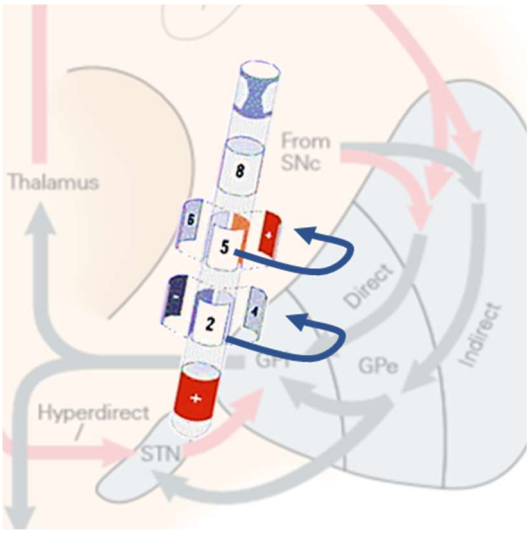

Figure 3.5 Quadripolar stimulation. In this stimulation configuration, stacked pairs of electrodes serve as join cathode or anode for stimulation. In this figure, stimulation is between (2,5) and (4,7).

For stimulation and evoked potential (EP) analysis, sequences of single, 200µs pulse-width per phase, biphasic square wave stimulation were delivered across a quadripolar electrode configuration for 2 minutes (Figure 3.5). Single, biphasic pulses were delivered at a rate of 2Hz, granting 500ms of time for EP analysis between stimulation pulses, as seen in Figure 3.6, middle. In quadripolar stimulation, a stacked pair of electrodes are together the anode (or cathode) and a neighboring stacked pair the cathode (or anode). An example configuration is depicted in Figure 3.5, in which vertically aligned electrodes 2 and 5 serve as the positive pole and electrodes 3 and 6 the negative pole, of a paired bipolar stimulation (i.e., quadripolar). This provides three unique pole combinations of stimulation orientation: (2/5 - 4/7), (2/5 - 3/6), and (3/7 - 4/7). Reverse orientations can be collected by driving negative current across the quadripolar configuration; a negative amplitude reverses the cathode and anode assignments, reversing the direction of the injected current. This quadripolar electrode configuration was selected to facilitate common mode rejection on the traditional, cylindrical DBS electrodes (electrodes 1 and 8).

During the two minutes of stimulation, constant-current amplitudes of the stimulation waveform are varied cyclically between two, polarity-matched magnitudes (as in: 3mA, 5mA, -3mA, -5mA, repeated). In total, 240 stimulation trials were collected for each underlying stimulation orientation at the sequence of amplitudes (±3mA and ±5mA) described.

This patient consented to 8-lead cortical ECOG implant for the duration of the surgery. As before, the strip was placed subdurally over the left central sulcus, parallel to the longitudinal fissure, and approximately spanning the hand primary motor and primary sensory cortices. Cortical electrode localizations relied on Freesurfer coregistered preoperative MRI and intraoperative CT, and LEAD-DBS software was used for dDBS localization and orientation.[143–145]

3.3.2.2 Cortical Evoked Potential (CEP) Analysis

For CEP analysis, recorded neural data were epoched around individual stim pulses, from 20ms prior to 500ms following the onset of stimulation (Figure 3.6, top). Cortical recordings were epoched around each individual dDBS stimulation pulse to yield 240 individual stimulation trials per stimulation block. To baseline each trial, the average magnitude of the 20ms pre-stimulus period, the DC offset, was subtracted from every point in the stimulation trial. Trials were individually baselined to the average pre-stimulation mean voltage, and then group baselined to the average pre-stimulation voltage per stimulation amplitude.[61]

Root Mean Squared (RMS)

To calculate the windowed root-mean-squared CEP metric, a 5ms rms smoothing window was used to reduce noise and high frequency oscillations in the post-stimulus CEP. Then, the maximum rms value ('RMS') between 10ms and 90ms post-stimulus onset was recorded.[61] The post-stimulus time at which this maximum occurred was recorded as 'rms_latency.'

High Gamma (70-110Hz) Bandpower Estimate (hiG)

Here, the stimulation artifact was removed from Following this, zero-phase digital filtering with an IIR bandpass filter for the gamma band was performed. Using Hilbert method envelop

extraction, the mean of the squared magnitude of the Hilbert envelop between 10-220ms was extracted as the evoked gamma band power following stimulation, per trial ('hiG').

For the windowed high-gamma metric, the stimulation artifact was removed from each stimulation trial using a weighted signal inversion technique validated by Schalk et al, 2019.[36] This low-cost weighted signal inversion method was shown to preserve pre- and post-stimulation frequency content. In this method, a predetermined window of signal around stimulation onset is removed from the signal and replaced with "synthetic" activity using a bidirectional linear window and summation technique. In this technique, a window of signal prior to the onset of the stimulation is time-reversed, linearly diminished to zero, and then added across the removed stimulation artifact window. This process is then applied for a window of signal beginning at the end of the removed artifact window and continuing for the same length as the removed artifact window. This signal is time-reversed, linearly diminished, and added across the removed stimulation artifact window. This method prevents jump discontinuities and preserves overall spectral representation of surrounding neural data.[36] The artifact-free, continuous signal was then bandpass filtered to extract time-series spectral information for 70-110Hz, called high gamma. The squared amplitude of the resultant signal was then averaged across a 10ms and 220ms post-stimulation period to calculate the average high-gamma power evoked by single pulse DBS stimulation.

Polynomial (0.01Hz Butterworth Low-Pass) Peak-to-trough

A third method calculated a post-stimulus peak-to-trough metric on evoked neural data that had been smoothed with a 5ms windowed polynomial smoothing function, equivalent to a 4^{th} order 0.01Hz low-pass Butterworth filter. The maximum displaced, peak-to-trough magnitude was labeled the 'p2t_window' metric.

3.3.2.3 Statistical Analysis

Multifactor analysis of variance (ANOVA) was conducted to explore the impact of cortical electrode position, dDBS stimulation orientation, and stimulation amplitude, including all interaction effects between these factors on the resultant CEP metric, i.e., the 2- and 3-way interaction effects were considered. Multifactor ANOVA evaluates the variance in the EP metrics attributable to dDBS stimulation orientation, stimulation amplitude, cortical electrode, and their interactions.

3.3.3 *Results*

In this one patient, ANOVA revealed a significant impact of orientation, electrode position, and stimulation amplitude on RMS ($p<0.001$), as well as a significant interaction effect of orientation and amplitude on RMS (Figure 3.6, c1) and rms_latency (Figure 3.6, c2). Variance of hiG was also significantly explained by stimulation amplitude. Looking at the bottom high-gamma plot, for example, we can clearly see the periodicity of hi-gamma fluctuations by electrode label though the classic ANOVA did not result a significant effect of electrode on hiG.[9]

Localization of ECOG electrodes revealed that CEP expression and modulation was strongest over sensorimotor cortices (electrode 3), the cortical tissue immediately anterior and posterior of the central sulcus. The orientation sensitivity of some cortical CEPs metrics may make them useful biomarkers for directional DBS programming, localization, and adaptive therapy.

Completed stimulation analysis results for one subject reveal a significant impact of stimulation orientation, electrode, and stim amplitude on the rms_max EP metric (all $p<0.001$), as well as a significant interaction effect of orientation and amplitude on rms_max ($p<0.001$). Additional N-

[9] If the electrode label was not correctly recoded as a non-quantitative label or category, the ANOVA would have been looking for continuous or linear effects of electrode number on CEP metric.

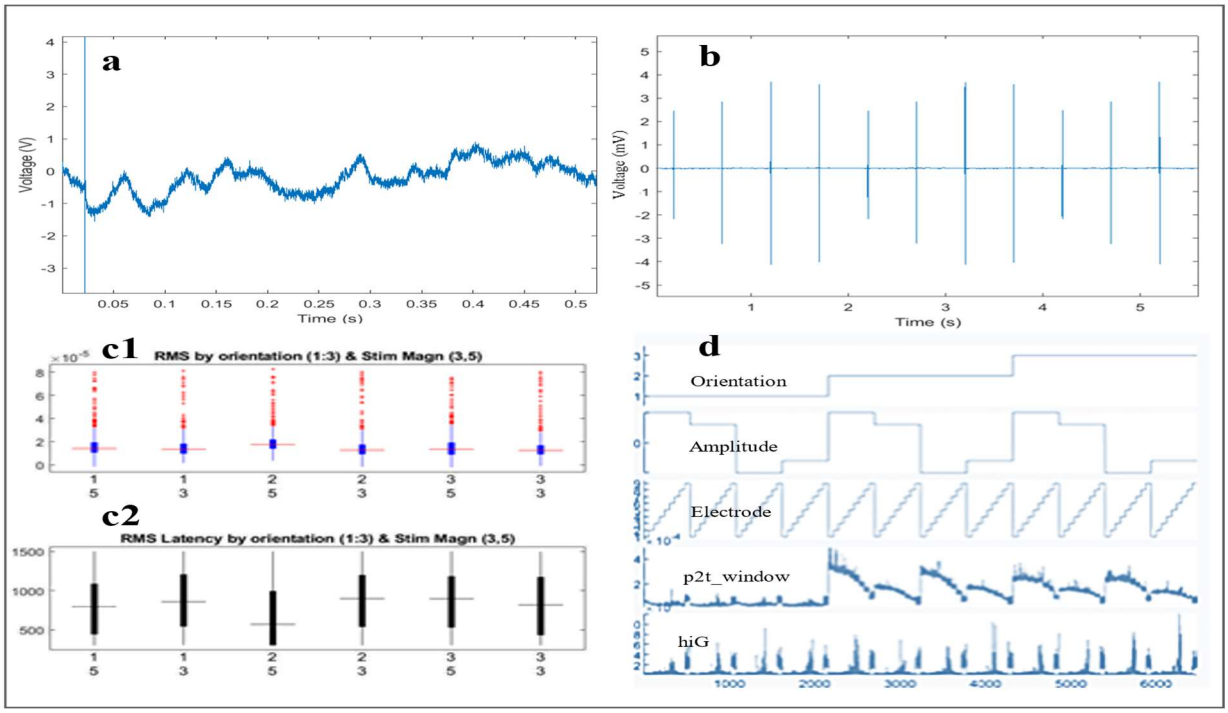

Figure 3.6 Effects of quadripolar dDBS stimulation on CEP metrics. (a) An exemplar baselined stimulation trial. (b) Series of single stimulation pulses regularly varying in amplitude. (c1) RMS values by orientation 1-3 and magnitude of the stimulation amplitude (3,5mA). (c2) Distribution of rms latency also by orientation-amplitude pair. (d) Stacked parameters (Orientation, Amplitude, Electrode) and CEP metrics (p2t_window, hiG) by sequential stimulation trial. Note effect of orientation on p2t_window and of CEP electrode and amplitude on hiG.

way ANOVA analysis of these factors on the gamma-power filter-Hilbert approach ('hiG') reveals a significant effect of only amplitude on evoked gamma-power ($p = 0.0098$).

3.3.4 *Discussion*

This preliminary stimulation analysis is included to discuss and demonstrate analysis of stimulation-locked (cortical) evoked potentials. It is unfortunate this work was not able to be continued once development began in earnest on the virtual reality experimental platform detailed in subsequent chapters. The results, by ANOVA and visual inspection, suggest a clear relationship between CEP magnitude and location, and the orientation and amplitude of directional DBS.

CEP metrics may offer an "active" way to evaluate neural state and response to neuromodulation or other treatment and may serve as a biomarker that can either be continuously evaluated during

therapeutic stimulation or elicited by specific stimulation parameters to periodically "probe" functional networks.

It is worth noting for future work that jitter above minimum temporal separation between individual stimulation trials should be implemented in a repeated stimulation study such as this one. Strict temporal patterns may introduce confounds as the network adapts to reliable stimulation.

Chapter 4. A New Experimental Platform: Clinical Intracranial Virtual Reality

4.1 Introduction

Immersive virtual reality (VR) grants unprecedented experimental control over visual stimuli alongside precise tracking of somatic and ocular movements. In VR exists not only a powerful environment for creative and efficient experimental design, but also an integrated platform able to collect synchronized datasets consisting of any explicit VR environmental variable or user parameter, including any rendered or unrendered object state, real-world tracking of the 6 degree-of-freedom movement of the subject controller, headset, and optional external trackers, the timing and type of all controller and headset button interactions, ocular dynamics including pupil metrics and gaze direction, facial dynamics, and external camera recordings.

In addition, VR offers an intuitive and flexible design platform for complex experiments and grants access to the manipulation of variables that are impossible to control in a natural world context, such as the constants of global and local physics, the visual details and optional rendering of every virtual object and personal avatar, or the precise probability distribution underlying any interaction. The level of control granted by a VR experimental platform is unprecedented and has the potential to greatly influence neuroscience experimentation and to refine canonical experiments and their associated understandings of human cognition and neural processes.

And yet, VR had yet been integrated for use with intracranial electrodes in a hospital setting. This patient population offers one of the few reliable opportunities to record intracranially from awake and interacting humans for up to weeks at a time.

As immersive VR had not been brought into the clinic for use this in-patient and post-operative research population, I carefully explored and refined subject protocols over time. I present my outline of safe and effective patient protocols refined over VR studies with 10 subjects, ages 7 –

47 years old, VR-naïve (n=8) and VR-experienced (n=2). I also present recommendations for designing virtual environments and interactions that support VR-naïve subjects.

4.2 Virtual Reality Hardware & Software Selections

4.2.1 *Unity Game Engine*

The critical first step towards building a virtual reality neural engineering and research platform was the identification of the VR and neural electrophysiology interface components. Unity[130] is a cross-platform game engine ideal for its status as a mature VR development tool, ease of use, and extensive set of tutorials, called Unity Learn[10], updated regularly and tiered for both novice and advanced VR developers. Unity is also supported by a fantastic list of YouTube content creators, including Justin P. Barnett and Valem Tutorials, both of whom significantly assisted my first steps along this VR journey.[151,152]

Game/Experiment design in Unity is built on interdependent use of the Unity Editor, a graphical user interface (GUI) for environmental variable, asset and game management, and C# scripting.[131] Unity also provides plug-in support for a wide variety of virtual (VR), augmented (AR), and extended (XR) reality devices. In 2019, Unity adopted the Khronos Group OpenXR API[153] for nearly universal operability with commercial devices (the list is extensive but not complete). This means that any solution developed on Unity for one hardware platform (i.e., Vive Pro VR system) should deploy on any other supported platform with no or minimal platform-specific changes. Experiments developed over the course of this thesis also used the OpenVR SDK[154] from Valve to support use of SteamVR and its custom Interaction system. I also used OBS Studio[155],a free and open source software suite for recording in-game video. This software was used to capture the

[10] https://learn.unity.com/

images from the right display screen at 3840x2160 resolution at 48 frames per second (fps), in-game audio, and subject verbal response during VR tasks.

4.2.2 *Commercial Virtual Reality Hardware*

In terms of hardware, there are a variety of VR headsets and systems on the commercial market. To avoid Virtual Reality Sickness, which is a feeling of nausea or discomfort that may result from virtual immersion, it is recommended that you buy the system with the highest refresh rate you can afford. Industry standard is moving towards 90Hz with higher end headsets now offering 120Hz refresh rates. A wider field of view and higher resolution bicameral screens may also help reduce discomfort in VR. Beyond this, some systems offer onboard eye tracking, external camera-based room or hand-tracking, controller, and additional object tracking, and either a wired or wireless headset connection. Controller designs differ between manufacturers, with some controllers offering more natural object interactions in VR. It is important to pair your headset with a sufficiently powerful and VR-ready gaming desktop or laptop in order to use your headset at its full capacity.

I selected the HTC Vive Pro Eye to ensure integrated eye tracking. This headset offers up to a 90Hz refresh rate with 110-degree field of view, onboard eye tracking, hand tracking, and multiple objects as well as hand-held controller accuracy. The headset system is wired, although a wireless option exists, and utilizes up to four base stations for reliable and submillimeter tracking resolution. This presents some added difficulty in terms of in-room setup compared to a wireless system. In our case, this was worth the added on-board functionality and render specs.

The VR task platform utilizes the Alienware m15 R4 (32GB RAM NVIDIA GeForce RTX 3070 8GB) VR-ready gaming laptop, and the HTC VIVE Pro Eye head mounted display (HMD) for VR immersion. Selected to reduce the chance of virtual reality sickness (VRS),[156] this HMD supports

a 90Hz refresh rate, a net field of view of 110°, dual high-density AMOLED displays, and onboard integrated eye tracking. The HTC VIVE Pro Eye uses two SteamVR 2.0 base stations for submillimeter tracking of controllers and headset along 3-euclidian and 3-rotational axes (6D). Base stations were mounted on extensible tripods and positioned a few feet from the hospital bed to ensure coverage of all potential dynamic movements during VR tasks.

4.2.3 *Custom API Development*

4.2.3.1 The Synapse-C# interface

Synapse, the software interface of the TDT neural recording hardware, offers a RESTful API with bindings for Python, MATLAB, and C++, but does not support C# which is needed for Unity integration. Synapse also provides a UDP interface for minimal latency data transmission[11] between an external computer and the neural signals processor, the RZ unit, for configurable use inside a Synapse-defined project.

In one route towards Synapse and Unity integration, Maurice Montag and I built and evaluated a custom API to manage the query and update of Synapse and Unity state variables during an ongoing experiment and govern data transfer between the TDT and VR task computers (Figure 4.1). Key design and evaluation metrics for the API included safety, within-experiment functionality, minimal lag, and ease of integration into standard Unity code. Integration of Synapse and Unity required development of a pure C# version of the provided Synapse API. Although a C# wrapper the existing API could have been built, it was determined that a new Synapse API in C# would be a more robust solution. This was due to Synapse's existing RESTful API being created with dynamically typed languages in mind, specifically Python and MATLAB. Although

[11] TDT documentation suggests that the maximum data throughput for UDP communication is 38.4 kBps, with 192 32-bit words being sent/received at 50 Hz.

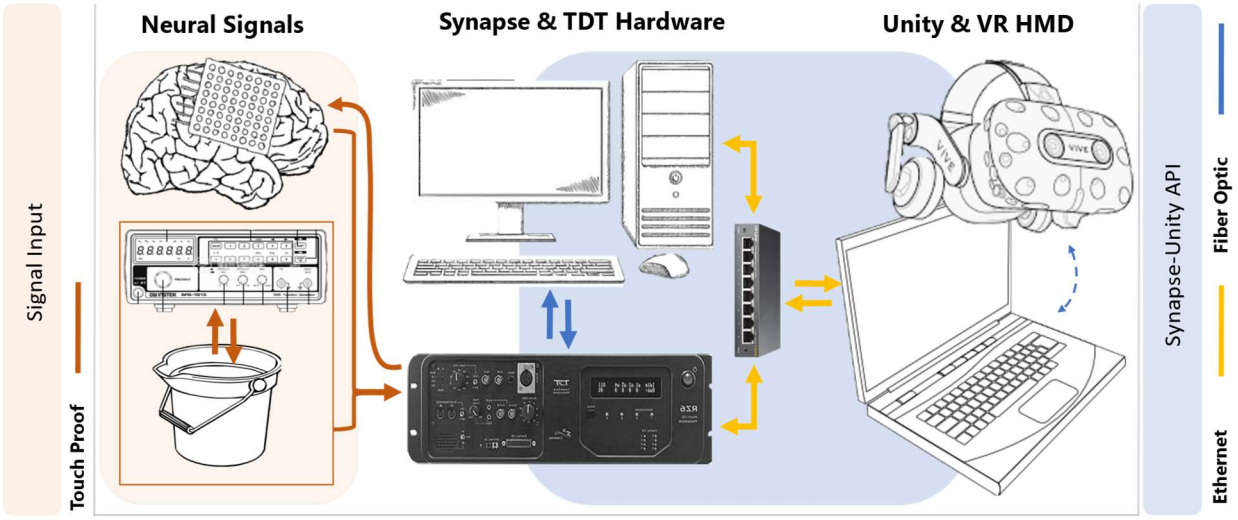

Figure 4.1 Benchtop testing and development setup. (left, orange) Neural input was synthesized using a function generator and electrodes submerged in a saline tank. (middle) TDT recording hardware connects to the TDT computer hosting Synapse, which connects (right) to a separate task computer hosting Unity and capable of supporting VR hardware. The custom API (blue) was deployed on the Unity-hosting laptop. Connections include standard touch proof (red), fiber optic (blue), and ethernet (yellow). Wired and wireless VR headset integration is supported within Unity (dashed blue).

the existing C++ bindings of the RESTful API addressed the problem of dynamic typing by treating all data types as doubles, this solution did not allow for strict type safety. Human research demands fail-safe control of neural stimulation, so accurate data typing is requisite. Future solutions minimized the access of the VR environment to experimental variables to guarantee patient safety during neural stimulation.

Additionally, the existing bindings for Python, MATLAB, and C++ were distributed as a static Windows object library (.lib). Our API was compiled in dynamic link library (.dll) format, for easier integration with Unity and other standard C# projects.

Finally, the existing RESTful API for Synapse was not object-oriented and mostly string-based, requiring unnecessarily clumsy syntax to work directly with Unity. In contrast, our C# Synapse API bindings facilitate the “getting” and “setting” of data inside Synapse in a simple, object-oriented fashion. This allows the code that interacts with Synapse to merge seamlessly with Unity code, eliminating awkward changes in syntax and allowing Unity developers to ignore the

underlying complexity of the provided API, working instead with familiar object-oriented patterns. Our API also enables a more robust error handling system that eases the burden of interpreting error information returned from Synapse in Unity. Error handling in this context is extremely important. We use the C# concept of nullable value types to force the checking of potentially null data before use. For example, if a user tries to retrieve an API parameter that is not enabled in the API menu for the specific Synapse gizmo, the function will return a null value type. The user will have to check whether the value returned is not null before being able to use it unless they specifically use a cast to knowingly bypass the checking. Using this system instead of exceptions helps to eliminate the possibility of API generated crashes, leaving Synapse in an unwanted state during an experiment.

In Synapse, "Gizmos" are the functional units for recording and stimulation control. In our API, each Gizmo is given its own class, containing all API parameters and associated data. At startup, each Gizmo is instantiated with their name and type, and information is retrieved from the Synapse environment to determine the parameter boundaries of the configured Synapse experiment. These parameters and boundaries can then be called and modified from within the Unity environment. One of these gizmos is a generic purpose UDP interface which allow 32bit words transmitted to or from the RZ neural processor as an input or output to other gizmos. Our API also exposes the ability to read or write this RZ UDP port directly as a low latency input or output.

It is important to note that in this implementation data are being sent in the clear as JSON or UDP packets. Although TDT may address security concerns in the future, we linked our Synapse and the Unity computers via a network (LAN) that was not connected to the external internet in order to keep patient behavioral and neural data secure.

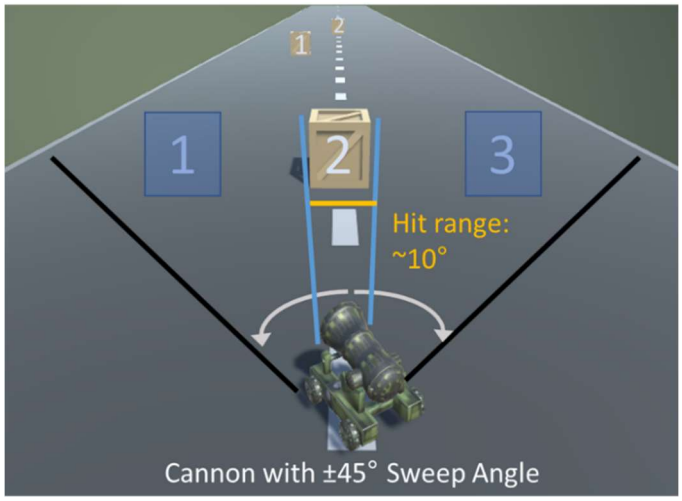

Figure 4.2 Visualization of the Cannon Task in Unity. Band power in Beta (10-30Hz) was used to rotate the cannon in place with 90-degrees of swing. Two thresholds, low and high, defined the beta power values that yielded no, counterclockwise, or clockwise rotation of the cannon. Power estimates completed by the TDT were updated each frame of the Unity task. Projectiles were launched when a countdown timer reached zero. If the projectile collides with the target box, then the API triggers the TDT to deliver stimulation across specified electrodes.

4.3 Benchtop Validation

4.3.1 *The Cannon Task*

To demonstrate the bidirectional capabilities of the Synapse-Unity API, a "BCI-inspired" task was designed in Unity (Figure 4.2). In this task, a cannon is rotated clockwise or counterclockwise according to the beta power (10-30Hz) recorded by a selected electrode. This signal was recorded by the TDT via a sEEG probe immersed in the saline solution (Figure 4.1). Using onboard digital signals processing hardware, the TDT band-passed the signal 10-30Hz and applied a Hilbert transform to extract the continuous power envelope, in real time.

Power estimates completed by the TDT were updated each frame of the Unity task. Two thresholds were selected based on post-hoc standard deviations of beta power, creating low, medium, and high ordinal labels, corresponding to no, clockwise, and counterclockwise rotation. After between 10 and 15 seconds of beta-driven targeting, the cannon fires a cannonball. If this cannonball hits the depicted box target, the collision detected in Unity triggers a train of stimulation to be delivered by the TDT.

Synthetic neural recordings were delivered in two ways. To test the coupling between beta-band power and cannon angle, a function generator and a bucket of saline solution set to mimic brain

resistivity were used (Figure 4.1). With the function generator, we introduced a complex voltage signal with a 2Hz sinusoidal power oscillation in the beta band (Figure 4.3). By design, the signal was created to have oscillating power in a desired bandwidth fluctuating with a frequency of 2 Hz (1). The cannon was seen to rotate as expected with this input.

$$Signal(t) = \cos(\pi f_b t) * e^{2i\pi f_c t} + \mathcal{N}\left(0, \tfrac{1}{2}\right) \quad (1)$$

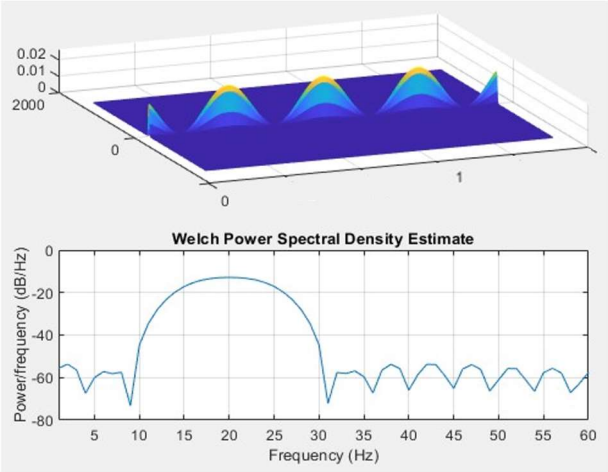

Figure 4.3 Complex voltage signal. (top) Spectrogram demonstrating oscillatory power in a narrow band. (bottom) Welch method power spectral density estimate shows the narrow band to be approximately 10-30Hz. This signal was designed to evoke a regular ~2Hz oscillation on Beta power for benchtop evaluation of the Synapse-C# API, VR-TDT system integration. Beta power was defined at 10-30Hz for the benchtop validation work.

To better approximate real neural signals, we utilized TDT's neural emulator software, Corpus which both simulates the spectral characteristics of human neural recordings and can emulate TDT hardware to reduce benchtop validation complexity. To clarify, Corpus is a neural emulator and does not replay actual neural recordings. Data were processed in real time, as before, to extract beta-band power. For the Corpus emulator, the thresholds determined labels of $\beta_{LOW} \leq$ 2.2E-10 dBW, $\beta_{HIGH} \geq$ 3.2E-10 dBW, and 2.2E-10 < β_{MEDIUM} < 3.2E-10 dBW. The ordinal label β_{LOW} triggered no cannon rotation, β_{MEDIUM} triggered counterclockwise rotation, and β_{HIGH} triggered clockwise rotation (Figure 4.4). If a cannonball collided with its appropriate target in Unity, stimulation was triggered. In our demonstration, stimulation was delivered as a train of constant current, biphasic pulses with pulse widths of 200us and a total train duration of one frame.

To assess the real-time performance of the developed software interface, we assessed system latency by measuring the delay from collision detection to stimulation onset. This was performed using a USB-to-BNC TTL generator that delivered pulses at the start of each collision detected event. These TTL pulses were fed into an analog input channel and sampled at 24.4KHz by the TDT system such that the speed of the API in relaying collision, triggering stimulation, as well as any TDT hardware delays in executing the stimulation command could be measured.

4.3.2 *Results*

The tight coupling between the constructed signal's beta power in black and the change in the angle of the cannon in blue demonstrates the rapid communication between the TDT recording hardware and the Unity task environment (Figure 4.4). With the emulator, we collected over 550 trials of performance data to demonstrate the stability of the API. A trial is defined as one approximately ten second period aiming followed by one launch of a projectile. Trial number 552 is depicted below in Figure 4.4, right, as it had a high collision rate for an input that was effectively a random walk, in terms of task dynamics.

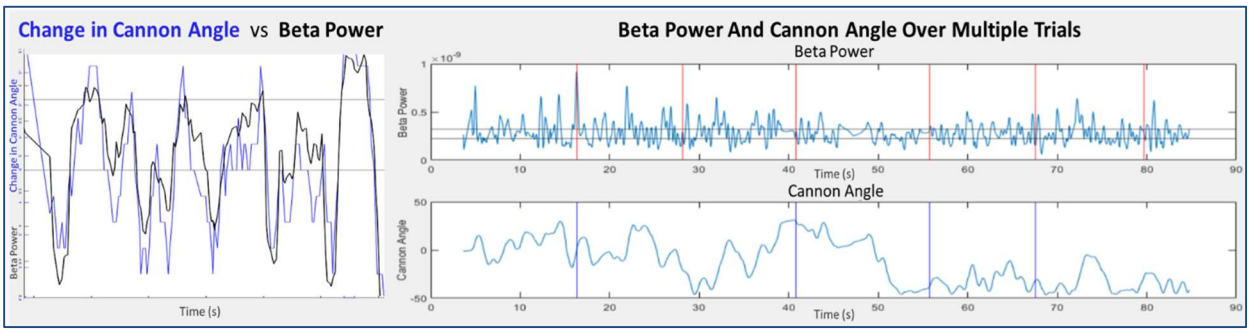

Figure 4.4 Continuous Beta Power and Cannon Rotation. Three graphs depicting the relation between beta-band power and smoothed cannon angle. (left) The superimposed time series of the change in cannon angle (blue) and Beta (10-30Hz) power (black), demonstrating apparent and near-immediate correlation. (right top) A plot of continuous beta power over multiple aim-and-shoot trials, and (bottom right) a concurrent plot of the cannon angle over time. The horizontal black lines are the thresholds for counter- and clockwise cannon rotation. The vertical red lines indicate when cannon balls were fired at their targets, and vertical blue lines indicate when the target was hit, and stimulation delivered.

As seen in Figure 4.4, the cannon fires once every 10 to 15 seconds, marked by a vertical red line in the top graph showing beta power. The extended delay visible between the third and fourth cannon fire is the result of a delay between one batch of trials and another, a circumstance unique to the continuous stability test. If the cannon fires while it is at the appropriate angle to hit the target, the Unity experiment marks that trial as a successful collision, depicted in Figure 4.4 as a blue vertical line in the lower graph showing cannon angle.

The delay from collision detection to stimulation onset was shown to be small with little variation, on average 6.8ms ± 1.7ms standard deviation across 217 collision-stimulation trials (Figure 4.5). Over 96.7% of delays were under 10ms with the maximum delay being 16.8ms – well below the detectable visuohaptic delay of 45ms.[157]

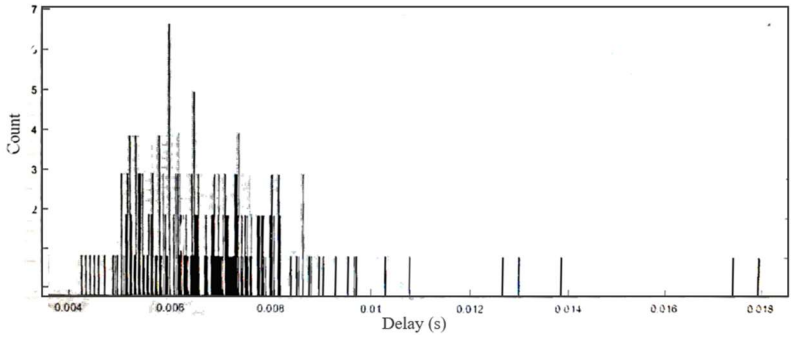

Figure 4.5 Distribution of delay in seconds from collision detection to stimulation onset. This captures the lag in communication from the VR environment to the TDT, and any circuit lag within the TDT hardware over 217 trials.

4.3.3 *Discussion*

By designing this integrated VR and human neurophysiology platform, we have provided experimentalists with a highly capable and flexible resource for developing virtual reality tasks, including bidirectional VR-BCI experiments. Our API permits rapid communication of task-relevant dynamics, such as ongoing band power measures or collisions within the virtual task, that are below visuohaptic and audiovisual perceptual delays.[157,158] While a researcher could instead use the newly released Python APIs from both Unity and TDT, the stability and temporal characteristics of this approach remain untested.

Our interface with the Unity game engine also enables support for augmented reality, mixed reality, mobile and PC-deployed applications. Additionally, Unity provides high-definition rendering, three-dimensional sound, and the integration of human physiologic data, like gaze-tracking, during task performance. Moreover, as an actively supported development platform, Unity is constantly integrating the latest hardware and improved software performance solutions. Our API links standard neural recording and neural stimulation hardware to this powerful engine for game-like and VR behavioral task design – a new frontier for neuroscience experimentation.[15,159]

This API is stored on GitHub, soon to be publicly available. The current API supports UDP-based synchronization as well as synchronization with analog signals such as USB bit output, audio cueing, and photodiode voltage recording. If requested, the Cannon Task could be "baked" and built for distribution as a SynapseAPI experiment with a .synexp file that would demonstrate implementation of the API alongside an approachable BCI-inspired task.

4.4 Experimental Validation

4.4.1 *Noise Analysis & Feasibility*

In this section, I present noise and feasibility analysis from the first implementation of a VR platform with implanted ECoG and sEEG electrodes in human, in-patient subjects. The goal of this part of my research was to demonstrate the feasibility and neural signals preservation of immersive VR to support ongoing VR research in this awake intracranial patient population. To this end, a noise analysis was performed on neural data collected in two subjects, one child and one adult, including both ECOG and sEEG electrodes. Both subjects were VR-naïve prior to completing this study.

In these two subjects, neural signals during unstructured activity in virtual reality immersion (with headset on) were compared to signals recorded during unstructured activity with the headset off. Noise analysis revealed an increase in line noise (60Hz and harmonics) that is almost completely mitigated by common average rereferencing, and no significant increase in the high-frequency noise floor that could subsume the high-frequency neural power bumps. This study was completed in response to a similar VR-in-EEG analyses in which wearing a VR headset that demonstrated significant signal perturbation.[10,160]

In contrast, results from this analysis demonstrate an increase in line noise power (57-63Hz) while wearing the VR headset that is mitigated effectively by common average referencing (CAR), and no significant change in the noise floor bandpower (125-240Hz). To our knowledge, this study represents first demonstrations of VR immersion during invasive neural recording with in-patient human subjects and supports the further use of VR hardware with concurrent intracranial electrode recording.

4.4.2 *System Specification*

For this analysis, only neural signals from the Natus clinical recording system were used with audio synchronization from the VR task and in-room video for headset on and headset off behavioral labeling (Figure 4.6). VR immersion and an object interaction task were presented using the Alienware m15 gaming laptop and HTC Vive Pro Eye.

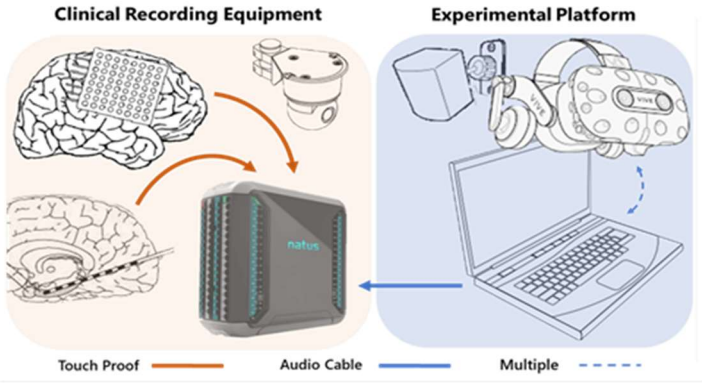

Figure 4.6 System diagram. (left) Clinical recording hardware includes implanted electrodes, Natus Quantum clinical neural recording suite, and in-room cameras recording continuous video and audio data. (right) The experimental VR platform includes a VR-ready gaming laptop, HTC Vive Pro Eye headset, Vive controllers 2.0, and SteamVR base stations 2.0.

4.4.3 *Methods*

4.4.3.1 Data Collection & Demographics

Data from two subjects implanted with intracranial electrodes for seizure localization were collected. Subject 1 was a 16 -year-old male with a prior left temporal lobectomy, implanted with 24 left temporal ECOG and 90 left hemisphere sEEG electrodes (114 in total). Subject 1 remained in VR for over 26 minutes in one continuous session. Subject 1 is, as far as the we are aware, the first in-patient subject to don an immersive virtual reality headset while undergoing invasive neural recording. Subject 2 was a 20-year-old female implanted with 142 left hemisphere sEEG electrodes. Subject 2 spent 68 minutes in VR over two sessions (12 minutes on the first day and 56 minutes on the second). As we limited analyses to controlled task periods, only data from the first session of Subject 2 were analyzed.

Concurrent in-room clinical video was used to define epochs of time during which the headset was on, off, being donned, or being removed. In Subject 1, 22 continuous minutes of neural recording during which the headset was on were identified (HMD On), as well as 22 minutes with the headset off (HMD Off). On day 1 in Subject 2, epochs of 4.75 minutes and 7.23 minutes HMD On were separated by 23 minutes of neural recording HMD Off. From the intervening 23 minutes, duration-matched headset-off epochs were identified for use in subsequent analysis. In Subject 2, the neural signals recorded during headset placement enabled visualization of the headset donning and removal process on clinical recording. These data were not available in Subject 1.

4.4.3.2 Signal Preprocessing

Neural data were minimally preprocessed to preserve recorded noise. In Subject 1, four of 114 total channels were removed from subsequent analysis due to excessive volatility. This is a standard preprocessing step as such electrodes are unlikely to be recording neural signals (e.g., may not be fully implanted in neural tissue or may have a broken connection wire[161]). Two were

removed due to repeated amplitude variations in excess of 4 standard deviations in both HMD On and Off conditions, and one was removed for line noise (57-62Hz) band power in excess of 4 standard deviations compared to other channels in HMD On and HMD Off. The fourth channel was removed due to broadband noise floor bandpower (125-240Hz) in excess of 6 standard deviations compared to other channels, but in HMD On only. Visual inspection of this channel's signal showed it to be quite noisy in both HMD On and Off conditions, though noise power increased markedly in HMD On. Noise levels decreased after headset removal, confirming the recording channel was not damaged during headset placement. This uniquely affected channel was a cortical ECoG electrode localized to the left frontal pole and was removed from the noise analysis as an outlier. In Subject 2, data from all electrodes were kept for analysis, as all sEEG channels demonstrated both similar amplitude variances and noise floor bandpower variances in HMD On and HMD Off.

Unprocessed or "raw" neural signals are local field potential (LFP) recordings natively referenced to a scalp needle electrode and grounded to a skull screw. For common average referencing (CAR), channels within each patient were referenced to the mean signal of all electrodes of a similar type. In Subject 1, all subcortical sEEG channels underwent CAR independently of ECOG channels, which were rereferenced to their own average. This independence was necessary as ECOG and sEEG electrodes have different impedance profiles. In our data, cortical ECOG channels had an average of 2.41 times the line noise power of sEEG channels in HMD On and 1.54 times in HMD Off. These ECOG vs. sEEG ratios did not change much with independent rereferencing (2.99 and 1.61, respectively) but shifted noticeably after non-independent rereferencing (0.01 and 0.02). This suggests that improper CAR may redistribute the noise in ECOG signals onto sEEG signals.

4.4.3.3 Noise Analysis: Noise Ratio

To help interpret the effect of noise in HMD On and Off, with and without CAR, bandpower ratios were calculated between the different recording conditions (On vs. Off) and preprocessing steps (raw vs. CAR) for each electrode. As shown in Equation (2), the noise ratio metric was calculated as the average of the power in the HMD On vs. Off conditions for each frequency:

$$Noise\ Ratio = \frac{1}{n}\sum_{i=1}^{n}\left(\frac{P_{on,i}}{P_{off,i}}\right),\ Power \sim \frac{V^2}{Hz} \quad (2)$$

4.4.3.4 Noise Analysis: Welch's Method Power Spectral Density

To evaluate the spectral differences of neural signals, Welch method power spectral density (PSD) estimates were calculated in 1Hz frequency steps from 2 to 240Hz (1 second Hamming windows, 50% overlap, see Figure 4.7). The line noise peak spanned 57-63 Hz on the PSDs, setting the frequency range for line noise analysis. In addition, a qualitative change in high frequency power was visible in HMD On vs. Off in the raw signal PSD of each patient, so a separate "noise floor" analysis was completed to quantify the power changes in this broad high frequency band (125 - 240Hz). In both line noise (57-63Hz) and noise floor (125-240Hz) bands, total band power was calculated using an area-under-the-curve estimate by rectangular method.

4.4.3.5 Noise Analysis: Jensen-Shannon Divergence Metric

To evaluate the significance of band power changes between HMD On and HMD Off conditions, the distributions of band powers across all electrodes were compared. The noise distributions were determined to be non-normal by chi-squared goodness of fit and Anderson-Darling tests. In response, a Jensen-Shannon Divergence (JSD) metric was used to evaluate the difference in line noise and noise floor spectral power PDFs in HMD On and HMD Off, for both raw and CAR preprocessed data. The JSD metric quantifies the distance between two probability distribution

functions (PDFs), does not assume normality, and is sensitive to both translations between PDFs (e.g., a shift in noise power at all electrodes) and differences in shape (e.g., noise power changes at only a subset of electrodes).

In each frequency band, the probability distribution of bandpower values across all electrodes was fit using a kernel method (Figure 4.7). While multiple standard PDF fit functions were evaluated, the nonparametric kernel method yielded the best goodness of fit for all conditions, as assessed by a chi-squared goodness of fit (g) test calculated between the actual data's pdf and a given parametric estimate of the distribution. For Subject 1 in HMD On, for example, only the nonparametric kernel estimate yielded a statistically significant goodness of fit (p=0.9553, g = 0.6672), though other parametric fits demonstrated moderately good fit, including exponential (p = 0.0017), Pareto (p=0.0033), Log-Normal (p=0.022), Birnbaum-Saunders (p=0.0310), and Inverse Gaussian (p=0.06) parametric distributions. Following kernel method fit, the JSD distance metric was calculated between HMD On and Off, in both raw and CAR preprocessed data.

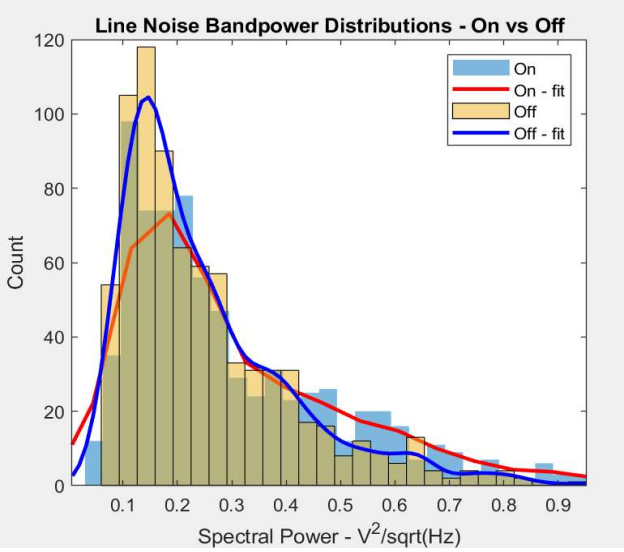

Figure 4.7 Line Noise Bandpower Distributions. Distribution of line noise (57-62Hz) bandpower values for Subject 1 during 22min of neural recording with the VR headset on (blue bars) and matched duration of neural recording with the headset off (yellow bars). Distributions were estimated using kernel method for the on (red line) and off (blue line) conditions and the distance between the distributions calculated as the symmetric Jensen-Shannon Divergence (JSD).

To determine the statistical significance of the resultant JSD values, null distributions of JSD metrics were calculated using two distinct randomization schemes. In one, HMD On and Off labels were randomly shuffled one thousand times to create 1000 unique sets of

"null" HMD On and Off distributions of spectral power values. The JSD metrics of these shuffled distributions were then calculated to create the null distribution of JSD values. This null distribution was designed to capture the range of JSD values under the null assumption that the headset condition (HMD On or Off) did not affect noise power overall, across electrodes. In the second randomization approach, 100 random power values from each of the HMD On and Off bandpower estimates were compared, bootstrapping a JSD metric to give context to the overall JSD. Though the subsamples were compared asynchronously, this randomization scheme was devised to express the range of potential JSD values within each condition's recorded data, analogous to a "confidence interval" for a given JSD comparison.

4.4.3.6 Exploratory Analysis: Noise Regression

Scatter plots of line noise bandpower and noise ratio vs. electrode number as an ordinal label were also drafted to visualize potential trends in the bandpower. In intracranial implants, channel 1 is the furthest from the wire bundle leaving the skull, making electrode number a rough proxy for depth from cortex, with the higher numerical labels corresponding to electrodes nearer the cortex and lower numerical labels corresponding to electrodes at greater depths. In Subject 1, all cortical ECoG electrodes were recoded to have a label of 17, which is one greater than the largest sEEG label of 16. Visible trends of the ratio of noise band power by contact number were then explored using a linear regression. The noise ratio metric was used to evaluate noise from the headset proportional to baseline (HMD Off) noise. To measure the effect size of a calculated regression coefficient, the Δr^2 value between it and a null regression coefficient was calculated. This null regression coefficient ($\hat{r}_{null}$) was defined as the average r_{null} of 1000 regressions with shuffled label permutations.

4.4.3.7 Exploratory Analysis: Headset Positioning Noise

In a final exploration, continuous neural recordings during headset positioning (donning and doffing) were identified in Subject 2 and time-frequency spectrograms built by the modified Welch method (80% overlap, reassigned center frequencies, 1 second time resolution, 2-140Hz). The spectrograms were used to visualize spectral effects during headset positioning.

4.4.4 *Results*

4.4.4.1 Noise Analysis

CAR demonstrates robust line noise removal (60Hz and calculated harmonics) in HMD On and Off in both subjects. Figure 4.8 visualizes the power spectra of HMD On and Off, raw and CAR signals, in an example cortical electrode (channel 105) from Subject 1. This figure also highlights the noise floor reduction in HMD On versus Off for both raw and CAR signals in Subject 1.

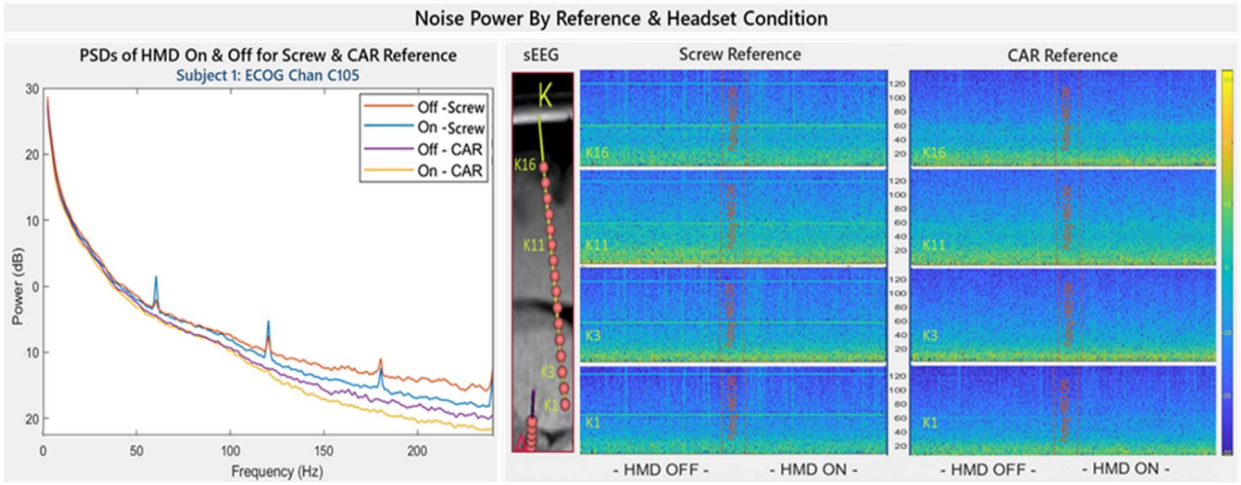

Figure 4.8 Power spectral density plots. (left) Welch power spectral density plots of screw referenced (raw) and CAR signals in the HMD On and HMD Off conditions for an ECOG electrode (C105) in Subject 1. Note the successful removal of in-phase line noise with simple common-average rereferencing. (right) Reconstruction of an in situ sEEG electrode and stacked spectrograms for four electrodes along the probe, representing decreasing electrode label and increasing implant depth. Specifically, spectrograms of contacts 16, 11, 3, & 1, from top to bottom, are depicted. The left column depicts the screw referenced data and the right column, CAR data. Each spectrogram visualizes continuous neural signals recorded during headset donning: from HMD Off, through headset positioning (delineated by vertical red lines), to HMD On. Spectrograms demonstrate noise reduction by CAR and no significant signal perturbation during headset positioning.

	Subject 1		Subject 2 Set 1 Set 2	
	57–62 Hz	***125–240 Hz***	***57–62 Hz***	***125–240 Hz***
Noise Off (CAR) [a]	0.25 (0.15)	0.03 (0.01)	1.85 (0.27) 1.50 (0.26)	0.02 (0.01) 0.03 (0.01)
Ratio On/Off (CAR) [a]	1.27 (1.02)	0.58 (0.87)	1.01 (0.95) 0.99 (1.13)	0.56 (1.71) 1.06 (1.32)
JSD sEEG ECOG	4.48 (0.43) 2.93 (0.35) 1.55 (0.08)	14.44 (0.87) 11.65 (0.50) 2.79 (0.36)	 28.62 (0.92) 2.55 (2.87)	 156.20 (8.96) 4.66 (3.63)
Shuffled Range [b]	19.22 - 23.99	21.373 - 22.501	409.55 - 512.52 372.10 - 456.94	119.19 - 125.01 54.51 - 57.25
Bootstrap Range [b]	1.50 - 4.39	13.694 - 14.671	29.146 - 71.386 25.686 - 60.484	0.830 - 1.468 0.126 - 0.684
Regressions [c] ON (CAR) OFF (CAR) RATIO (CAR)	**0.08** (***0.04***) ***0.06*** (0.04) 0.002 (0.002)	**0.08** (**0.06**) **0.80** (**0.06**) **0.01** (0.002)	-0.07 (-0.21) -0.01 (-0.04) ***0.002*** (0.005) 0.009 (0.05) 0.09 (-0.04) **0.01** (**0.04**)	-0.05 (0.03) -0.03 (0.01) 0.01 (0.002) 0.02 (0.07) -0.04 (0.02) 0.01 (0.01)

Table 4.1 Results by metric and subject & frequency band. Band power (dB) and noise ratio averaged across electrodes[a] are listed in the first two rows (Noise Off (CAR) and Ratio On/Off (CAR)). In row 3, smaller JSD results indicate greater similarity between two distributions. In rows 4 and 5, the Shuffled Range[b] results approximate a null distribution and the Bootstrap Range[b] results are interpretable as an estimate of a confidence interval. In the last row, the Regressions[c] results for each condition and the calculated power ratio are presented as Correlation (r) values. The statistical significance of the value is encoded by style font, with bold-underlined indicating **p<0.001**, bold-italicized indicating ***p<0.01***, & plain font indicating trend-level correlation, but not significant (p>0.01).

Table 4.1 lists the mean power estimates of line noise (57- 62 Hz) and high-frequency broadband noise (125-240Hz) in HMD On and Off, both before and after CAR, for both subjects. Also listed are the noise ratios comparing HMD On and Off by frequency band and reference type. These results demonstrate that CAR can efficiently remove the noise introduced by the headset: for Subject 1, the line noise ratio (on/off) was 1.266 in the raw data, indicating more line noise in HMD On. This ratio reduced to 1.017 following CAR. The noise floor ratio of 0.583 in Subject 1, raw signal, indicates a reduction in noise floor bandpower in HMD On. This ratio increased to 0.871 after CAR.

For Subject 2, results are presented for each of the epochs of matched HMD On and Off data. Again, CAR is shown to greatly reduce the noise magnitude in line and noise floor frequency bands.

Table 4.1 also lists the results of the JSD analysis. Smaller JSD values indicate similarity between two distributions. The results here show much smaller JSD values between the On and Off conditions for the CAR than raw data, with JSD values much less than the range of values generated by the comparison of 1000 distributions using shuffled labels. This means that the actual On-Off distributions are more similar than 1000 random distributions generated from the data and suggests a low impact of the headset on either line noise or noise floor bandpower.

For example, in Subject 1, the JSD metric for line noise bandpower in HMD On and Off was found to be 4.482 for screw-referenced and 0.432 for CAR signal (Row 4 'JSD' in Table 4.1 Column 1). In 1000 randomized shuffles of on-off labels, the range of the resultant JSDs was 19.22 – 23.99 (Subject 1, line noise, raw), and in 1000 bootstrapped comparisons, the range was 1.5040 - 4.3845. For the shuffled randomization result, the real JSD was much less than the null distribution range (4.4820 < [19.22 23.99]), suggesting that the real On and Off distributions were much closer than the distances between 1000 random distributions generated from the on-off bandpower data. The bootstrapped randomization statistic (4.4820 > [1.5040 4.3845]) indicates that the calculated JSD is consistent across our data, supporting the use of the JSD metric to characterize the magnitude of difference in noise bandpower between HMD On and Off conditions.

4.4.4.2 Exploratory Analysis

Regressions were completed for HMD On and Off, raw and CAR, in line noise and noise floor bandpower values against electrode label. This was done to explore the relationship between VR headset noise and electrode depth. The last row of Table 4.1 lists abridged results for this regression analysis and visualizes the results of line noise bandpower regressions for Subject 1.

For Subject 1, line noise bandpower significantly correlated with depth in both HMD On and Off, for both sEEG and ECOG electrodes. The strength of the correlation is larger in HMD On (Table

4.1, last row & Figure 4.9, red and blue lines), indicating an increased noise gradient due to the HMD. Preprocessing with CAR reduces but does not eliminate the correlations in HMD On and Off, so while CAR may reduce both line noise magnitude and line noise gradient, it does not completely redistribute the increased line noise in the more surface sEEG electrodes and ECOG. While the regressions may be statistically significant, their Δr^2 are very small ($\Delta r^2_{on\text{-}null}$ =0.0055, $\Delta r^2_{off\text{-}null}$ =0.0027, Δr^2_{CAR} =0.0016). The noise ratio regressions for line noise bandpower conclude no significant correlation between HMD On and Off conditions for neither CAR nor raw signal. High-frequency noise floor bandpower was shown to correlate significantly with electrode depth in HMD On and Off, both before and after CAR (Table 4.1). Again, the Δr^2 are quite small ($\Delta r^2_{on\text{-}null}$ =0.0055, $\Delta r^2_{off\text{-}null}$ =0.0027, Δr^2_{CAR} =0.0016). The correlation is much stronger in the off

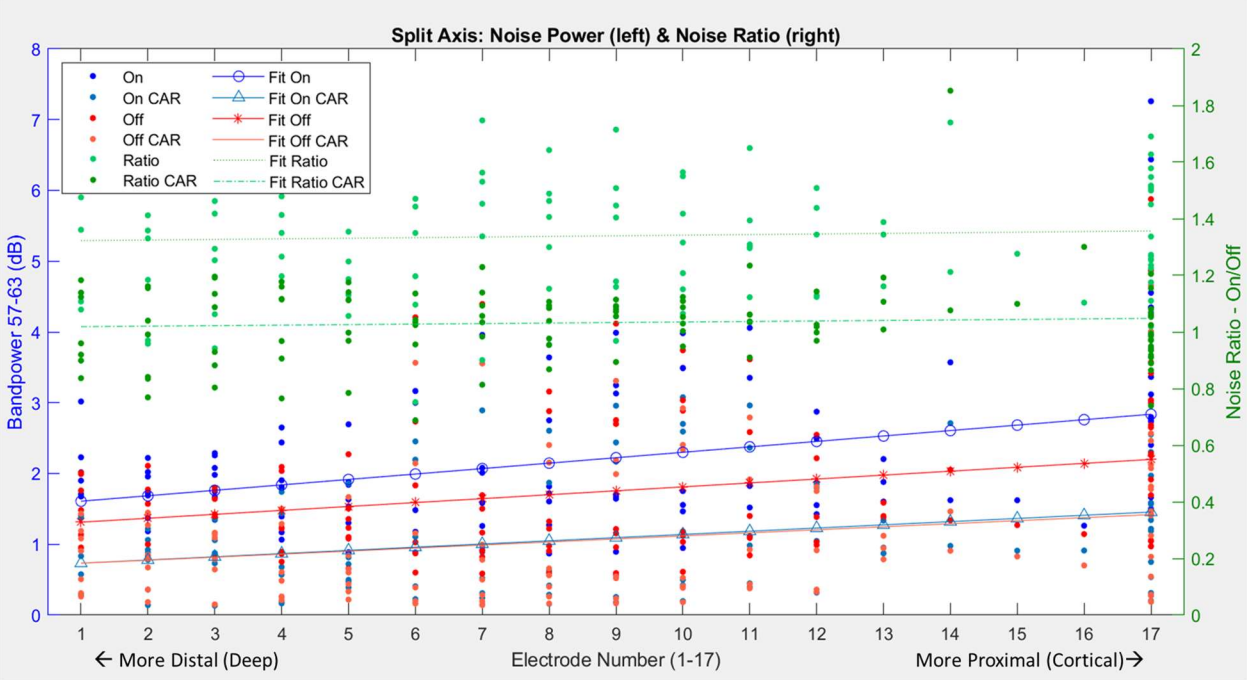

Figure 4.9 Line noise bandpower and regression results. The left y-axis encodes line noise band power (57-63Hz) for HMD On (blue & muted blue) and HMD Off (red & muted red). The right y-axis encodes noise ratio (green & muted green). The shared x-axis encodes electrode labels from 1-17, with 1 deepest to 16 shallowest/most cortical sEEG, and ECOG recoded as 17. The scatterplots show data distribution per condition. For Subject 1, a significant noise correlation with electrode label for HMD On (blue) and Off (red) is seen, with a steeper regression slope in HMD On. CAR reduces HMD On and Off (muted red & muted blue) noise power and flattens the HMD On gradient. (left axis) Raw noise ratio data show a nearly flat regression and are reduced towards 1 by CAR.

condition, which agrees with the earlier result that the headset reduced the overall noise floor in Subject 1. This result suggests it does so by reducing high-frequency noise in the most cortical electrodes, seen as a reduced gradient (regression slope) in HMD On vs. HMD Off. The significant correlation of noise floor ratio and electrode label seen in the raw data does not survive CAR, suggesting that CAR redistributes high-frequency broad band noise. In Subject 2 (sEEG only), bandpower did not significantly correlate with depth in any condition or frequency band. While the ratio of headset bandpower correlated with electrode label in both raw and CAR data for set 2, the effect sizes were very small ($\Delta r^2_{ratio\text{-}null}$ =0.00004, $\Delta r^2_{ratioCAR\text{-}null}$ =0.00080). Ratio correlations were not significant in the noise floor frequency band. Stacked spectrograms (Figure 4.10) were used to visualize continuous resting state spectral data during HMD Off, headset positioning, and

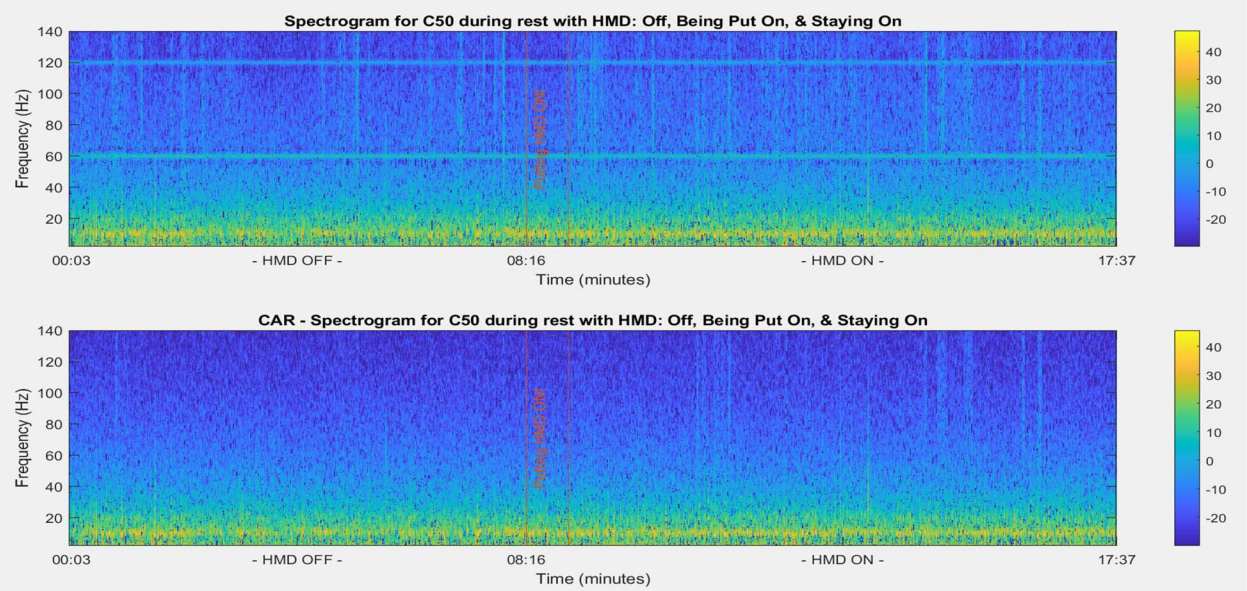

Figure 4.10 Stacked spectrograms depicts the spectral power content in 1Hz frequency bands from 1-140Hz, with 1 second temporal resolution across a recording over 3 minutes in length in which the VR headset is put on. The left portion of these spectrograms depict a headset off condition, the segment between the red lines during headset donning, and the right portion of the spectrograms depict a headset on condition. The top plot is of raw signal and the bottom plot is of the same signal following CAR. Data presented were from an electrode localized to Brodmann Area 6 (BA 6) in Subject 1. Note again the successful removal of in-phase line noise with simple common-average rereferencing. Each spectrogram visualizes continuous neural signals recorded during headset donning: from HMD Off, through headset positioning (delineated by vertical red lines), to HMD On. Spectrograms demonstrate noise reduction by CAR and no significant signal perturbation during headset positioning.

HMD On. Figure 4.10 presents results from a different electrode from Figure 4.8 Power spectral density plots. (left) Welch power spectral density plots of screw referenced (raw) and CAR signals in the HMD On and HMD Off conditions for an ECOG electrode (C105) in Subject 1. Note the successful removal of in-phase line noise with simple common-average rereferencing. (right) Reconstruction of an in situ sEEG electrode and stacked spectrograms for four electrodes along the probe, representing decreasing electrode label and increasing implant depth. Specifically, spectrograms of contacts 16, 11, 3, & 1, from top to bottom, are depicted. The left column depicts the screw referenced data and the right column, CAR data. Each spectrogram visualizes continuous neural signals recorded during headset donning: from HMD Off, through headset positioning (delineated by vertical red lines), to HMD On. Spectrograms demonstrate noise reduction by CAR and no significant signal perturbation during headset positioning. and at greater scale for visual inspection of the HMD Off, positioning, and HMD On epochs. In both figures, stacked spectrogram represents the same epoch of time, during which Subject 1 was at rest and not wearing the VR headset, then donning the headset with assistance, and then sitting in a virtual "waiting room" depiction of a dark sky at dusk. The spectrograms demonstrate the effectiveness of CAR in reducing line noise in both On and Off conditions. They also confirm that headset donning procedure does NOT evoke significant changes or artifacts in the spectral time series. Signal stability was present during all epochs of headset manipulation.

4.4.5 *Protocol Development*

4.4.5.1 Patient Protocols

In the hospital setting, base stations were mounted on extensible tripods and positioned a few feet from the hospital bed to ensure coverage of all potential dynamic movements during VR tasks. Prior to VR immersion, patients developed familiarity with the trigger, grip, and trackpad inputs

of the controllers. Our protocol for donning the headset is as follows: First, outline the full procedure to the subject -- a little nervousness is common before first immersion. Next, extend the VR headset to its maximum fit settings and note the fit mechanisms (e.g., straps or ratchets) to the subject as this is done. Then, invite the patient to hold the headset against their face in the most comfortable position for them while a researcher positions the headset strap over the "braid" of electrode cables gathered at the back of the patient's head and onto the occipital area of the skull. Finally, guide the subject's hand to the pre-introduced fit mechanisms so they may tighten their own headset for themselves. Even highly attentive researchers will not get the fit as perfect as a subject will for themselves. Secure headsets are much more comfortable over time than loose or ill-fit ones, and patient involvement in headset donning also seems to reduce pre-immersion nervousness. To remove the headset, have the patient hold the headset firmly against their face while the fit settings are loosened, and then removes the head strap mindfully. In our experience, once the subject understands the fit of the headset, they may be able to don and remove it themselves with minimal assistance from the researchers.

The two subjects in this study reported ease and comfort with donning, doffing, and wearing the headset for extended periods of time − collectively, for over an hour. In fact, both subjects opted to remain in VR when given the choice to either explore additional VR experiences (e.g., Google Earth) or remove the headset. Subject 1 spent time exploring a SteamVR mountaintop lodge scene, and Subject 2 toured Paris, Tokyo, and Volcanos National Park, HI by Google Earth VR. It may also be worth noting that while neither subject had prior experience with immersive VR (both were "VR naïve"), they each adapted to the VR tasks readily and reported neither discomfort nor symptoms of virtual reality sickness (VRS) during their experimental sessions. We highlight this

to allay concerns of VRS in well-constructed VR tasks and to suggest that prior VR experience is not a prerequisite for VR task engagement.

Prior to VR immersion, subjects developed familiarity with the trigger, grip, and trackpad inputs of the controllers, we discussed the donning and doffing procedures for situating the headset on their headwrap and over the braid of cables usually gathered at the back of the head. Subjects are familiarized with the multiple fit mechanisms (dials, ratchets and straps) used to make the HMD as comfortable as possible to wear.

4.4.5.2 Initial Immersion & Task Design

First, while careful design is required to ensure an enjoyable experience, the notion that VR-Naïve patient will not be able to complete a VR task is incorrect. Nearly 75% of subjects I have worked with have been VR naïve and enjoyed my simple experiments. In fact, VR-Naïve subjects are much more engaged with immersive but repetitive tasks, more that the few VR experienced subjects I have seen.

It is important to have the same VR Familiarization protocol for all patients. Begin with reviewing the controller inputs while the headset is off. Adjustment to the virtual environment seems to occur quickly, so long as the initial immersion environment is soothing and simple. We have preferred to utilize a SteamVR loading scene that features a distant, mountainous horizon backlit with a twilight or dusk-lit sky and moving aurora borealis. It's very pretty, very soothing, and very simple in terms of potential object interaction. All tasks should minimize the potential for virtual reality sickness (VRS) using established best practices for VR gaming[159,162] and the VRS Questionnaire adopted to evaluate patient comfort during VR tasks (Appendix A). Controller and headset position, velocity, and angular velocity are recorded during the task, as is a video of the right eye

VR display. To reduce VRS potential, tasks were designed to have simple, neutral backdrops with infinite horizons, few moving objects, and minimal requirement for head movement.

4.4.5.3 First Task: Object Interaction

The Object Interaction Task adapted prefabs from the open-license Interaction Demo Scene within the SteamVR OpenXR plugin. Stations of distinct virtual object interaction profiles were created, and teleportation enabled for non-locomotive transportation between the virtual task stations. A preliminary exploratory analysis revealed a post-teleportation increase in alpha band power in cortical electrodes localized to the medial temporal lobe. This may indicate a flurry of "self-localization" by sensory integration after the very unnatural maneuver of spatial teleportation.

At Station 1, subjects are asked to reach, grasp, move, and then release two virtual objects, ten times each with the left and right hands (Figure 4.11, first two VR overlay images). A floating countdown timer lists the number of remaining interactions per object. Subjects are asked to use their left to engage with the left object and right hand for right object. Movements are self-initiated and voluntary in path and duration. I called this a directed or stereotyped reach task as the grasped virtual object, once released, returns to its starting position. In this way, the reach motion is a stereotyped motion towards a fixed location in world space.

At Station Two (third VR overlay image, Figure 4.11), undirected and dynamic object interactions were encoded. Here, hand and object animations during object interaction enable deformation proportional to force applied to the grip button of the controller: objects at this station may squish with grip strength, for example. Additionally, altered physics are encoded, such that objects may float or fall with gravity, bounce with elastic recoil, or explode into flowers when dropped. These are termed dynamic object interactions.

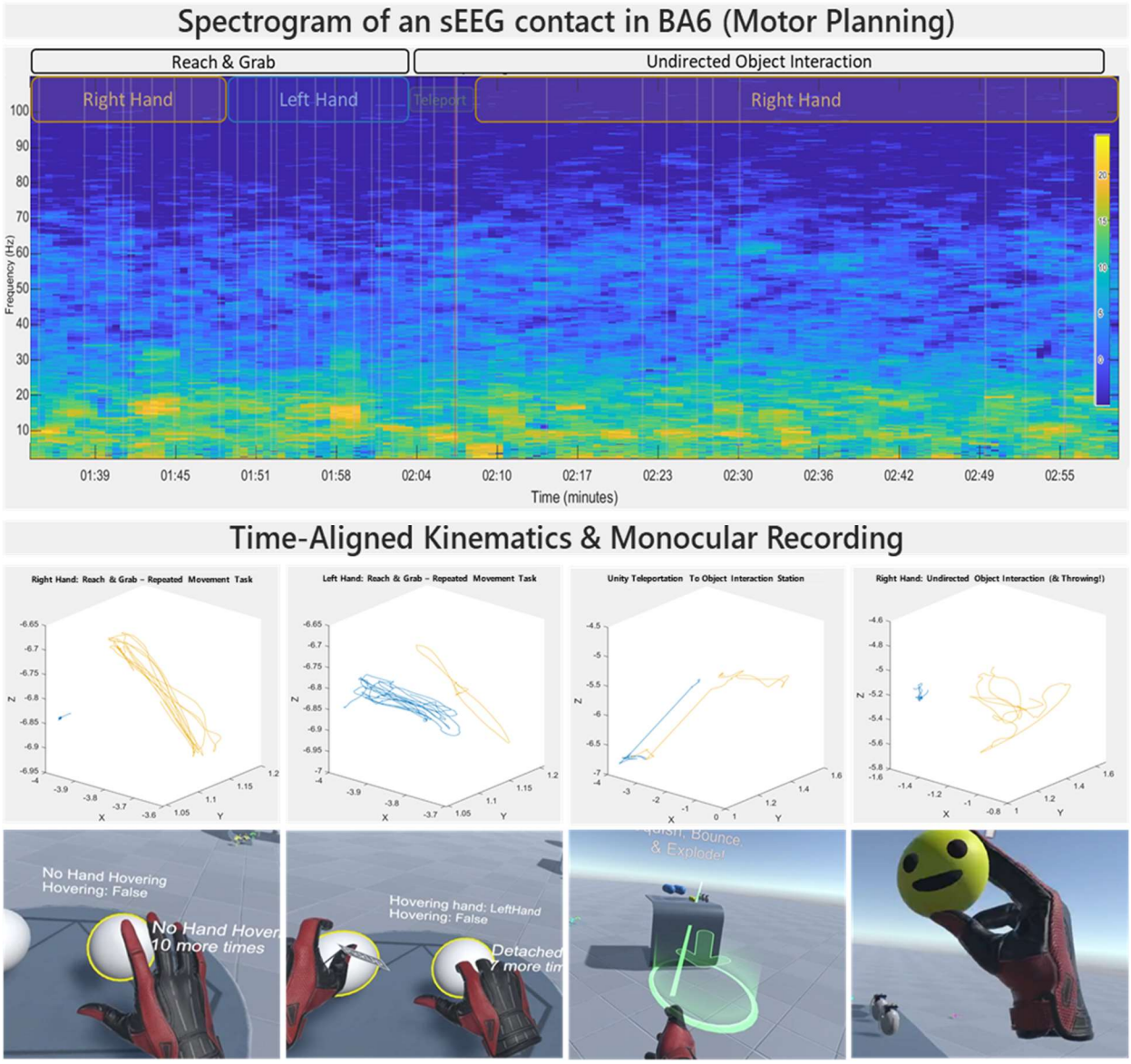

Figure 4.11 Object Interaction Task. (top) The spectrogram of a left Brodmann Area 6 (BA6) cortical electrode in Subject 1 (1Hz frequency bins from 1-110Hz). Color magnitudes depict power (dB), from -5 to 35dB, blue to yellow. The vertical lines superimposed over the spectrogram represent grab and release synchronization cues, extracted from the audio cue signal. The labels "Right Hand" and "Left Hand" (in orange and blue, respectively) superimposed at the top of the spectrogram indicate the dominant hand during movement. (middle) Four kinematic traces depict the position of the right and left controllers (orange and blue, respectively) relative to the subject's headset. The tracings are time aligned using collision-based audio synchronization to the spectrogram. The first two positional tracings represent movement during a stereotyped reach and grasp task in which a virtual ball is grasped, moved, and released, resetting the ball to its starting position. This is repeated ten times for each hand, as shown by (bottom) the left-most in-game image in which the countdown message "10 more times" hovers over the virtual ball. The third kinematic positional trace and third in-game image demonstrate teleportation, marked by a small green label between the Left Hand and second Right Hand labels. Teleportation is a common travel mechanic in immersive virtual reality. The final kinematic plot depicts a naturalistic object interaction in which objects were designed to bounce, explode, squish, or float as if unaffected by gravity --multiple throwing events occurred, as evident in the chaotic kinematic trace.

At Station Three (not depicted), graspable cubes are presented on a table and a large target is rendered at a perceptual distance of 5-meters. While no directions are given, subjects quickly surmise the nature of the task and begin throwing cubes towards the target. The presented cubes are unlabeled and have different kinematic approximations that alter their release velocity when thrown, presenting an unreliable (or probabilistic) throwing experience. This task may be considered both a naturalistic reach task and a ballistic movement task.

An optional Station Four (not depicted) presents a virtual bow and arrow, a static balloon-generating target, and a moving balloon target. While there is no declared game dynamic (no point system), the variable difficulty of this task is unexpectedly engaging for the patient and demonstrated the unique opportunity for casual gamification in VR.

4.4.6 *Discussion*

Virtual reality behavioral task design represents a new and emerging platform for human neuroscientific research. In this chapter, I discussed a first implementation of a VR experimental platform with in-patient subjects undergoing invasive neural monitoring for seizure localization. I also quantified the impact of the VR system on electrophysiological signal quality in intracranial recordings. In the noise analysis, I explored the impact of electrical noise from the VR headset, demonstrating efficient removal of headset-induced line noise (57-63Hz) using simple CAR preprocessing. In Subject 1, an exploratory regression analysis revealed a significant relationship between line noise band power and electrode label, a proxy of electrode depth, in HMD On and Off. This indicates an increased susceptibility to line noise in more cortical electrodes. The regression remained significant following CAR, although the magnitude of the line noise and the Δr^2 (effect size) of the regression were reduced. Collectively, these results suggest that while the headset increases line noise in neural recordings, this increase is readily addressed by a simple

CAR preprocessing step. The headset was also seen to either decrease or minimally impact the broadband high frequency noise floor (125-240Hz), preserving this important and often low signal-to-noise spectral region.

In this chapter, I also discussed patient protocols, task design, and approaches to VR immersion in this in-clinic, invasive neuromonitoring patient population. I outlined VR hardware selection, familiarization, and basic room setup. I addressed concerns about VR skill acquisition in VR-naïve populations and noted the ready immersion, task engagement, and genuine enthusiasm from two early subjects, who not only tolerated their VR experiences but were eager to remain in VR. In all nine subjects I have worked with, not one has, at any point, expressed discomfort with VR immersion or demonstrated signs of VRS.

Chapter 5. Designer Touch: Neurohaptic Engineering

5.1 INTRODUCTION

Currently, sensory DES feedback studies rely on single-axis stimuli, interpretable as intensity, to deliver one-dimensional feedback.[4,79,117–119] Prior work has demonstrated the use of three level of S1-DES amplitude (none, low, and high amplitude) to successfully guide a motor grip task.[79] My research expanded upon this work by exploring novel stimulation protocols that modulated pulse-train shape with the intent of developing stimulation paradigms that can better simulate the natural diversity and complexity of touch.[79,80,122,128,163,164]

Inspired by prior results integrating TMS for game feedback in humans[13] and DES for virtual object exploration in monkeys[4], I sought to advance neurohaptic research by integrating S1-DES with naturalistic motor behavior during object exploration. Leveraging new stimulation flexibility with the TDT IZ2 stimulator, I sought to also evaluate the subjective effect and discriminability of dynamic, or temporally structured, sequences of S1-DES. My hypothesis was that temporally dynamic stimulation would evoke percepts more akin to natural sensation than what had been previously described.

Regardless of the naturalness of evoked percepts, however, amplitude and frequency modulation are parameters of multi-pulse S1-DES not yet evaluated for perceptual discrimination in humans. In this study, I limited my investigation to dynamic amplitude modulation. To accomplish the second goal of integrating S1-DES with naturalistic behavior, we extended the functionality of a VR experimental platform we had recently developed[1] to both record human neural data from intracortical electrodes during VR task immersion, and now also deliver stimulation directly to the brain in response to VR task dynamics (Figure 5.2). This enabled us to design behaviorally

dependent and contextually relevant neurohaptic stimulation paradigms embedded in a set of engaging and gamified VR object discrimination tasks.

5.2 METHODS

5.2.1 *Demographics & Electrode Localization*

Subject 1 was a 15-year-old male implanted with ECoG and sEEG electrodes, and Subject 2 was a 19-year-old male with sEEG electrodes only. Collected data included neural signals, in-room sound and video, kinematic vectors and object interaction flags, as well as subjective descriptions of experimental events acquired by questionnaire and free response.

For Subject 1, ECoG electrodes were identified over the left somatosensory hand (LGT 15:16) and lower arm (LGT 23:24) cortex as potential targets for percept-eliciting stimulation (Figure 5.1 Electrode Localization to Identify Primary Somatosensory Cortex. Localization for each subject was completed and candidate electrodes identified for direct cortical stimulation of the hand area

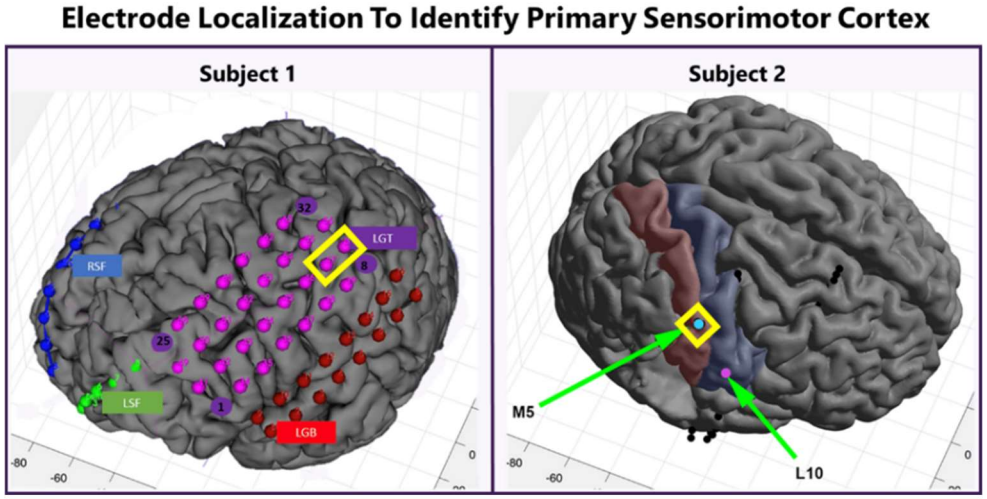

Figure 5.1 Electrode Localization to Identify Primary Somatosensory Cortex. Localization for each subject was completed and candidate electrodes identified for direct cortical stimulation of the hand area of the somatosensory cortex (S1-DCS). (left) The cortical electrodes highlighted in yellow overlay the hand area of the left somatosensory cortex and S1-DCS at these contacts elicited a somatic percept in Subject 1's right thumb and index filter. (right) Surface sEEG electrodes boxed in yellow intercept the hand area of the right sensorimotor cortex and S1-DCS at these sEEG contacts induced an interesting sensorimotor percept of a clenching movement across the left palm despite no indication of actual movement.

of the somatosensory cortex (S1-DCS). (left) The cortical electrodes highlighted in yellow overlay the hand area of the left somatosensory cortex and S1-DCS at these contacts elicited a somatic percept in Subject 1's right thumb and index filter. (right) Surface sEEG electrodes boxed in yellow intercept the hand area of the right sensorimotor cortex and S1-DCS at these sEEG contacts induced an interesting sensorimotor percept of a clenching movement across the left palm despite no indication of actual movement.). For Subject 2, depth sEEG electrodes in the right somatosensory cortex for hand (M4:6), motor cortex for face and tongue (L 8:10), and hand (I 14:15) were identified. Figure 5.2 shows the most superficial electrodes of Subject 2's depth sEEG probes with primary motor and somatosensory cortex coverage.

5.2.2 *Hardware Design & Validation*

Between the HTC VIVE Pro Eye and Natus clinical system, audio cues were used to align the experimental VR data and clinical neural data, and UDP used to synchronize the Unity experimental environment and neural data recorded by the TDT (Figure 5.2). In Synapse, a custom TDT circuit was built to manage recording, stimulation, and rapid switching between these two hardware states.

Perception and stimulation parameters were assessed using single-pulse or short burse stimulation for each subject prior to each day's first neurohaptic task. Threshold values were approximated

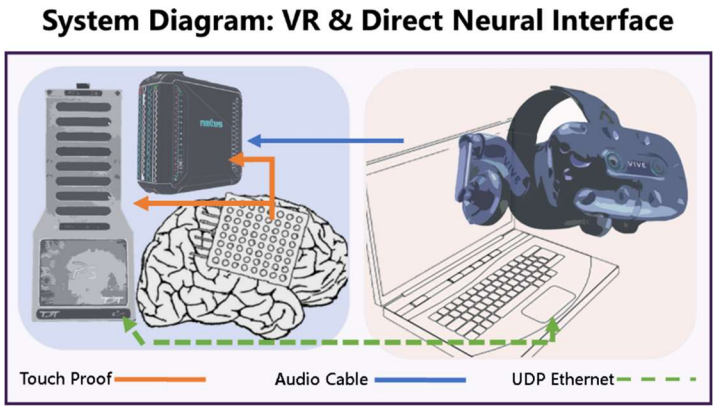

Figure 5.2 System diagram: Haptic. This diagram depicts hardware connectivity and synchronization. An HTC VIVE Pro Eye virtual reality headset was used in concert with a Tucker Davis Technologies (TDT) neural recording and stimulation suite and Natus Quantum clinical recording suite, with data synchronization between these and the VR task-hosting laptop by UDP (dashed green) and audio inputs (solid blue).

using a manual search of candidate electrodes with stimulation values of 1000µA-6500µA and pulse counts of 1, 5 or 20 pulses at 30Hz. The presence, strength, location, and character of any evoked percept was determined by subject report. Once the range of stimulation values was set for a given subject on a given day, stimulation sequences were tested for subjective response and preliminary discriminability. Up to two seconds of each sequence were delivered and initial subjective descriptions were collected. Manual 1-back comparisons between sequences that elicited distinct subjective descriptions were completed until a pair of sequences was found to exhibit some preliminary, untrained differentiability.

A prebuilt sequence was selected and stepped through pulse-by-pulse using Unity-triggered USB outputs, recorded by the TDT as a C0 BNC input. This circuit enabled only one stimulation sequence to be delivered at a time. For multiple sequences to be implemented, as required by the HapticSort_ABØ task, a new stimulation control circuit was designed in Unity that leveraged the UDP interface of the TDT RZ-2 unit.

To enable task-responsive stimulation, the VR task sends stimulation related timing and information to the TDT system using a UDP interface between the TDT RZ unit and the VR laptop ethernet port. The TDT is capable of providing stimulation to the subject through the same electrodes used for sensing, and all stimulation will be delivered in accordance with known safety limitations.[129]

5.2.3 *Complex Stimulation Design*

To enable task-responsive stimulation, the circuit was designed to receive indices as integers (1:15) from the Unity laptop, sent over a UDP interface between the TDT RZ unit and the VR laptop ethernet port (Figure 5.2). The integers were used to trigger stimulation at an amplitude indexed by the integer value from a 15-element, patient-specific array. For example, the amplitude array

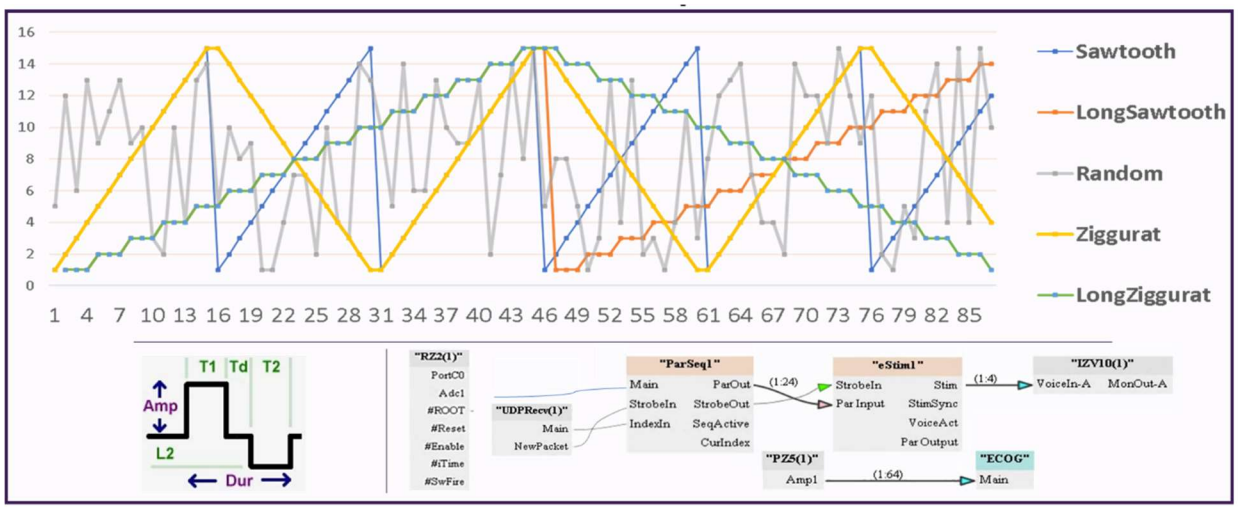

Figure 5.3 Sequences of stimulation indices were used to deliver structured trains of amplitude-modulated, charge-matched biphasic square wave pulses that ranged across an array of amplitudes customized to the percept thresholds of each subject on each new day of neurohaptic experimentation. (top) Depiction of the stimulation sequences by index along the y-axis and stimulation count along the x- axis. (bottom left) An exemplar biphasic waveform. (bottom right) Our custom Synapse circuit receives an integer over UDP from the Unity experiment hosted on another computer and delivers a single biphasic pulse at the current amplitude indexed by the received integer from the customized array of simulation threshold values.

for Subject 1 Day 1 was 3900µA to 6000µA in 150µA steps, with the lower bound set at the approximate short-train (5 pulses at 30Hz) perceptual threshold and the upper bound at the amplitude of a reliably received single-pulse stimulation. Fortunately, in this study, both subjects could reliably detect a single pulse stimulation of sufficient amplitude, with a maximum explored amplitude of 6500µA in Subject 1 and 5000µA in Subject 2.

For the HapticSort task in Subject 1, a Synapse circuit with multiple, preset stimulation sequences of 15 index values (1-15) was created (Figure 5.3, upper). These indices called values in a 15-step amplitude range customized for each subject before each day of haptic experimentation. For example, the 15-step amplitude range for Subject 2 on Day 1 stepped from 2000µA - 3400 µA in 100 µA increments. The low end of this range approximates a 50% detection threshold for short-burse (5 pulse) stimulation and the high end of this range is suprathreshold for single pulse stimulation that elicits a comfortable and non-spreading percept. Evoked percepts can sometimes

be uncomfortable at higher amperages, or the sensation may begin to “spread” somatically. Stimulation amplitudes in this study stayed well below such effects.

Stimulation trains are sequences of single, constant-current, biphasic, charge-matched pulses (single pulse architecture seen in Figure 5.3). Pulse frequency is defined by the delay between individual pulses and burst frequency is defined by the delay between stimulation trains. Pulse amplitude indicates the current magnitude across the electrode surface and is the same in magnitude during both phases of a single, biphasic pulse.

In this study, pulses were triggered by Unity at a rate no faster than 50Hz (pulse frequency), set by a minimum delay counter which required that some number of “physics updates” (20ms each) be processed between stimulation triggers. Stimulation was also triggered only while an object was being actively held. Five amplitude-modulated sequences were constructed (Figure HapticSort) and nicknamed based on shape. These sequences represent a structured variation of the indices (1:16), shown along the y-axis of Figure 5.3, used to select stimulation amplitudes from a patient-specific, linear array of percept-inducing values. The lowest value in the array approximates the percept threshold amplitude of a short burst (5 pulses at 30Hz) of stimulation, and the highest value is a suprathreshold amplitude for a single stimulation pulse.

The sawtooth sequences rise from the lowest stimulation value (index 1) to the highest (index 15) and immediately cycle again from index 1 to 15, 1 to 15, etc. LongSawtooth spends three “time steps” at every index or stimulation value, and Sawtooth only one. The ziggurat sequences rise from index 1 to 15 and then slowly and symmetrically decrease back to 1. LongZiggurat takes 3 “time steps” at every index, and Ziggurat one. The Random sequence was generated by Synapse and was the same sequence in both subjects. It has a much faster oscillatory structure.

The index sequence patterns have an envelope period ratio of ~1:3:6:9:18, corresponding to Random : Sawtooth : Ziggurat : LongSawtooth : LongZiggurat sequences.

5.2.4 *Task Design*

Two tasks around a similar game mechanic were created. The basic game mechanic is a throw-to-target task in which points are earned for successfully hitting the correct target with the correct object. Subjects use controller-based interactions in which objects are grasped by pulling the controller trigger with a dynamic animation that renders the partial pull of the controller trigger to generate congruent visual feedback of the grasping action. Upon grasping of the virtual object, DES is delivered, and when the object is released, DES stops.

5.2.5 *Binary Discrimination: HapticSort*

HapticSort is a binary discrimination task in which virtual objects are classified based on whether they deliver haptic feedback when grasped or does not. Objects are identical. The subject is instructed to depress a virtual button to generate an object that is then grasped, classified, and either thrown towards a target for points or dropped onto a "trash" target. Points increase subject engagement by introducing a game mechanic. First, during Training of this task, haptic feedback is delivered as continuous controller vibration while the haptic object is grasped. Objects delivering haptic feedback are thrown towards the target. Once the game mechanic is understood using controller-based vibration, the task is relaunched, and now haptic feedback is delivered exclusively by DES.

Stimulation parameters align with prior work in the lab[23] and clinical stimulation (bipolar, biphasic, with 300-500ms total pulse width). Before beginning the VR task, perception of DES is evaluated with single pulses as well as short trains (<20 pulses) and the perceptual amplitude

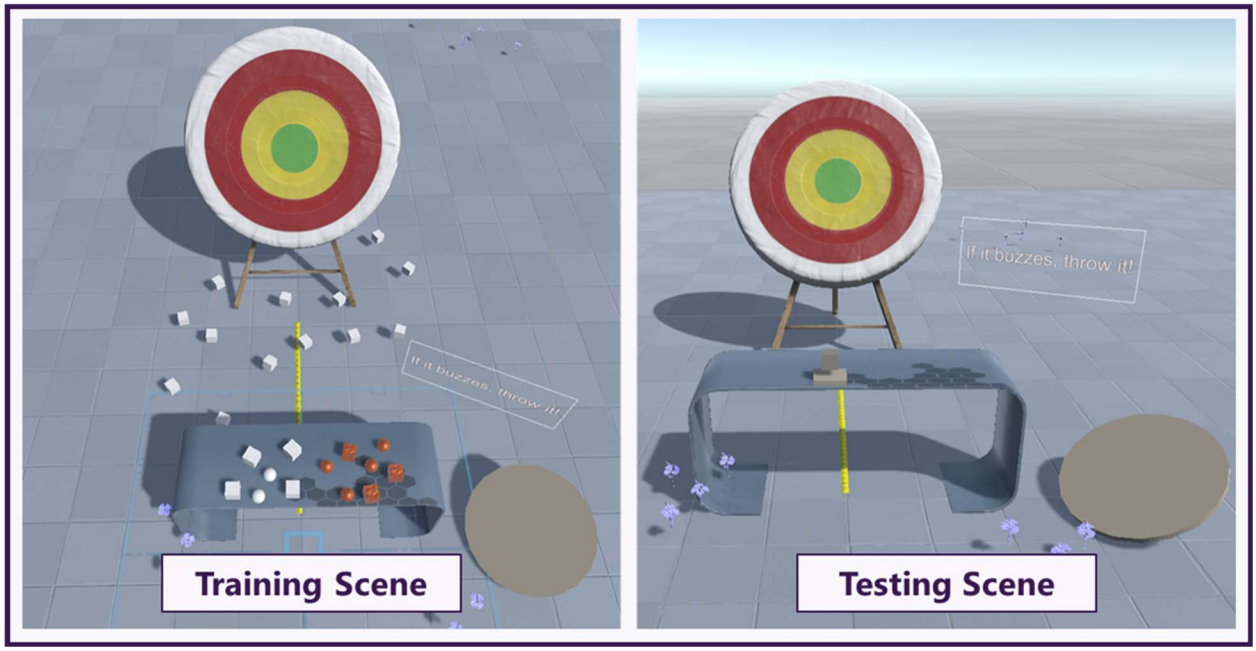

Figure 5.4 HapticSort training and testing scene layouts. (left) The training scene renders 13 interactable objects that deliver either no haptic feedback when grasped (matte white), or haptic feedback when grasped (metallic orange). (right) The testing scene utilizes an object-generating button and presents an object without visual encoding for pure haptic discrimination. Haptic objects are thrown towards the bullseye target.

threshold determined by simple yes/no query. Stimulation electrode pairs may be identified from post-operative electrode localization or during clinical language mapping.

HapticSort is a simple binary (yes/no) discrimination task presented in two scenes: a training scene and a testing scene (Figure 5.4). In the training scene, shown in overhead view by the left panel of Figure 5.4, a subject is placed before a table with 13 objects that are all approximately within an arm's reach. As these objects do not regenerate after being thrown, the training scene is limited to 13 trials. Behind this table is a large ringed target with a green center bullseye. Objects on the table are intermixed spheres (six) and cubes (seven), each rendered with either a matte white material (six, left side of table) or a metallic gold/orange material (seven, right side of table). The materials indicate whether haptic feedback will (gold/orange) or will not (matte white) be delivered upon grasping and holding the object. Stimulation is delivered continuously while the object is held. Subjects are encouraged to determine the neurohaptic state of the object quickly but accurately,

and to throw a haptic object towards the bullseye target and a non-haptic object towards a matte brown “waste bin” target.

If the subject correctly identifies the haptic object and hits the target, then upon target collision the haptic object explodes into a colorful archery arrow that remains permanently lodged in the target and adopts the color of the ring hit (e.g., green for bullseye). This serves as an ongoing visual indicator of success in addition to the game score projected into the task table. Behavioral data regarding accuracy of haptic identification was recorded by a script running within the HapticSort scene and confirmed by review of both in-room video and recordings of the VR screen overlay.

After completing the training scene, the testing scene is launched. In this scene, subjects are placed before the same table, with the same set of ringed bullseye target and “waste bin” target, and with the same instruction to throw haptic objects toward the bullseye target and non-haptic objects towards the matte brown target. Instead of pre-placed objects on the table, though, there is instead a simple button actuator that, when depressed, generates an object offset to a small space to the right of the button. This button is seen as a simple floating square above a matched, matte brown button base (Figure 5.4). The site of object generation can be modified easily to accommodate left-hand dominance or various task performance challenges.

Generated objects are pulled from a pre-allocated pool of haptic and non-haptic objects. This is done to reduce memory management of game-instantiated objects and to facilitate even distributions of randomly selected haptic and non-haptic objects. All objects in the training scene are rendered with identical visual characteristics of material (matte white), shape (cube), and size. No visual or VR perceptual characteristic identified a haptic vs. non-haptic virtual object, except the delivery of neurohaptic feedback upon contact. Behavioral accuracy was recorded, as before.

To introduce the HapticSort task and to validate task design, subjects were asked to complete the binary discrimination task with traditional vibrotactile haptic feedback, delivered through the VIVE controller, during object interaction. Once the HapticSort task was understood, the vibrotactile haptic feedback for object interaction was disabled and only neurohaptic feedback by S1-DES was delivered.

5.2.6 *HapticSort_ABØ*

HapticSort_ABØ ("Ay-Bee-Null") retains the haptic discrimination goal of the original HapticSort task. In this version, however, objects are presented during training with visual cues that correlate to DES stimulation pattern A, pattern B, or no stimulation. There is no controller-based vibrotactile introduction and each object is thrown toward its unique and learned target. Targets and their associated simulation profile (A, B, or Ø) are learned during the training phase, in which objects

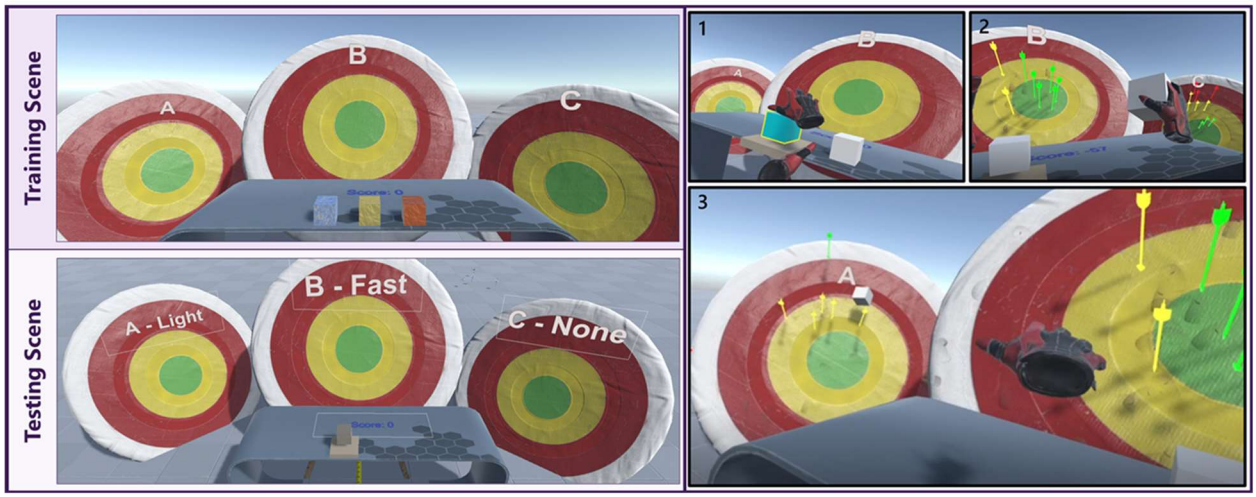

Figure 5.5 HapticSort_ABØ training and testing scenes. This task leverages the same principle of visual encoding during training and button-generated nondescript objects discriminable only by haptic profile during testing. In HapticSort_ABØ, two types of haptic object and one non-haptic object must be discriminated, and each thrown onto their own bullseye target. (left) The Training and Testing scenes. (right) A sequence of 'live-action" HapticSort_ABØ discrimination, in which (1) a random and unknown object is generated by button press, (2) the object is grasped, and the resulting haptic information evaluated, and finally (3) the object is thrown towards its designated target. Each arrow indicates an accurate discrimination trial.

are visually distinguishable (e.g., null stimulation is visually encoded as a blue, icy cube while stimulation pattern A is encoded as a red, metallic cube).

In the one patient collected so far, stimulation patterns were amplitude modulated (AM) sequences. Various AM sequences were presented in an informal one-back comparison task with verbal response (e.g., yes, these are different or no they are not/I can't tell). The range of presented amplitude values was determined as with HapticSort, by verbal response to single pulse DES. The two AM sequences repeatedly reported as noticeably different were selected for the task.

It is worth noting that verbal descriptions of the AM sequences included statements like "That one is more bumpy and the other one more smooth." This is significant because DES percepts are notoriously non-tactile, difficult to describe, and often characterized with works like "buzzing" or "tingling."[106] I hypothesized that AM stimulation would evoke a more sensorimimetic sensation.

The subject performed over 50 individual grasp and throw trials of HapticSort_ABØ.

HapticSort_ABØ is an extension of the binary HapticSort task and demands discrimination between two distinct stimulation sequences in addition to the 'null' no-stimulation case. In the training scene of this task, the subject is again placed before a table, but now faces three bullseye targets with visible, in-game labels of A, B, and C (Figure 5.5). Placed already on the table are three cubes, each rendered with a distinct material: (left) a blue, translucent, ice-like material, (middle) an opaque, yellow-gold metallic material, and (right) an opaque, orange-red metallic material. These were nicknamed "ice, rock, and lava" by Subject 1. The structure of HapticSort_ABØ task parallels that of the burst frequency discrimination task conducted with non-human primates, mentioned above, in which monkeys were trained to discriminate between two stimulation sequences and a no-stimulation condition.[4]

The goal of the training scene is for the subject to learn which stimulation condition is mapped to which material and which target. The far left "ice" cubes are non-haptic objects, and their correct target is C (Ice → Ø, C). The middle, yellow gold "rock" cubes elicit one stimulation sequence (e.g., Ziggurat) and their target is A (Rock → A). The rightmost orange red "lava" cubes elicit a second stimulation sequence (e.g., Sawtooth) and go with target B (Lava → B). Once thrown, each cube will regenerate, so the training scene for HapticSort_ABØ is not limited to a preset trial count. These visually distinct materials were introduced to facilitate performance on the training task by providing a visual cue to identify the correct target. This is especially important for subject engagement early in the task when the stimulation sequences may be difficult to distinguish and remember. Chosen materials and animation effects may also be used to give context or to prime the subjective experience of neurostimulation.

As before, if an object hits its correct target, an archery arrow prefab colored by where it lands on the target is generated, with fanfare. If an object contacts an incorrect target or the floor, it bounces off and does not generate an archery arrow. Once contact with any target or the floor has been made, cubes are returned to their original position on the tabletop after a 3 second delay. The number of trials completed during the training scene of HapticSort_ABØ is determined by the subject, though a minimum of fifteen trials is encouraged.

In the testing scene of HapticSort_ABØ, the same matte brown button from HapticSort replaces the three, visually distinct cube objects. Upon button press, a nondescript, matte white cube object appears to the right of the button, as in HapticSort. This cube was randomly selected from a pre-instantiated pool of haptic (two of each A and B) and nonhaptic (one Ø) objects, each rendered with matte white material to be visually identical. Based on the learned target-haptic associations, subjects throw each cube towards the target indicated by its neurohaptic profile. In Subject 1,

although subjective descriptions of the stimulation profiles were elicited, these descriptions were not incorporated into the testing scene. This led to memory errors that caused decreased behavioral performance confounded interpretation of target accuracy as an indicator of only perceptual discrimination of the stimulation sequences. In Subject 2, to remove the behavioral confound of needing to memorize target representations (e.g., Stimulation Ø → Target C), one-word descriptors, chosen by the subject, were added to the targets in the testing scene (Figure 5.5). For example, Target B read "B – Fast" for Subject 2 during one testing scene. The subjective labeling of the targets in the testing scene was reportedly useful and will continue to be implemented with future subjects.

5.3 RESULTS

5.3.1 *Subject 1*

Subject 1 completed three non-consecutive days of neurohaptic VR experiments. Thumb & index finger percepts (Figure 5.1) were elicited by stimulation between contacts LGT 15 and LGT 16, and on day 1, biphasic pulses of 200µs pulse width elicited percepts in an amplitude range of 2mA – 4.5mA.

Subject 1 completed familiarization and task validation of HapticSort using controller-based vibrotactile haptics at a binary stimulation detection accuracy (AB-Ø or Stim-Null) of 100%. No S1-DES was delivered, only traditional haptic feedback. For all subsequent trials, vibrotactile feedback was disabled. Subject 1 then completed multiple rounds of HapticSort with only S1-DES, at various pulse widths and stimulation amplitudes. Although haptic objects are visually encoded in the HapticSort training scene, AB-Ø accuracy was only 88.1% (Table 5.1 Subject 1 Percent Accuracy (%) of HapticSort Trials, row 1 - gray). This reduced accuracy despite visual encoding

Table 5.1 Subject 1 Percent Accuracy (%) of HapticSort Trials

Subject 1			
Stimulation Details	Stim Binary	Percept Ternary	Percept Binary
	AB – Ø	A – B - Ø	A - B
13 trials, 200µs, 3mA [a]	88.1	-	-
28 trials, 200µs, 3mA [b]	92.9	-	-
3 trials, 200µs, 2mA [b]	0	-	-
48 trials, 150µs, 3mA [b]	95.8	-	-
52 trials, 400µs, 4 -6.1mA [b] LongSawtooth	100	-	-
32 trials, 400µs, 4 -6.1mA [a] Sawtooth - LongSawtooth	86.2	84.4	87 of 23
20, 400µs, 4 -6.1mA [b] Sawtooth - LongSawtooth	90	50	57.1 of 14
46 trials, 400µs, 4 -6.1mA [b] LongSawtooth - 3.85mA	86.9	73.9	77.8 of 27

a. Training scene: visual encoding of objects.

b. Testing scene: no visual encoding.

of the objects demonstrates the importance of task familiarization in both haptic and neurohaptic paradigms as S1-DES, while innately localizable, may not feel natural and may require a short period of familiarization.

In the first HapticSort testing scene, binary stimulation detection (AB-Ø) accuracy was 0.929 over 28 trials in which neurohaptic feedback was delivered by biphasic square pulses with 200µs pulse width and a constant amplitude of 3mA (Table 1, row 2). Three additional rounds of HapticSort were completed, including one in which the stimulation was sub-threshold and undetectable, resulting in a 0% AB-Ø accuracy over 3 trials. Decisions regarding the presence or lack of neurohaptic feedback took noticeably longer in nonhaptic trials, although grasp duration was not specifically recorded.

Description of the evoked percept from constant amplitude S1-DES was that it “may be buzzing.” This response may have been influenced by both the preceding controller-based vibrational haptics and the use of the word “buzz” in the task description.

On day 2, one week later, 400µs pulse width stimulation yielded a 4mA - 6.1mA percept threshold range, with 150µA intervening steps to build the 15-index array. Subject 1 was unable to remember if the subjective nature of the short-burst stimulation percept had changed between the first and second day. Compared to “maybe buzzing” from the week prior during constant amplitude

biphasic square pulse stimulation, the structured stimulation yielded interesting subjective responses: the Sawtooth pattern was described as having a "pulsing effect" with a quick, ~2Hz rhythm. The LongSawtooth and LongZiggurat sequences were both described as "bumpy" with different bumpiness -- specifically that the bumps of the LongSawtooth sequence were "sharper." Compared to this, the Random sequence was described as "smoother" and a constant amplitude stimulation train as "flatter."

Subject 1 completed two rounds of a misfunctioning HapticSort_ABØ that encoded a LongSawtooth stimulation object and two null stimulation objects when a second sequence failed to actuate. If we consider this a form of binary HapticSort with extra steps, then the AB-Ø stim discrimination accuracy was shown to be 100% over 52 trials (17 haptic and 35 non-haptic, Table HapticSort, row 5).

Four days later, on day 3, Subject 1 completed three fully functioning rounds of HapticSort_ABØ. The training round contrasted null stimulation, Sawtooth, and LongSawtooth sequences using the same 4mA to 6.1mA in 150µA steps percept threshold range as before. LongSawtooth was described as "slow" and Sawtooth as "fast."

In the training scene, ternary A-B-Ø discrimination accuracy dropped to 50% as A and B seemed to be increasingly difficult to distinguish, yielding a specific binary A – B discrimination accuracy of 57.1% over 27 stimulation trials (Table 5.1, row 7). However, in terms of simple stimulation detection, the AB-Ø accuracy was still 90%. This round highlighted the confounding impact of memory in the first implementation of this task. Multiple mistakes were made not because A and B were indistinguishable, but because remembering target assignment was difficult. Learning from this implementation error, the targets in Subject 2's HapticSort_ABØ testing scenes were labelled

with the subjective description of the associated stimulation sequence as well as the A, B, and C designators.

In the second round of HapticSort_ABØ, a constant amplitude stimulation at 3.85mA was contrasted against the LongSawtooth sequence and null stimulation (Table 5.2, row 8). LongSawtooth was described as described again as "bumpy" and the constant amplitude stimulation as "smooth, no bumps."

5.3.2 *Subject 2*

Subject 2 also completed three days of neurohaptic VR experiments. Stimulation across right hemispheric cortical sEEG contacts M5 and M6 elicited somatic percepts in Subject 2's left hand, which was partially paralyzed but retained natural touch perception.

Table 5.2 Subject 2- Percent Accuracy (%) of HapticSort Trials

Subject 2			
Stimulation Details	AB - Ø	A – B - Ø	A – B
6 trials, 400µs, 2 -3.4mA [a] Sawtooth - Ziggurat	100	100	100 of 5
16 trials, 400µs, 2 -3.4mA [b] Sawtooth - Ziggurat	81.3	68.8	80 of 10
29 trials, 400µs, 2 -3.4mA [b] Sawtooth - Ziggurat	89.7	72.4	79.2 of 24
50 trials, 400µs, 2 -3.4mA [b] Sawtooth – 2Hz Burst	98	82	79.5 of 39

a. Training scene: visual encoding of objects.

b. Testing scene: no visual encoding.

On day 1, a burst of twenty biphasic square wave stimulation pulses of 400µs pulse width at 2mA elicited an interesting motor sensation but not muscle activation across the palm of Subject 2's left, paralytic hand. Subject 2 stated, "I felt like I was clenching" while making a gripping gesture with the right hand, opening and closing in a regular rhythm. The stimulation was repeated with 10 and 5-count bursts, confirming no actual motor behavior but the sensation of movement. This could be interpreted as the induction of a motor intention through DES or a unique interaction with neural tissue that has undergone some level of cortical remapping following functional paralysis of the left hand -- a "phantom motor" sensation. An increase in stimulation amplitude to 4.5mA

did not change the percept of movement, although inverse polarity of the biphasic pulse (-4.5mA) reportedly created a “more intense” feeling of movement or clenching. Clear sensation was also elicited by single pulse stimulations at -4.5mA and by 5-pulse, short burst stimulation at -1mA. From this, stimulation current between contacts M6 and M5 was refined to the range of 2mA - 3mA in 100μA steps. Reversed contact polarity is equivalent to a negative stimulation current.

One second of the Sawtooth stimulation sequence across this stimulation range was described as having an irregular “pulsing” rhythm, the LongSawtooth was clearly felt as “a little faster,” and the Random pattern evoked lingering perceptual effects that were initially concerning as evidence of after-discharge activity. Stimulation was suspended for one day to confirm by neural signals visualization and consensus of the clinical team that the sequence had not evoked irregular or epileptiform neural activity, simply an unexpected and lingering percept. The percept elicited by the Random sequence seemed to persist with decaying intensity for more than 3 seconds.

When we returned to the VR neurohaptic task a day and a half later, the stimulation range of 2mA to 3.4mA in 100μA steps was again found sufficient to evoke percepts from short burst through single pulse stimulation. Stimulation sequences were again evaluated using a one second duration of each sequence. This time, the LongZiggurat sequence was barely perceptible with no particular character, the Ziggurat sequence was perceived as a regular “bump, bump, bump, bump” percept, the Sawtooth felt “faster,” the LongSawtooth was felt as “pulsing” but was “not clearly different” from Sawtooth, and the Random sequence, cautiously evaluated, was perceived as “just fast pulsing” with no lingering percept.

For familiarization and validation, as before, the HapticSort scenes were completed using controller-based haptic feedback. Then, in the interest of time, only HapticSort_ABØ was

evaluated using S1-DES (Table 5.2, rows 1 & 2). With comprehended visual encoding during training, the task was performed with perfect accuracy.

On day three, two rounds of HapticSort_ABØ were completed. The previously identified stimulation range was again retained. In the first round, Sawtooth, Ziggurat, null stimulations were again contrasted for a ternary A-B-Ø accuracy of 72.4% across all 29 trials. Within these, binary AB-Ø accuracy was 89.7% and binary A-B percept discrimination accuracy was 79.2% across 24 detected stimulation trials.

In the second and final round, Ziggurat was contrasted with a new stimulation condition that more closely replicated the burst frequency approach outlined in the non-human primate study discussed earlier.[4] In this stimulation approach, a 5-pulse burst of stimulation at 50Hz was repeated approximately twice per second for a 2Hz burst frequency. Approximate frequency is due to small changes in processing rate that may occur during VR game updates. A-B-Ø accuracy was 82% over 50 trials, with binary AB-Ø stimulation detection accuracy of 98% and binary A-B percept discrimination accuracy of 79.5% across 39 detected stimulation trials (Table 5.2, last row).

5.4 Discussion

This work demonstrated the utility of traditional and novel S1-DES for neurohaptic feedback during naturalistic object interaction. In both of our human subjects implanted with intracranial electrodes, amplitude modulated S1-DES elicited distinct and memorable percepts, suggesting a new dimension for complex and dynamic neurohaptic design. Moreover, the structured S1-DES sequences elicited perceptual descriptions that seemed to approximate real tactile experience of texture in one subject, and phantom or intended movement in the paralyzed hand of the other.

Acknowledged limitations to this study include the patient count, the limited time to explore multiple stimulation profiles, and many hand-tuned and estimated stimulation parameters. Despite

this, the well-above-chance discrimination performance of both subjects attests to the strength of percept discrimination from dynamic S1-DES in the simple binary (on-off, AB-Ø), ternary (A-B-Ø), and percept binary (A-B) evaluations. The clear interpretation of amplitude-modulated S1-DES into rhythmic "bumps" with "sharpness" and sequences of relative "flatness" also attest to the interpretability and variety of induced percepts possible with this approach. We look forward to evaluating these stimulation dynamics in future subjects, and to leveraging a higher patient count to identify "universal" stimulation features to guide transferrable neurohaptic feedback.

Both subjects demonstrated occasional and temporary drift in their ability to discern elicited percepts that had been clear, or even differentiate stimulation on and off conditions that had also been obvious a few trials before. Understanding the neural dynamics governing receptivity to S1-DES would undoubtedly improve stimulation delivery and design and may give insight into the learning mechanisms important for adaptive bidirectional-BCI.

Finally, by leveraging VR, we were able explore the integration of neurohaptic feedback in response to complex, self-directed, and spontaneous human interaction with virtual objects. It would have been nearly impossible, for example, to present objects in the real world that could be grasped without also being felt. Working in VR allowed us to rapidly update our tasks to accommodate limitations in both of our subjects: motor weakness in Subject 1 and paralysis in Subject 2. Modifications included things like adding a multiplier to the release velocity of a thrown object, so that our subjects could more successfully and enjoyably engage with the throwing mechanic of our tasks and adjusting the location of game objects so they could be more easily accessed according to the body position and needs of the subject.

VR opens incredible opportunities for flexible, creative, and insightful experimental design not possible except in virtualis re. This study suggests a virtual route forward for neurohaptics design with implications for BCI and neuroprosthetics.

Chapter 6. A Bidirectional VR-BCI: Linking Neural Triggers & Neurohaptics

Figure 6.1 Visualization of the Bidirectional VR-BCI in use. Actual screen overlay from VR-BCI scene depicted in the VR pop-out shown here.

6.1 Introduction

Bidirectional BCI, in general, had not yet been implemented with ECOG or sEEG macroelectrodes. In my search of the literature, no bidirectional BCI in any modality has been integrated with a virtual reality environment. As stated, virtual reality offers a uniquely capable environment for exploring and developing novel BCI strategies. For example, complex behaviors can be initiated in VR by simple neural triggers that each yield a half-dimensional of control over

a virtual avatar or other output effector of the VR-BCI. Half-dimension control describes a "neural trigger," which can be thought of as a mouse-click by the brain. This does not constitute a full dimension of control as it is not considered a continuous decoder. My goal was to connect real-time neural signals decoding to task-relevant sensory stimulation within a VR visuohaptic task to yield a bidirectional VR-BCI.

This chapter presents the culminating implementation of the VR experimental platform I developed over the last year and a half of my PhD. First, I describe the VR-BCI task environment and gaze integration. I then present the behavioral cueing protocol and neural signals analysis pipeline I used to identify robust "neural triggers." These specific and reliable neural triggers rapidly decoded overt movements from neural signals in two subjects. The first subject was not able to attempt the VR-BCI task due to a hardware communication error resolved only after explant. Subject 2, then, became the first VR-BCI "cerebronaut" – Subject 2 coined this term after VR-BCI immersion to describe users of a VR-BCI. I then present the behavioral results from this first implementation of a bidirectional VR-BCI. This work leads the way in designing the next generation brain computer interface by leveraging the power of immersive virtual reality for bidirectional BCI.

6.2 METHODS

6.2.1 *Task Design & Gaze Integration*

The VR-BCI task was designed and implemented in collaboration with Iman Tanumihardja at the University of Washington. The task involved gaze-selection of one of three virtual objects: floating red, green, and blue spheres, presented visually left to right, at a graspable distance and about head height, as seen in Figure 6.1. Real-time neural signals were decoded to trigger a rigged-skeleton animation sequence that would reach out, grasp, and interact with the gaze-selected virtual object.

Each object had, for this experiment, its own attached animation that would be activated when the object was selected by gaze and the VR-BCI registered a neural trigger. During the animation, while the virtual hand was in contact with the selected object, the VR-BCI delivered S1-DES stimulation as neurohaptic feedback. Percept tangibility was confirmed by verbal report. Animation sequences could only be activated by real-time decoding by the VR-BCI of the neural trigger and concurrent gaze selection of an object.

To implement gaze-based object selection, the SRanipal Runtime was installed on the tethered Alienware VR-capable laptop and the HTC SRanipal Unity SDK was imported into the VR-BCI scene.[165] This SDK provides a solution for gaze interaction within VR, built on the output variables of the native Tobii eye tracker[12] on the HTC Vive Pro Eye headset. These variables include device and system timestamp, gaze origin, gaze direction, pupil position, pupil size, and eye openness. Following a 5-point eye tracker calibration, a script called Gaze Ray Selector was written to continually cast gaze direction as a physics ray within the VR scene. Collisions between this "gaze ray" and any of the rendered set of interactable objects was used to select one of the three hovering spheres.

Before completing the VR-BCI task, the subject was guided through an onboard eye tracking calibration protocol in which (1) the HMD was repositioned as needed to center the eyes, (2) the interpupillary distance (IPD) knob on the front of the headset was physically rotated until the visual alignment indicator within the VR scene was centered, and finally (3) the gaze calibration was completed by having the subject look at five specific locations in the visual display indicated by highlighted dots. These dots map the four corners of a 2D plane intersecting the visual 3D world

[12] Specifications: 110° trackable per-eye field of view (within 20° FOV) for 120Hz binocular gaze data output at 0.5°-1.1° accuracy following successful 5-point calibration. Manufacturer notes that eye surgery, eye disease, heavy makeup, and high myopia may affect eye tracking performance.[165]

to calibrated high field-of-view angle and a resting centered gaze position. Eye tracking, very useful for cognitive research, is used for dynamic foveated rendering of VR games to reduce GPU load by reducing the required resolution of VR elements outside of the foveal focus.

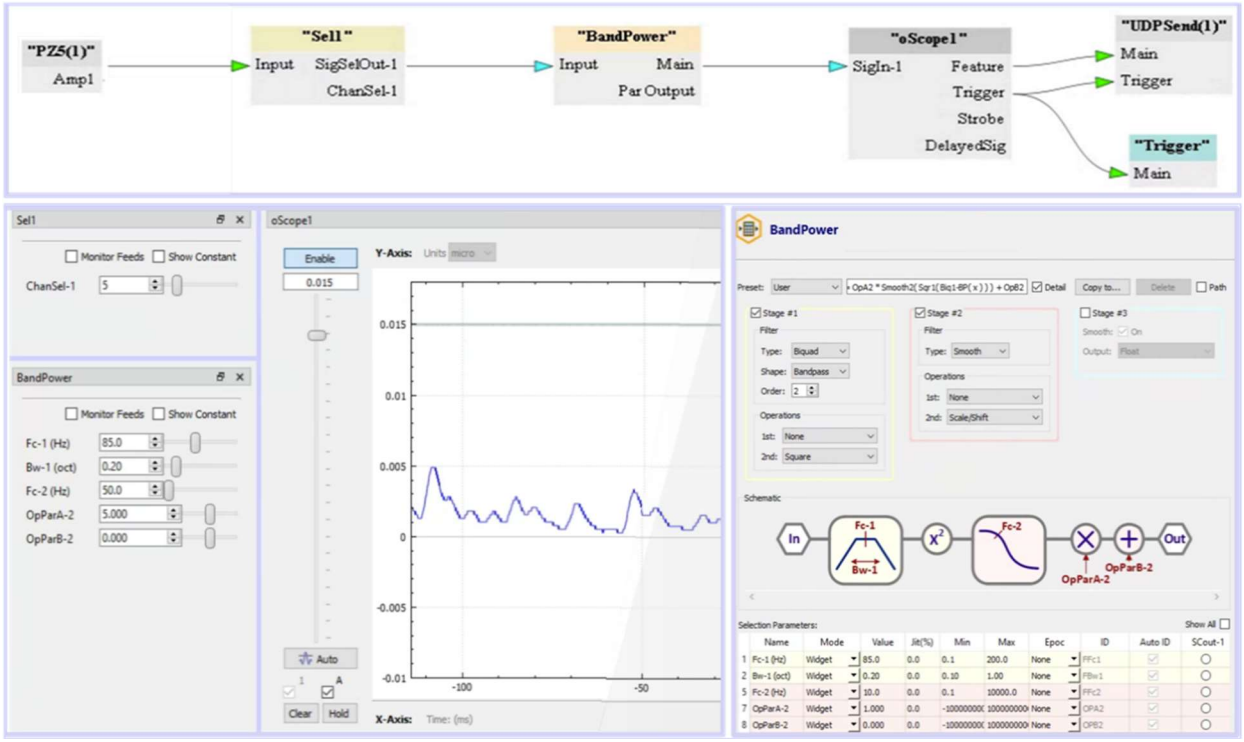

Figure 6.2 Synapse Circuit Diagram for VR-BCI Decoder. (top) In this half of the VR-BCI control circuit, a channel selector ('Sel1') isolates a single channel of neural signals to undergo real-time filter-Hilbert processing ('BandPower'), producing a continuous bandpower waveform that may be visualized, transformed, and thresholded ('oScope') for neural trigger detection ('Trigger') and VR task updating in Unity ('UDPSend(1)'). (bottom) The front panel of the decoder permitting updating of some parameters during runtime, including channel selection, bandpass filter settings, bandpower and threshold calculation settings.

6.2.2 *Real-time Neural Decoding*

The hardware diagram for the bidirectional VR-BCI implementation system is the same as the neurohaptic object discrimination tasks (Figure 5.2). For the extended functionality required by the bidirectional VR-BCI task, the UDP socket script needed to be updated to enable bidirectional communication between the VR-hosting laptop and the TDT RZ unit. Once bidirectionality had

been confirmed, the decoding half of the Synapse control circuit for neural recording, onboard digital signal processing (DSP), and thresholding for neural trigger identification was developed (Figure 6.2). In this circuit, a single channel is selected for onboard digital signals processing of bandpass filtering, followed by amplitude-squaring (power estimate), then smoothing by 10Hz lowpass filter, and then optional vertical translation or scaling (set to 0 and 1 for initial circuit design).

6.2.3 *Neurohaptic Stimulation*

The rigged-skeleton animation registered object collision, sending an index integer via UDP to the TDT RZ Unit, as in the HapticSort tasks previously described (Section 5.2.2). Neurohaptic stimulation was delivered only while the animated virtual hand grasped the virtual object. For the first and only session of VR-BCI task implementation, constant amplitude stimulation was delivered using biphasic square wave pulses of 200μs pulse width at a pulse frequency of approximately 50Hz. The functionality for complex stimulation to enable neurohaptic-based object discrimination is available for future experiments.

Electrode localization was used to guide candidate neurohaptic stimulation electrodes. For Subject 2, sEEG electrodes in the hand area of the left primary somatosensory cortex were identified. Prior to VR-BCI task immersion, percept tangibility was confirmed on the localized electrode and threshold of 5-pulse burst stimulation was evaluated.

6.2.3.1 Definition: Neural Trigger

As described, a Neural Trigger can be liked to a “mouse click” by the brain and offers 1.2-dimmension of control. To achieve the quick “click” of decoded neural activity, a neural trigger can be implemented a threshold decoder. While amplitude can be used as a straight-forward feature on which to threshold, it is highly variable and very subject to both line and broadband noise. I

elected instead to threshold the power estimate of a bandpass filtered signal. A candidate neural trigger by this implementation, then, is defined by the frequency band from which the bandpower signal is estimated, the recording electrode capturing neural data, and a cued behavior shown in offline processing to uniquely elicit a bandpower increase in the target bandpower range. The threshold is set during live evaluation of each candidate neural trigger.

Candidate neural triggers were identified using an informed search and either automated or manual evaluation of neural features to support a real-time powerband estimate method for Neural Trigger state decoding. These steps are described individually in the subsections below.

6.2.3.2 Informed Search: Electrode Localization & Behavioral Cueing

Electrode localization was completed as described in section 2.3, page 32. Electrodes localized to the primary somatosensory (S1) and primary motor (M1) cortices were used to construct a list of motor actions likely to elicit cortical activity from recorded cortex (Figure 6.3). Sensory cortex is

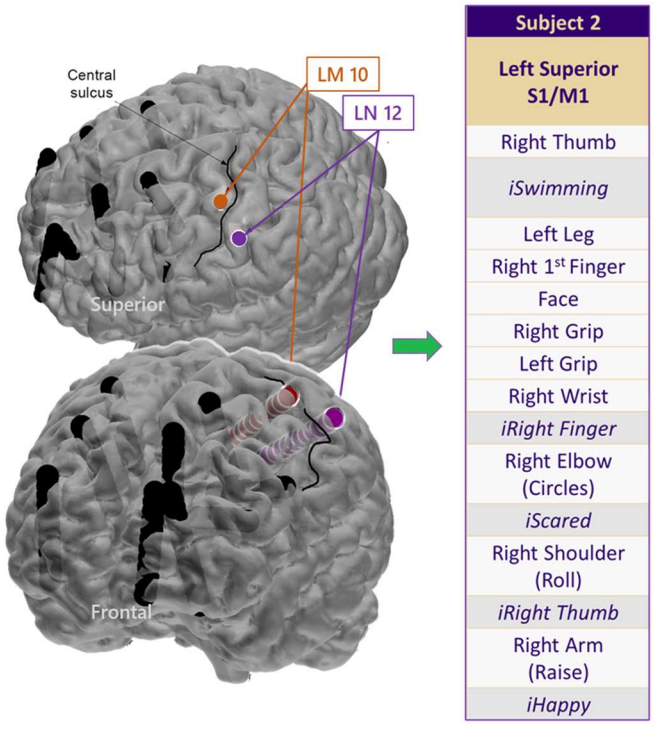

Figure 6.3 Behavioral Cue List Informed by Electrode Localizations Electrode localizations were used to identify electrodes implanted in the primary somatosensory or primary motor cortices. In Subject 1, electrodes 10 and 12 on probes Left Motor (LM) and Left Sensory (LN) were localized to the shoulder/arm and hand areas of their respective cortices. From this, a list of behavioral cues shown here was constructed. This list contains movements likely to be decoded given electrode coverage (e.g., 'Right Thumb' movement), interleaved with contrasting cognitive and behavioral cues of actions unlikely or remotely likely to elicit decodable neural activity (e.g., '*iSwimming,*' which stands for 'Imagine Swimming (but don't actually move).'

known to reflect motor activity[166–168] which is why localizations to S1 were also used to design the motor behavioral cue list.

This list was interleaved with a second list of cognitive and motor cues unlikely or remotely likely to be decodable by the real-time BCI. This list of interleaved behavioral cues ((Figure 6.3) was used to build a dataset of continuous neural activity during sequential 30-second cue-and-action epochs.

To begin, behavioral neural signals collection was preceded and followed by 2 minutes of resting state data. Then, the subject was instructed and guided in the completion of 30-seconds of the cued behavior. For example, for Subject 2, the first cued behavior was "Right Thumb" (Figure 6.4). To fulfill this cue, the subject *and the researcher, together,* did 30-seconds of right thumb circles. In a prior cued motor behavior task, I learned that concurrent activity improved task engagement over the course of the 30 seconds. The second cued task, after 30-seconds of right thumb circles, was "*iSwimming*," which stands for "Imagine swimming." All cued behaviors were completed for a minimum of 30 seconds each, in the order listed, once through the list. This protocol was demonstrated in Subject 1 to be sufficient to reveal 6 candidate neural triggers. In Subject 2, the behavioral cue list was lengthened to support the identification of additional candidate neural triggers.

Subject 1
Right M1 – Hand & S1 Arm
Right Hand
Left Hand (Touch)
Right Elbow
Left Elbow
Shoulders (Both)
Jaw / Mouth
Tongue

Figure 6.4 Subject 1 Behavioral Cue List. This list demonstrates the first iteration of the informed neural trigger identification pipeline. Electrode localization identified an electrode in the hand area of the right Primary Motor (S1) cortex and the arm area of the Primary Somatosensory (S1) cortex. Offline analysis of these seven cues was sufficient to identify six candidate neural triggers. VR-BCI was not collected in this patient due to a hardware communication error, resolved after explant.

6.2.3.3 Offline Neural Signals Analysis

Offline neural signals analysis included windowed Fourier decomposition on for time-frequency visualization, followed by filter-Hilbert bandpower evaluation. As discussed before, each offline "candidate neural trigger" is defined by the recording electrode, frequency band, and behavioral cue. For Subject 1, an automated candidate detection process yielded 6 strong candidate neural

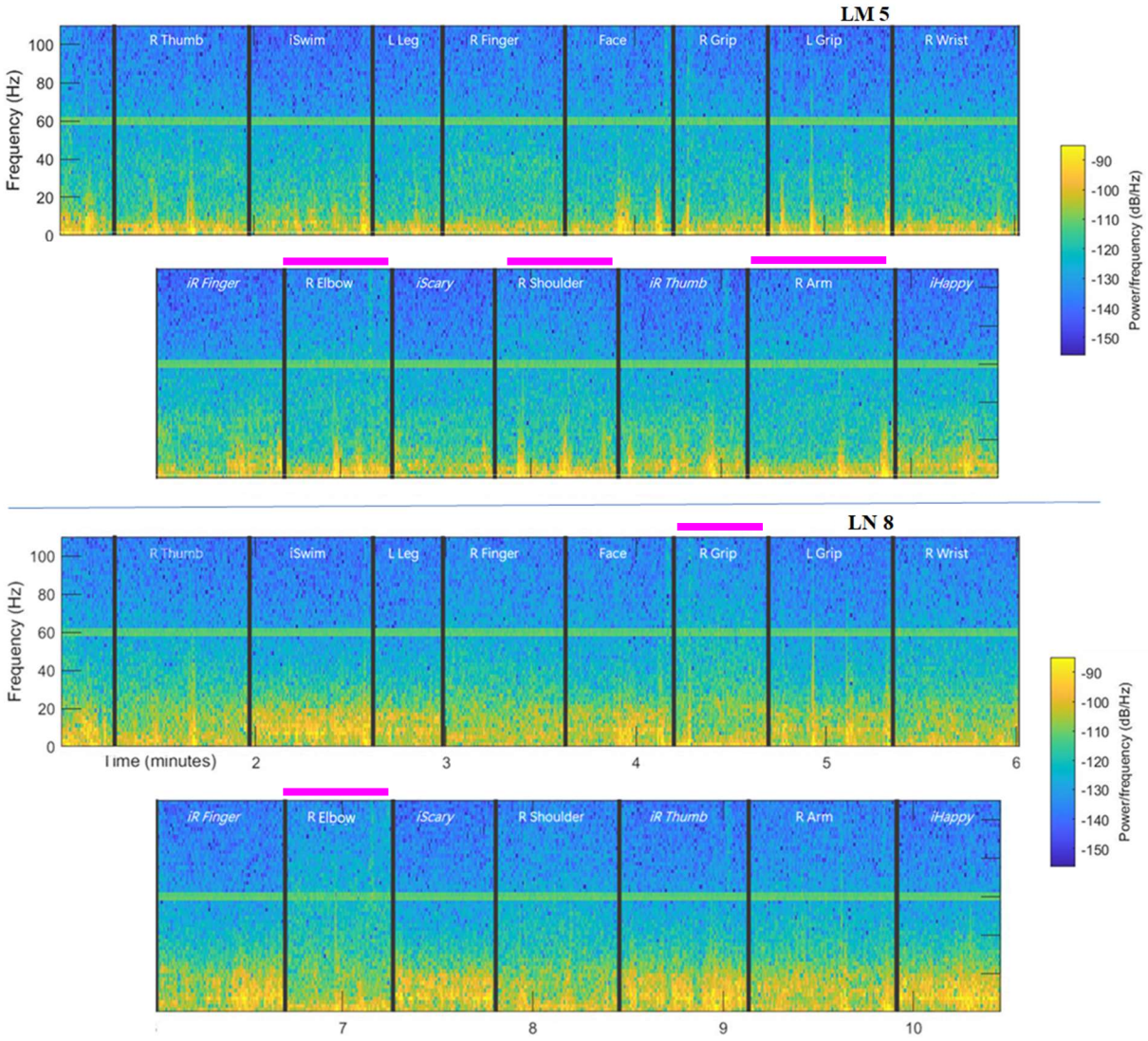

Figure 6.5 Spectrograms from two channels during a sequence of cued behavior. Continuous time-frequency activity is depicted across 15 epochs of cued behaviors on channels LM 5 and LN 8, each a minimum of 30 seconds in duration. Dark vertical bars frame these behavioral epochs, each with abbreviated cue label (e.g., the first epoch is 'R Thumb'). Time along the x-axis is in minutes, frequency along y-axis is 1-110Hz. Power values are dB-scaled from -150 to -90 dB/Hz. Hot pink bars identify behaviors per channel with visibly distinct spectral activity throughout the behavioral epoch.

triggers. In this automated approach, average power comparisons between cued activity and resting state were used to identify behavioral activities that elicited a 20% or greater average power increase in any canonical spectral band and on any electrode during a 30-second cued epoch.

For Subject 2, the automated process yielded too many initial candidates. As a result, I modified the offline signals analysis protocol, implementing a more manual approach. In this approach, continuous time-frequency data across the entire behavioral cue list for all 23 implanted electrodes (from which we could record with the TDT) were extracted by windowed Fourier Transform, as before, and visualized as spectrograms. Electrodes with visible power differences between behavioral epochs were manually identified (Figure 6.5), and from this, frequency bands of visible activity difference were approximated. Visual comparisons of the spectrograms of candidate electrodes within these specific spectral bands across all cued behaviors (Figure 6.6) were then used to rank order candidate neural triggers by behavioral cue, frequency band, and electrode. Neural triggers decoded from the neural activity of actual movement also facilitated behavioral evaluation of the VR-BCI task. I leveraged the visibility of Subject 2's stereotyped, neural trigger-evoking movement to mark the onset of their intent to trigger the BCI. From this overt action, I can calculate the temporal delay, for each VR-BCI trial, from visible movement initiation – representing the intent to trigger – to triggered action (Figure 6.7).

6.3 RESULTS

6.3.1 *Electrode Localization*

The bidirectional VR-BCI Neural Trigger task was implemented only with Subject 2. Electrode localization (i.e., LM 10 and LN 12) informed a behavioral cue list emphasizing right hand, arm, and shoulder movement (Figure 6.3). Contrasting behavioral cues included imagined movements, actual face and ipsilateral leg and hand movements, and cognitive prompts (e.g., '*iScary*' is

"Imagine being very frightened. Imagine something scary."). Electrode localization also identified electrodes LN 10-12 as a potential left cortical hand-area S1-DES targets.

6.3.2 *Neurohaptic Evaluation*

Medial thumb sensation was elicited using bipolar S1-DES between electrodes LN 10 & 11 with a remarkably low sensitivity of 0.25mA-3mA eliciting 10-pulse burst to single pulse stimulation percepts. Subjective response to amplitude modulated S1-DES (as described in Section 5.2.3) yielded interesting results, and 'Sawtooth' S1-DES was integrated into the ultimate VR-BCI demonstration (Table 6.1). Meaning, Sawtooth modulated (Figure 5.3), bipolar S1-DES was delivered as neurohaptic feedback during VR-BCI object interaction. The range of experiences with different complex stimulation profiles was dramatic and unexpected.

Table 6.1 Subjective Responses to Complex S1-DES

Stim Profile	Channels	Range	Description
Single & 10-pulse	LN 10-11	3mA	Medial thumb percept, feels like a "bark collar" [electrical buzzing], both
Sawtooth VR-BCI	"	0.25-3mA	"Like a boat going over a wave"; fluctuating percept in time with the peak-descent profile of the stimulation; also "like a bark collar"
Random	"	0.25-3mA	Movement from thumb to first finger
Ziggurat	"	0.25-3mA	Felt "warm" and evoked a muscle twitch with the peak-descent profile of the stimulation
Constant 1-sec continuous	"	3mA	Percept moved to pointer finger, with felt and visible movement
Sequence-7 5-pulse bursts at 2Hz, constant amp	"	3mA	Percept at pointer finger; stronger twitch
Single pulse	"	3mA	Percept moved (back) to medial thumb
10-pulse	LM 1-2	3mA	Right trapezius motor twitching

6.3.3 *Neural Trigger Selection*

In Subject 2, a behavioral cue list of 15 behaviors was collected, yielding 10.47 minutes of continuous and behaviorally labelled data, recorded on 23 sEEG electrodes using the TDT neural recording suit. Visualization of this activity as continuous spectrograms (Figure 6.5) identified potential channels, frequency bands, and behavioral cues for further evaluation and rank ordering, namely: (1) on LN 8 (channel 15), in the alpha (9-23Hz), beta (30-50), and gamma (70-100) bands, the right thumb, finger, grip, wrist, and elbow actions, and (2) on LM 5 (channel 5), in beta and gamma bands, the right grip and elbow actions. Power across behavioral cues in these extracted bands was visualized as in Figure 6.6.

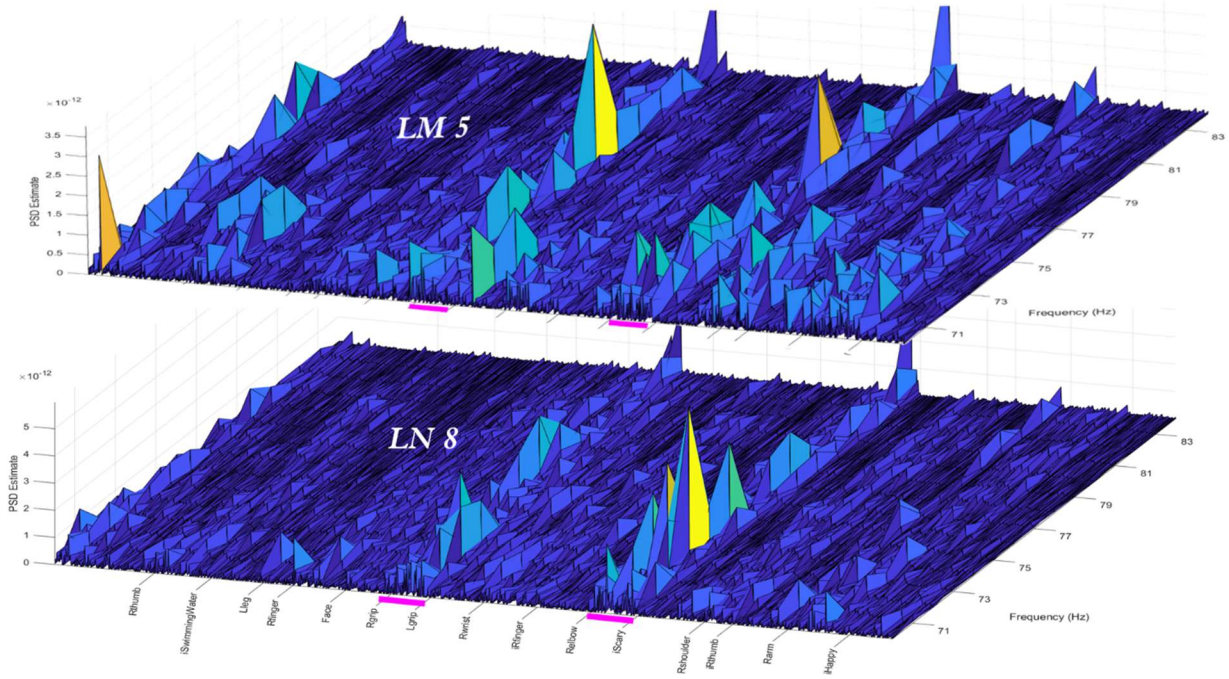

Figure 6.6 Gamma band (70-100Hz) visualization across behavioral cues for two channels. (top) On channel LM 5, a reduced gamma band (71-83Hz) of frequencies shows power increases with right grip and elbow movements (epochs highlighted in hot pink). (bottom) On channel LN 8, gamma activity rises most with right elbow movement.

This manual analysis pipeline yielded three top candidate triggers: gamma (70-100Hz) power on LN 8 for right elbow movement, and gamma power on LM 5 for right grip and right elbow movement.

6.3.4 *VR-BCI – Trials*

Subject 2 completed 15 VR-BCI trials over 8.77 minutes using a Neural Trigger of gamma power, defined by the real-time neural circuit (Figure 6.2) as 0.2 octave around a center frequency of 85Hz, recorded by electrode LM 5 (Figure 6.6). Real-time gamma bandpower was seen to increase during elbow circles.

During live evaluation of the neural trigger prior to headset donning, a stretch factor (multiplication) of 5 was applied to the gamma bandpower waveform and the neural trigger threshold was set to 0.011 in the live Synapse 'oScope' gizmo (Figure 6.2). The trigger was set such that motor behaviors of elbow circles focusing on deltoid arm lift could activate the neural trigger (with visual correspondence between motor activity and neural trigger activation), but resting activity did not reach threshold. It was not required during initial evaluation that every relevant arm movement activate the trigger, simply that resting activity did not trigger while motor activity showed some efficacy in reaching threshold. S1-DES to LN 10-11 was confirmed to evoke a percept on right medial thumb prior to headset donning and VR-BCI task launch, as well.

The headset was donned and an example trial demonstrating animation reach toward the center green sphere (Figure 6.1) was completed, introducing the VR-BCI task structure and confirming neurohaptic perception only during virtual hand-object contact. Control was passed to the real-time neural decoder and the subject completed 12 trials at the listed 0.011 threshold, and 3 trials at a higher threshold. The higher threshold was explored briefly after an accidental trigger

activation following movement in bed. It was too high for neural trigger activation despite active, intentional right arm movement and right-hand grip, so the initial threshold was restored.

The delay from intentional motor activity to neural trigger activation is presented for each of the 12 trials at the initial threshold, demonstrating a remarkable reduction over this first VR-BCI session (Figure 6.7). Gaze-selection demonstrated highly accurate and responsive ocular tracking with accurate object selection by gaze ray collision.

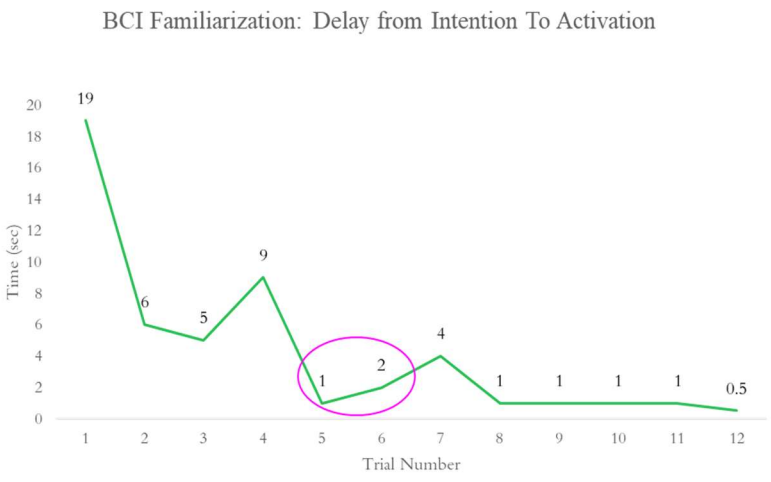

Figure 6.7 Delay across VR-BCI trials. Delay was defined as the seconds from the onset of motor activity with an intent to trigger, to the onset of the animation following successful neural trigger activation. Trials 5 and 6 are circled as these were "errors" in the VR-BCI neural trigger decoder, in which the trigger was not intentionally activated. In trial 5, Subject 2 was watching the animation and thinking about activating the trigger when it activated. In trial 6, Subject 2 was adjusting body position.

From these data (Figure 6.7), the average neural trigger delay was 4.86 seconds ± 5.47 seconds, standard deviation (stdev), and the overall neural trigger decoder "accuracy" was 10 of 12, or 83.3%. The two circled trials in Figure 6.7 highlight the two trials in which the VR-BCI neural trigger was not intentionally activated. However, in trial 5, the subject was watching the animation and thinking about activating the trigger when it activated, an in trial 6, the subject was adjusting body position. These are strictly non-intentional neural trigger events but may still represent "accurate" functioning of the simple neural trigger VR-BCI decoder. Neurohaptic feedback by S1-DES was delivered for all except one catch trial and was reported tangible for all except the catch trial.

Finally, periods of "intentional rest" were recorded in an effort to validate the specificity of the neural trigger to volitional activation. Intentional rest was defined as any period of time greater than 2 seconds in which the subject was intentionally *not* engaging the live neural trigger VR-BCI. In total, across twelve trials, six such periods of intentional rest greater than 2 seconds were recorded, for a total of 54 seconds and an average of 9 seconds ± 8.2 seconds, stdev. The longest and most interesting period of intentional rest was a 25 second run in which the subject was talking to a parent in the room and using the left controller to attempt to interact with the floating spheres. This was immediately followed by a volitional VR-BCI trial (trial 8, Figure 6.7) in which the neural trigger was activated in 1 second (rounded up to the nearest whole second).

6.4 DISCUSSION

In this chapter, I discuss the implementation and evaluation of a bidirectional BCI in virtual reality that leverages gaze tracking for object selection, a real-time neural trigger decoder for VR-BCI control over initiating a rigged-skeleton animation sequence, and neurohaptic feedback delivered during object interaction. I demonstrated that 30-second epochs of cued neural activity are sufficient for the offline identification of candidate neural triggers, and I validated these triggers during online neural trigger decoding. I demonstrate sharp reductions neural trigger delay across sequential trials, demonstrating increased efficiency in neural trigger engagement over time and potentially rapid learning of VR-BCI. This work constitutes the first implementation of a bidirectional VR-BCI in humans and presents an approachable protocol and circuit design to support new VR- BCI architectures, to include continuous neural state decoding.

I would also like to acknowledge the amazing patient who participated in this research and coined the term for an operator of a VR-BCI: Cerebronaut.

Chapter 7. Recreating Canon: A Virtual Rubber Hand Illusion

7.1 Statement of Collaboration

In this chapter, I present an application of the VR experimental platform for cognitive neuroscience research. This work was completed in healthy human subjects by a team of two researchers, Sophia Lowe-Hines and Iman Tanumihardja, led and advised by me. I discuss here the design and implementation of a virtual Rubber Hand Illusion experiment, touching specifically on design considerations, challenges, and solutions, as well as innovation. I present the group's approach to analysis and behavioral results.

7.2 Introduction

The Rubber Hand Illusion (RHI) is a classic perceptual illusion in which a rubber hand and a subject's real hand are synchronously and congruously stroked. The rubber hand is visible and offset in some way from the subject's real hand, which is hidden from view. Discovered by Botvinick and Cohen in 1998, the RHI[169] demonstrates that the visuotactile synchrony of seeing a rubber hand stroked while a congruously stroke is felt on one's own hand is sufficient to evoke a sense of ownership or embodiment over the rubber hand. The strength of this sense of embodiment is assessed using questionnaires and a metric called proprioceptive drift. Proprioceptive drift is the linear distance between a subject's actual hand and the proprioceptive sense of where the hand is. Traditionally, subjects are instructed to point with their other hand[119] or verbalize alignment to present hashes[170] along a ruler or other estimator to identify the location of the induced hand. Normally, our sense of self-location is accurate and variability in self-location is low. However, after inducing the RHI, the proprioceptive sense of self is seen to drift towards the rubber hand.

The stronger the sense of false embodiment in the rubber hand illusion, the more pronounced the proprioceptive drift towards the rubber hand.

While powerful, the classic RHI experiment is constrained by physical reality – e.g., the impossibility of superposition of a rubber hand and a subject's real hand – or requires complex experimental apparatus.[170] VR is freed from such constraints. However, prior attempts to implement a VR-RHI were restricted by hardware and design limitations that affected real-world object tracking and precise rendering of complex real-world collisions. For example, a VR-RHI implementation published in 2021[171] was forced to use pre-recorded animations to synchronize virtual rendering of touch with actual touch of a subject's hand, making the induction phase highly stereotyped and unnatural, and dependent on precise execution by the researchers for visuotactile synchrony and alignment. The VR experimental platform presented in this thesis, however, integrates the newest VR hardware and software and can overcome these technical hurdles.

7.3 METHODS

7.3.1 *Participants*

Thirteen healthy individuals participated with informed verbal consent in a protocol approved by the University of Washington Institutional Review Board (IRB). All participants were right-handed adults, as assessed by self-report, and were recruited through email listings. Screening prior to participation ensured that subjects were above the age of 18 and free from cognitive, language, or physical disability, or a history of discomfort and/or nausea induced by virtual reality.

7.3.2 *Task Design & System Integration*

The VR-RHI implementation presented in this chapter integrated the newest collider-based physics system in Unity (LTS 202) with additional external trackers (HTC Trackers 3.0), and support from

the SteamVR hand pose estimator to achieve at-speed rendering of real-world collisions. These components alongside the advances in Unity allowed us to develop a VR-RHI task able to render precise and real-time visuotactile concordance during live induction of the RHI over a purely virtual hand. Leveraging onboard eye tracking in the HTC Vive Pro Eye system, a new gaze-based measurement of proprioceptive drift was implemented and compared to traditional "point to self" behavioral estimation of this drift metric. We hypothesized that a simpler and more innate means of self-localization would better represent the perceptual truth of proprioceptive drift and remove the confound of self-pointing. Finally, the VR environment grants great flexibility in determining what is rendered. Harnessing this, we explored VR-RHI induction when the subject's real hand was not visually represented in VR and when it was rendered using a semi-transparent gloved hand avatar. This exploratory experimental modification was used to evaluate whether (1) knowledge of actual hand position interrupted illusory embodiment, and (2) whether it induced a meta-cognitive awareness of the onset of illusory embodiment – as occurs in some implementations of real-world RHI.[119,172]

Figure 7.1 Task Protocol. Initial measurement phase (that serves as a baseline), the induction phase (where the participant's own hand and the virtual hand are touched), and the final measurement phase (where the participant is again asked to identify the location of their own hand). Semi-transparent hand is location of actual hand and is only for demonstration purposes.

Finally, we also elected to build our experiment in an open virtual environment with a distant, infinite horizon, pleasant bright ambience, and simple experimental objects outside of a realistic gloved hand avatar. This was done to reduce the chance of inducing virtual reality sickness, to make the virtual environment easy to rest in, and to simplify the visual field to only the items needed for the experiment: a floor, a table, hand or hands, and the induction object. During the measurement phases, a clear cyan blue line is used to indicate the location the subject is pointing to, either along the floating ruler during earlier experimental sessions or on the table now.

7.3.3 *VR-RHI Experimental Protocol*

Participants sat at a table adjacent to the experimenter, with their dominant hand placed inside a cloth black glove resembling that depicted in the VR environment during the induction phase (Figure 7.1). For the duration of the experiment, participants wore an HTC Vive Pro Eye VR headset. After donning the headset, participants were handed two VR controllers rendered in VR with left- and right-hand avatars. A small black strap was placed around the index finger of the participants' dominant hand, the hand over which the VR-RHI illusion would be induced, to secure their hand to the controller. A third controller, called the induction object, was used by the experimenter to induce the illusion on the participants dominant index finger over the glove.

Our VR-RHI protocol included the following sequence of actions, depicted in Figure 7.1:

(1) Initial Measurement Phase – baseline self-localization

(2) Induction Phase – colocalized physical and visualized touch

(3) Final Measurement Phase– post-induction self-localization

(4) Illusion Reset - movement or self-touch to reset proprioceptive self-localization

During the initial self-localization measurement (Figure 7.1, left), participants are asked to point and click on a virtual ruler that is placed in front of them in the virtual scene (Measurement Phases). The proprioceptive drift metric is the difference between the baseline and post-induction self-localization measurements, measured in centimeters of drift. The strength of the illusion is also quantified using a traditional questionnaire adapted for use in VR, designed to evaluate strength of ownership, agency, and localization as distinct properties of embodiment.

For the induction of the illusion (Figure 7.1, middle), the virtual hand and the subject's real hand are touched synchronously and congruously. To ensure congruous visual alignment of where the touch was being felt on a subject's real hand and where it was being rendered on the virtual hand, we gently fixed each subject's hand in a grasp of the controller with the index finger extended. This hand position was consistent across participants in our study and between induction sessions within each experimental session.

The final phase (Figure 7.1, right) is a post-induction measurement phase. Here again, any rendering of a virtual hand is removed, and the subject is asked to point to the location of their real right hand using their left hand, using the same mechanism as the pre-induction or baseline measurement from Phase 1. These two pre-and post-induction self-localization measurements are subtracted in order to calculate proprioceptive drift. After the post-induction measurement, we ask either a full (Appendix B) or a modified RHI questionnaire. This VR-RHI protocol was completed multiple times with different offsets to the virtual hand.

7.3.3.1 Gaze Based Proprioceptive Drift

For the gaze-based proprioceptive drift metric, the subject was instructed to use eye-gaze to select where they think their hand is located. During this self-localization measurement, a translucent blue ray is rendered, extending forward from the participant, based on headset tracking and camera

direction. This ray is visible in the VR scene and is used as a pointer to indicate where they believe their actual hand would be if it were resting on a table in front of them in the virtual scene. The Vive Eye Pro VR headset built in eye tracking and eye-tracking SDK enabled this new self-localization measurement.

7.3.3.2 Transparent Hand Avatar

In order to isolate visual from visuo-tactile integration cues in the VR environment, we have added an additional trial in which a second virtual hand is rendered with 25% transparency to visualize the actual location of the subject's hand while still rendering and inducing over the other offset virtual hand.

7.3.4 *Questionnaire*

In refining our study, we updated our approach to the VR-RHI questionnaire (Appendix B). The full questionnaire was too burdensome to ask after every trial, so we elected to ask it only once, at the end of the entire study, and instead asked a modified 5-question RHI questionnaire after each trial. This helped with patient engagement. We selected the questions for the abbreviated questionnaire based on subject comprehension -- some questions were consistently confusing and demotivating -- and correlation with illusion induction. The abbreviated questionnaire captured the key components of the illusion: embodiment/ownership, self-localization, agency. Catch questions were included to confirm faithful report of the subject's experience:

1. I felt as if I were looking at my own hand. (*Embodiment/Ownership*)
2. I felt as if I had 3 or 4 hands. (*Catch*)
3. I felt as if my hand was located where I saw the virtual hand. (*Self-localization*)
4. I felt as if I could control the movement of the virtual hand. (*Agency*)
5. I felt as if my real hand were turning virtual. (*Catch*)

The questionnaire responses were collected using a Likert scale from -3 to 3. It was collected by asking, “Do you agree or disagree with the following statement?” and then, “How much, on a scale of 1 to 3.” Disagreement scores were coded as negative. Uncertainty or inability to agree or disagree was coded as a zero score. Because subjects are in VR, they are not able to take a pen-and-paper version of the questionnaire, and we found the above approach to be the simplest was of eliciting a verbal Likert score.

The complete questionnaire was asked at the end of the experimental session (Appendix B).

7.4 Behavioral Results

7.4.1 *Questionnaire Results*

Figure 7.2 depicts the Likert scale ratings of each subject for the five questionnaire items as they relate to offset. Each color depicts a different trial with a different offset, ranging from 30 cm to

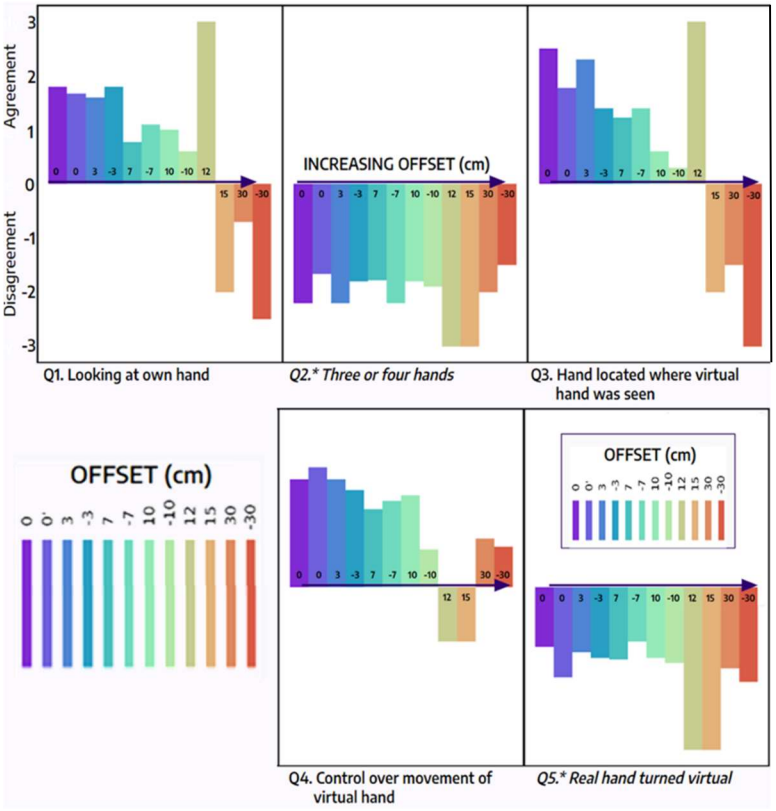

Figure 7.2 Modified Questionnaire Results. Asked after each RHI trial, Questions 1-5 evaluate embodiment, a catch question, self-localization, agency, and a final catch question, respectively. Catch questions ensure subjects are answering attentively and not merely trying to “please” the researcher. The colored bars in each plot represent one trial at the labelled offset in cm. Offset magnitude increases from left to right. For the two catch questions (2 and 5), the answers are consistently negative with no trend across offset magnitude. For Questions 1, 3, and 4, there is a positive response endorsing embodiment, self-localization, and agency following illusion induction, until a critical offset is reached. After ~12cm of offset, these subjective responses deny illusory embodiment, self-localization, and agency.

the left of the subject's real hand to 30 cm to the right of the subject's real hand. The more strongly the subjects agreed with the questions, the higher the bar. This visualizes how strongly subjects agree or disagree with different components of embodiment and the relationship of these subjective responses with increasing offset magnitudes. Questionnaire results (Figure 7.2) also indicate that embodiment over the virtual hand was induced, however as offset increased, the Likert rating slowly diminished. When offset magnitude reached 12-15cm, the Likert rating inverted, suggesting a maximum threshold of offset for which the VR-RHI may be induced.

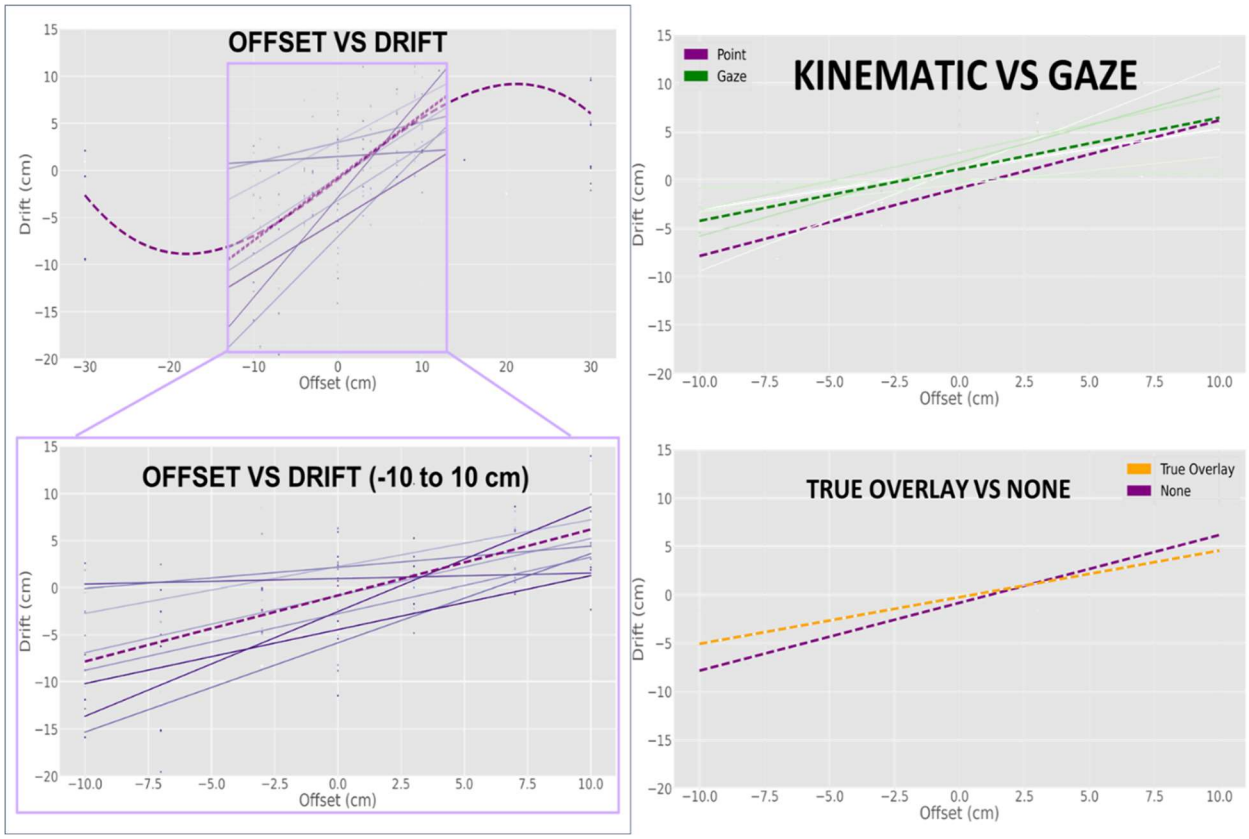

Figure 7.3 Proprioceptive Drift Results. (left) The two graphics forming the left column depict the results of proprioceptive drift by virtual offset. The lower graphic depicts the inset from the top graph and shows only offsets up to 10cm to the left (towards midline, negative offset) or right (lateral from body, positive offset) of the subject's hand. All subjects were right-handed and RHI induced on the right hand. These graphics show a strong linear relationship between drift and offset within the 10cm displacement (individual regressions in solid lines, average regression dotted). (top right) Drift measured using eye gaze still shows a linear relationship between drift and offset, but a weaker (flatter) correlation. (bottom right) Drift measured while a transparent indicator of actual hand position was rendered still shows a linear relationship between drift and offset, but a weaker (flatter) correlation.

7.4.2 *Relationship Between Offset & Proprioceptive Drift*

Proprioceptive drift towards the virtual hand was recorded following induction of our VR-RHI at offsets as extreme as 30cm between the virtual hand and our subject's actual hand. On average, strong proprioceptive drift was seen only at offsets ranging from 0 to 10 cm in either direction (Figure 7.3). This suggests a limit to RHI induction that corroborates the questionnaire results. A strong linear relationship between drift and offset suggests the VR-RHI paradigm we developed was highly effective at inducing a sense of embodiment and self-localization.

7.4.3 *Effect of Gaze & Overlay*

Proprioceptive drift measured using eye gaze also showed drift towards the virtual hand after RHI induction, though the strength of proprioceptive drift was less significant. This suggests that eye gaze may be a more accurate way of collecting self-localization measurements in VR-RHI as self-gaze seems less proprioceptively influenced by the visuotactile congruency of RHI, compared to self-pointing.

To replicate the real-world RHI experiment more strictly and to explore the limits of VR-RHI induction, we collected additional trials in two subjects in which a second virtual hand was rendered with 25% transparency. This exploratory study (Figure 7.33) still demonstrates a proprioceptive drift that follows offset. This parallels real-world experimentation, but was a surprise, nonetheless. Even when these subjects could see where their real hand was, the VR-RHI illusion of embodiment over the ”touched” virtual hand was significant enough to induce drift in self-localization.

7.5 DISCUSSION

Proprioceptive drift towards the virtual hand was observed at offsets as extreme as 30 cm, though strong embodiment as indicated by proprioceptive drift and questionnaire response seemed confined to offsets of up to 10 cm. Data from our healthy, right-handed human VR-RHI participants (n=13) demonstrated a strong bounded, linear correlation between VR render offset and proprioceptive drift, but only for render offsets within about 10cm of the correct hand location. This suggests that greater offset displacements are not "believable." There also seems to be greater accommodation of medial vs. lateral offsets. A slight difference in the extent of this believability in lateral (rightward) verses medial (leftward) offsets of the right virtual hand suggest different tolerances for medial and lateral offsets in the induction of the embodiment illusion.

When evaluated by self-gaze, the magnitude of perceptual drift towards the virtual hand was reduced. These results suggest that using gaze may refine the proprioceptive drift metric by minimizing the required movement of the subject's body and contralateral hand while self-localizing after RHI induction. Self-gaze may be a more accurate form of self-localization for future (VR) RHI studies. Movement during pointing may be a confound.

In trials in which the actual location of the subject's hand was also rendered, making the offset of the induced object explicit, our results demonstrate preserved, illusory embodiment and proprioceptive drift, despite knowledge of the actual hand position. This may suggest that visuotactile integration cues play a more significant role in embodiment than "prior knowledge" or that tactile integration cues play a more significant role than vision in embodiment.

Overall, our results suggest a strong illusion of embodiment induced by our VR-RHI protocol.

Chapter 8. Neuroethics for Engineers: Practical Considerations

In this chapter, I discuss both my work with the IEEE Brain Neuroethics community and present a secondary neuroethical evaluation of VR as a nascent technology with potential application to brain computer interface (BCI) development.

8.1 That's My Brand, Baby: Speculative Neuroethics

In a 2019 IEEE Brain Talks podcast, Dr. Joseph J. Fins, M.D. and Professor of Medical Ethics at Weill Cornell Medical College in New York, replied to a question about the definition of neuroethics by stating that there wasn't "an overall generic take" or consensus about what neuroethics is or even really, what it hoped to accomplish.[173] He offered that there was "speculative neuroethics that's concerned about cyborgs, neuro-privacy, enhancement and transhumanism" – but this, he quickly clarified, was *not* his brand of neuroethics.

It turned out, however, to be exactly my brand of neuroethics. Or, at least, the one I enlisted to serve.

As a veteran of the US Navy, medical student, and practicing neural engineer, I joined the IEEE Neuroethics Framework team and, given my experience, was assigned as an author to the Military Working Group and as an editor to the Medical Working Group. My two main goals in joining the IEEE Neuroethics team were **(1)** to work directly with neuroethics framework development to help build something useful to the neural engineering community, and (2) to hopefully transmute my perception of neuroethics from something gossamer – trivial at best and encumbering as worst – to something with practical utility and value. In the end, I learned a great deal about the challenges of founding a new brand of research, the earnest goals of neuroethicists, and some of the challenges facing this nascent field. Looking back, I would say my job as both a veteran of the US Armed

Services and a BCI neural engineer was to help bring speculative neurotechnological fiction and Hollywood-inspired visions of armed service a little closer to reality.

It is worth noting that had I not volunteered to join the IEEE Neuroethics Framework, the Military group would not have had a BCI or neurotechnology engineer on the team. This would have been disastrous, truly. Engineers and researchers must be actively recruited to neuroethics efforts. I would go further: neuroethics framework development should not be attempted in the absence of domain-expert stakeholders, including engineers, foundational researchers, and those delivering the technology to the public (i.e., physicians).

As far as my two goals for joining the IEEE neuroethics effort, I hope I helped create something useful, and while I leave my PhD with a sustained belief in the easy encumbrance of neuroethical frameworks, I now also believe in the useful potential of neuroethical study.

> *A task such as this should not simply be a group of people sitting around a table trying to reach some consensus, and then being satisfied enough to pat ourselves on the back, and merely stop at that point. Rather, the idea and plan is to approach this in a way that is going to create a body of work, a set of ethical guidelines, that is—and will be—highly usable beyond the scope of our meeting tables.*
>
> *And while this project represents a two-year effort, we see it as a rung—albeit hopefully an important and meaningful one—on an ever-extending ladder of neurotechnological developments and neuroethical address. To such ends, we view our work as part of a considerably larger work in progress, and one to which we are proud to contribute.* – Dr. James Giordano, founder of the IEEE Brain Neuroethics Subcommittee[174]

The complete neuroethical framework documents developed by both the Medical and Military Working Groups will be released in 2023 as the IEEE Neuroethics Framework: "Addressing the Ethical, Legal, Social, and Cultural Implications of Neurotechnology."[175]

8.2 Overview of a Nascent Field

8.2.1 *Definitions A Priori*

The NIH Brain Initiative currently defines neuroethics as "an interdisciplinary research area that focuses on ethical issues raised by our increased and constantly improving understanding of the brain."[176] A later Brain Initiative summary document answers, "What is neuroethics?" with "A tool for the advancement of neuroscience."[177] In the *Brain 2025: A Scientific Vision*, the document outlining the goals of the 2014 NIH BRAIN Initiative, neuroethics was tasked with ensuring that "brain research … proceed with sensitivity and wisdom" as it entails both bioethical challenges and "special ethical considerations."[178] This document clarifies that:

> *Because the brain gives rise to consciousness, our innermost thoughts and our most basic human needs, mechanistic studies of the brain have already resulted in new social and ethical questions. Can research on brain development be used to enhance cognitive development in our schools? Under what circumstances should mechanistic understanding of addiction and other neuropsychiatric disorders be used to judge accountability in our legal system? Can civil litigation involving damages for pain and suffering be informed by objective measurements of central pain states in the brain? Can studies of decision-making be legitimately used to tailor advertising campaigns and determine which products are more attractive to specific consumer bases?*[178]

The first neuroethical society, the International Neuroethics Society (INS), founded in 2006, defines neuroethics as "a field that studies the implications of neuroscience for human self-understanding, ethics, and policy." [179,180] In 2014, they identified in the top 12 areas of neuroethical consideration to include human enhancement, decoding mental states and decision making, and neuromarketing and addictive technologies, alongside more traditional bioethical considerations of device safety, patient consent, data transparency, and social stigma.[179] One of the challenges

facing the field of neuroethics is to distinguish itself from merely bioethics applied to interactions with the brain.

> *What neuroethical issues does the BRAIN Initiative prompt? Some are familiar bioethical issues pertaining to studies with humans, such as questions around acceptable degrees of risk for human patients, necessary levels of antecedent evidence before human trials, consent capacity, data sharing, privacy and confidentiality, and concepts of agency, identity, and normality. Often the context of neurotechnology research, development, and widespread application brings these familiar issues into sharper relief.*
>
> *In other cases, new ethical issues arise because the brain is the organ of the mind. Novel neural circuit monitoring technologies may be able to record brain activity underlying thoughts and moods, which will pose ethical, legal, and societal questions. Some of those issues may arise even before the technologies can be applied to living humans. Small scale circuit function can be studied in brain tissue that can be kept alive for days after removal from surgical patients.* ***At what point do we worry about decoding a person's memories stored in the tissue?***[181]

As evidenced by the above, current definitions of neuroethics are not exactly definitive. Rather, they tend to be skirting mashups of the words: ethics, brain, decoding, technology… etc. This highlights the real, daunting task of drafting a practical document guiding discussion and application of concepts from a new field still defining itself. On top of this, neuroethics seems very willing to onboard the role of speculator and to deal, occasionally if not in the end, definitively, in the purely *what-if*. This places on the shoulders of new neuroethicists the challenge of convincing colleagues of their speculative insight and its relevance.

In *Insiders and outsiders: lessons for neuroethics from the history of bioethics*[182], Dr. Winston Chiong notes that ultimate acceptance of bioethics as a valuable field of study relied on the (financially-valuable) integration of bioethicists into existing medical consults. At the time, these "bed-side consults" brought together clinicians, administrators, and other stakeholders to work

through ethically and medically complex decisions. Dr. Albert Jonsen, author of The Birth of Bioethics, believed that this practical integration

> *.. saved the life of bioethics, which (although it had no name in those years) was threatened by huge questions that drew it up into a hot air balloon of speculation. The ethical concerns had no purchase on concrete problems until the researchers and transplanters set to work on patients. Clinical ethics and research ethics (in the restricted sense of protection of human subjects) became the matter of bioethics and gave rise to its methods.*[183]

Neuroethics, currently caught up in its own hot air balloon of speculation, is earnestly searching for the same opportunity to ground and define its place alongside bioethicists, engineers, researchers, clinicians, and administrators in the broad field of neurotechnology. Neuroethics, in the words of Al Jonsen, belongs somewhere in the "unexplored continent lying between the two populated shores of ethics and of neuroscience." I believe neuroethics will define its own land, eventually. Until then, neuroethicists remain eager to ply their "disciplinary expertise in the human experience" to attain the "central tenant of neuroethics: to integrate the human experience into neuroscience." [184,185] This, truly, means absolutely nothing yet, but it is a sufficient placeholder for now.

8.2.1.1 Bid for Inversion: The Neuroscience of Ethics

For completeness, it is worth noting that there was a popular early proposal that the definition of "neuroethics" should encompass both the ethics of neuroscience and the neuroscience of ethics, with the latter studying the neurological basis of ethical thinking and ethical behavior.[186] Although this proposal was correct in identifying this latter aim as "an aspect of neuroethics that [would] distinguish it from traditional bioethics," [187] the proposal failed to address how this would

distinguish neuroethics from neuroscience, which has tackled the behavior and neurobiology of such topics for decades.[187]

8.2.2 *Methods of Speculation*

The most commonly stated goal of neuroethical research is to identify and stratify the challenges that a given neurotechnology may someday encounter, in order to mitigate negative outcomes by designing and engineering solutions to these potential challenges as early as possible in the development cycle of the new neurotechnology. In the Neuroethics Guiding Principles for the NIH Brain Initiative[188], neuroethicists are encouraged to "anticipate special issues related to capacity, autonomy, and agency" -- an admonition only second to assessing safety.

> *When we think about neuroethical questions when we're initially conceptualizing research, we can usually do a better job of anticipating challenges that might come up later in research.*[189]
>
> - Lauren Sankary, JD (Health Law & Bioethics, Cleveland Clinic).

> *Neuroethicists can help scan the horizon and assist in anticipating and navigating ethical concerns … [to] empower a neuroscience research team and help to inform how studies are designed, conducted, interpreted, and applied.*[177]
>
> - The Brain Initiative 2022 Summary Document

> *Neuroethics was not a policing mechanism for scientists, but instead offered strategies: serving a horizon-scanning function, anticipating ethical roadblocks, and surfacing and sometimes challenging unspoken assumptions of neuroscience research. Neuroethics could in this way ultimately advance and even accelerate good neuroscience.*[190]
>
> - Karen S. Rommelfanger, Founder of the Institute of Neuroethics[191]

> *An important, accepted role for neuroethics is an anticipatory one: to view emerging applications of neurotechnology through a lens that seeks to identify and prepare for both benefits and potentially unwanted outcomes.*[185]
>
> - Nita Farahany & Khara M. Ramos

Types of Neuroethics Research

Conceptual

- Analysis of specific concepts such as privacy or personal identity
- Philosophical research about normative questions (i.e., What ought to constitute desirable or acceptable social behaviors?) or theoretical questions (i.e., What is consciousness and how can neuroscience inform how consciousness in conceptualized?)
- Examples: How should one define and treat people with various levels of consciousness? Does fluctuating capacity from disease, a brain injury, or a brain intervention indicate a need to rethink informed consent?

Conceptual and normative neuroethics research may draw from existing literature and theories, as well as practices from law, philosophy, theology, and neuroscience.

Empirical

- Systematic data collection to ascertain views, values, or practices of researchers, patients, research participants, or the public; testing the application of norms, principles, etc.
- Use of social-science methodologies such as quantitative surveys or qualitative interviews, experimental designs for testing the impact of interventions and/or other experimental manipulations.
- Examples: The BRAIN Initiative® has funded a number of neuroethics empirical projects.

Figure 8.1 Types of Neuroethics Research. This inset text box produced by the BRAIN 2.0 Neuroethics Subgroup of The BRAIN Initiative®, outlines the research methods of neuroethics. Conceptual research is expected to incorporate theories of law, philosophy, theology, and neuroscience to research normative and theoretical questions or to analyze existing concepts (e.g., privacy, personal identity) in the context of a developing neurotechnology. Empirical neuroethical research is expected to collect and present data from quantitative surveys, qualitative interviews, or behavioral experiments to test the impact of interventions. In neuroethics, empirical seeks to understand the views, values, and practices of a specific population of stakeholders in a new neurotechnology.

To accomplish this, neuroethicists engage in both conceptual and empirical research (Figure).[192] Conceptual studies may include analysis and definition of key concepts, classification of the values at odds in ethical challenges, evolution of ethical theories, and the review of legal and ethical precedent, while empirical research often involves interviews and surveys to evaluate the various perspectives of identified stakeholders in any issue. Neuroethicists are encouraged to use these modes of investigation to anticipate and mitigate the value conflicts that may exists between relevant parties (e.g., navigating the competing interests in neural data privacy among administrators, researchers, clinicians, and clinical subjects).[177]

8.2.3 *Reframing Existing Frameworks: The New Framework*

Frameworks provide a structure from which to approach the open-ended world of neuroethical evaluation and, importantly, enable researchers from other fields, engineers, and clinicians to apply a neuroethical lens to the evaluation of their own work and ideas. It is recommended that a validated neuroethical framework be used to define what questions to ask and to decide which of the available neuroethical research models or study designs are appropriate for answering these questions.[185] Ethical frameworks generally offer a series of themes or open-ended questions to guide neuroethical evaluation, with suggested subthemes and often a nudge towards previously accepted conclusions. This encourages continuity in ethical research, prompting either explicit agreement or disagreement with prior understandings. In this regard, neuroethical frameworks are "alive" in that they are under constant revision and reformation, being confirmed, refined, and redefined over time by the contributions of various practicing neuro- and bioethicists.

It was in this spirit of framework refinement and perhaps standardization that the NIH Brain Initiative Neuroethics Subgroup, following the success of the framework developed by the international Human Brain Project, proposed the formulation and articulation of a new comprehensive neuroethics framework (Appendix C). The high-level goal of the NIH Brain Initiative Neuroethics Subgroup was to make progress along three main thrusts: (1) stakeholder empowerment: funding and integrating more stakeholders to "write a complete standalone neuroethics roadmap and then integrate [it]," (2) training: converting "online, non-interactive, multiple-choice-based learning" to more interactive options that promote collaboration without losing affordability and scale, and (3) framework development,.[190]

In response to the call for inclusive framework development, IEEE Brain established its own Neuroethics Subcommittee in 2021 to begin development of a robust neuroethical framework to

be named, "The One to Rule Them All." Just kidding[13] – to be named, "Addressing the Ethical, Legal, Social, and Cultural Implications of Neurotechnology."[175]

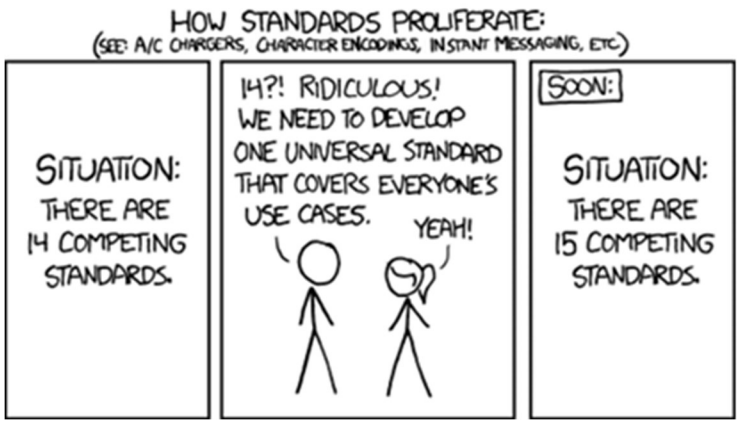

Figure 8.2 Standards Proliferation. "Fortunately, the charging one has been solved now that we've all standardized on mini-USB. Or is it micro-USB? [Oh no!]." Famed xkcd[77] comic humorously outlines the well-intended process of standards proliferation.

8.2.4 *ELSCI & An Interdisciplinary Salad*

The new IEEE Brain Neuroethics Framework uses the widely accepted Ethical, Legal, Social, and Cultural (ELSCI) implications framework – in contrast to the Responsible Research and Innovation (RRI)[14] framework used by the EU Human Brain Project and with the addition of Cultural implications beyond the classic ELSI framework. The IEEE Brain Neuroethics effort consists of multiple, independent working groups, each assembled as a salad bowl[184] of volunteers from relevant fields, all tasked with the development an ELSCI-structured document detailing the neuroethical implications of contemporary neurotechnologies and methods, as they apply to a particular domain. Each of the domains, called Applications, were addressed by a different group to include. These domains include: medicine, wellness, education, work and employment, military and national security, sports and competitions, entertainment, the legal system, and marketing and

[13] The IEEE Neuroethics Framework is expected to be released sometime in 2023 under the title: "Addressing the Ethical, Legal, Social, and Cultural Implications of Neurotechnology."[175]
[14] The framework of Responsible Research and Innovation (RRI) promotes a multidisciplinary approach to evaluating the ethical, philosophical, societal, and regulatory tangles that may accompany advanced brain research. The goal of RRI is to facilitate "a future where responsible digital brain research is proactive in its recognition of existing and emerging societal and ethical challenges."[192]

advertising. This matrix of working groups and considered neurotechnologies is visualized in Figure 9.2 of Appendix C.

The final IEEE Brain Neuroethics framework documents are expected to be released in 2023 and are intended to "provide the basis for the development of a set of guidelines for engineers, researchers, applied scientists, practitioners, and neurotechnology companies that will help ensure the responsible development and use of new neurotechnologies."[175,193]

8.3 SPECETH: NEUROETHICS IN A MILITARY CONTEXT

8.3.1 *Acknowledgement*

Over the course of 2021 and 2022, I worked as an author and member of the Military and National Security Working Group. Subsequent statements and discussion in this chapter reflect the still ongoing[189] collaboration and dialogue among our "salad bowl" of engineers, scientists, clinicians, ethicists, sociologists, lawyers, and other stakeholders. The text has been heavily modified and condensed to suit the purposes of framing the "Military Culture" section of which I was sole author. Outside of this section, any direct quotes are indicated as such.

8.3.2 *Statement of Intent*

Military use of any biomedical technology creates a complex layering of stakeholders and competing values that exist in tension between operational requirements and the traditional bioethical principles of autonomy, beneficence, nonmaleficence and justice.[194] These principles may even acquire conflicting interpretations when a particular technology is required to achieve legitimate military objectives. For example,

> *… does increased operator effectiveness outweigh the potential risks to autonomy and wellbeing? Should the use of technology that increases military efficiency and protects operators during combat operations override individual*

> *consent? … Is operator enhancement just[?] … do the goals of national security supersede adherence to bioethical principles?*

To facilitate posing and answering relevant neuroethical questions, the ELSCI neuroethical framework was utilized. This framework was selected for use by every IEEE Brain Neuroethics Working Group in order to provide "a system for ordering thought… a tool kit for risk assessment." Additionally, the ON-RAMP framework, discussed below, was introduced by the Military Working Group as a "methodology for operationalizing the [ELSCI] construct into the design process."

Ultimately, this document was written to facilitate ELSCI consideration during neurotechnology development for specifically military or national security purposes and is geared toward use by the neural engineers and developers of neural technologies for that domain. The goal of this document is to help build "a comprehensive understanding of consequences and implications [of neurotechnology] so all involved are responsible stewards of the technology."[189]

The authors acknowledge that although many of the discussed neurotechnologies are still in preliminary development, insightful speculation may identify and stratify potential long-term impacts of these technologies. Early consideration of potential negative outcomes or unintended use may facilitate development of alternative technology or strategies in response to projected long-term costs. Our intent is to mitigate foreseeable, preventable adverse outcomes. This is especially important in light of the fact that technologies for military use often develop in isolation from academic, commercial, and medical domains, but often transition from military to non-military (i.e., civilian) use, eventually.

8.3.3 *ON-RAMP: Operationalizing ELSI*

This working group introduced another accepted framework for neuroethical assessment of neurotechnological interventions called the Operational Neuroethical Risk Analyses and

Management Paradigm (ON-RAMP).[195] This framework is an open-ended pipeline of specific questions, designed for end-users who are not necessarily trained neuroethicists. The sequence includes the six Querying Ws (who, what, why, where, when, which), the six Framing Cs (capacities, consequences, character, context, continuity of care, consent)[195], and six Additional Consideration Rs (responsibility, realistic assessment, research, responsiveness to burdens, revision, and regulation).[189] The Querying Ws are designed to help "gather and assess all relevant fact", including the circumstances of the case, the parties involved and their respective roles, and the ethical issue or problem at hand. The Framing Cs are used to identify relationships between relevant facts, possible actions toward resolving issues or problems, and potential trajectories, outcomes, and effects of these actions. The Additional Consideration Rs are designed to help determine what actions would maximize the in-context, beneficial consequences. Champions of

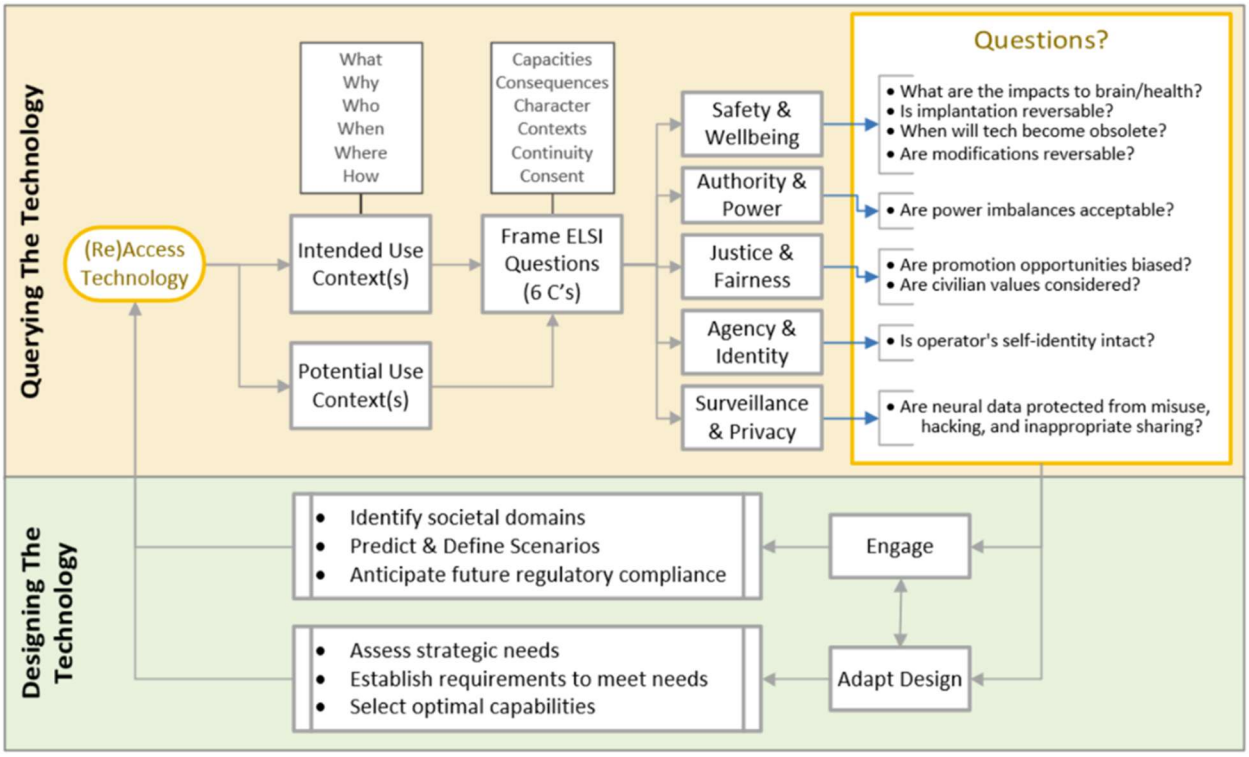

Figure 8.3 Operationalizing ELSCI with ON-RAMP. The discretized 18-step Operational Neuroethical Risk Analyses and Management Paradigm (ON-RAMP) was integrated into the overall Ethical, Legal, Social, & Cultural Implications (ELSCI) workflow to facilitate thorough neuroethical evaluation of a given neurotechnology or method.[168]

this framework believe it better captures the risk assessment context of ethical challenges and guides the implementation of ELSCI. Figure 9.2 was used to elucidate the intended workflow of neuroethical framework implementation.

8.3.4 *Scope & Terminology*

Neuroethical analysis was limited to ELSCI considerations. Both a traditional bioethical evaluation and evaluation of the weaponization potential of neurotechnology were deemed out of scope for the Military Working Group. Table 8.1. lists important terminology and definitions.

Terminology	Definition
Military	Any state-sponsored entity that engages in the use of force at or beyond the borders of the nation state
Operator	Any human agent of a military
State	All levels of government
Military Technologies	Any hardware, software/algorithm, or biological solution designed to improve the offense or defensive capacity of a military entity
Recording/ Sensing	Detect and interpret ongoing brain activity to facilitate teaming, machine-human interaction, cognitive enhancement, neurorehabilitation
Stimulating/ Actuating	Modify behavior or cognitive function through invasive or non-invasive technology (e.g., transcranial electrical stimulation)
Closed Loop	Closed-loop technologies record and modulate brain activity to titrate parameters in response to individual response and situational demands

Table 8.1 Terminology. Table extracted from text of the IEEE Brain Neuroethics Framework – Military Working Group document but is unique to this thesis.

8.3.5 *ELSI of ELSCI: Overview of Ethical, Legal, Social Implications*

8.3.5.1 (Bio)Ethical Implications

The specific subcategories of Ethical consideration within ELSCI were defined in the IEEE Brain Framework template as: safety, well-being, and risk; authority and power; justice and fairness; agency and identity; surveillance and privacy.

Safety, Wellbeing & Risk

While it is evident that safety for both short- and long-term implants must be assessed, this working group notes that "military use of enhancement neurotechnology is not to achieve a medical benefit, but rather to achieve mission success" and that "there may be no discernible benefit for the individual operator." Additionally, operators are often younger adults with still-developing neurological systems and present additional challenges in predicting long-term consequences of implanted neurotechnology. This group also recognizes "moral injury" as a risk, should there be ambiguity in the locus of decision making during operational engagement (see Agency). The working group explicitly advises:

> *Augmentations that render people as "single use" operators, not able to return to their pre-augmented selves but no longer "usable" due to technological advancements, should be considered unethical. Care must be taken during the design phase to proactively plan to maximize the lifecycle of the enhancement and ease the transition if/when it is removed or no longer used.*

Limited options for post-operational transition exist. Namely, the device can be (1) removed, (2) deactivated but remain implanted, (3) demilitarized so it retains some but not all original capabilities. For each of these scenarios, the biological, psychological, and social impacts must and have yet to be assessed.

Authority & Power

As operators must follow all legal directives from superiors in their chain-of-command, they may feel compelled to participate in even voluntary neurotechnological enhancement, if advocated by leadership. Moreover, there are non-experimental medical procedures operators are unable to refuse (e.g., vaccinations).

> *As combat readiness requires thorough physical and mental training, technology that enhances preparedness, overcomes fatigue, and accelerates skill acquisition has the potential to be mandated without individual consent.*

Justice & Fairness

In neuro/bioethics, justice refers to the fair distribution of the "benefits and burdens" of a technology.

> *Neurotechnology may not have the flexibility to enhance all users. This places a selection bias in favor of those amenable to neurotechnological enhancement, and thus may violate the principle of justice by limiting the distribution of the benefits of neurotechnology.*
>
> *We acknowledge that hand in hand with this unequal distribution of benefits may also be the unequal distribution of burdens.*

Regarding military context, we speculated that neurotechnological enhancement could be used to incentivize military recruitment, and perhaps the benefits and "the burden[s] of neurotechnological modification could become concentrated in more socioeconomically vulnerable sectors of society."

Agency & Identity

In neuroethics, agency is "the capacity of individuals to act independently, to make their own free choices, and to self-initiate actions." Neuromodulation can influence behavior and may interfere

with an operator's agency. Neurotechnology that influences an operator involuntarily would violate agency and identity[15]. This group also identified that neural enhancement could precipitate:

> *.. an increase of concentration, resilience, or other decision-making elements [that] may make it easier for the individual to be responsible for his/her/their own actions. Particularly in the specific cases of neuro enhancement that aims to reduce negative effects of stressful situations, a higher level of control--agency-- could be afforded that increases an individual's precision or stamina as well as optimized agency and legal liability.* (sic)

Finally, changes in personality, concepts of self, and expressed values have been reported with stimulating neural devices, which may lead to positive or negative perceptions by self and others, and alterations to a patient's sense of self-identity.[196] The working group noted that changes to an operator's perceived identity by others includes the adversary's perception. The consequences of this are unknown.

Surveillance and Privacy

This working group defines neural data as any "direct neural signal measurements as well as any information that can be used to deduce the identity of existing neural signal measurements, [or] infer about neurological states and traits." Examples of inferential data include sensorimotor response times or ocular dynamics including pupil reactivity. Especially in combination, neural and psychographic data[16] could be used to target an operator's cognitive or emotional vulnerabilities. Therefore, "considerable thought should be given to what types of data are stored in association with others, and how a hack in one part of a stacked system could …[confer] access to other associated data." At minimum, neural data must be encrypted.

[15] The final document includes a summary line within this heading that states: "Operators should not feel that they are tools for military use." I have repeatedly recommended this line be removed from the final document as it is deeply out of touch with the nature of military service. There is no question you are a tool for military use. The ethical limits of service are explored extensively in traditional military ethics.

[16] Psychographic data includes personality traits, political orientations, attitudes and dispositions towards specific topics or events, and other psychological indicators.

8.3.5.2 Legal Implications

The specific subcategories of legal consideration within ELSCI were identified as: informed consent, privacy and data ownership, and responsibility and accountability.

Informed Consent

In 1947, The Nuremberg Code[197] set a minimum standard of voluntary consent. Consent requires legal capacity, thus excluding minors and people with mental disability, and decisional capacity, free of force, fraud, or deceit, etc. Additionally, article 13 of the Geneva Convention states that:

> *In particular, no prisoner of war may be subjected to physical mutilation or to medical or scientific experiments of any kind which are not justified by the medical, dental or hospital treatment of the prisoner concerned and carried out in his interest.*[198]

Informed consent requires that a subject understand the procedure and potential outcomes, positive and negative. Finally, the procedure itself must meet the conditions of Necessity and Proportionality. Necessity requires that a procedure be the least harmful option to achieve a specified goal, and Proportionality requires that the benefits of a procedure outweigh the costs. In practice, proportionality is also interpreted to indicate that the benefits must be certain, and not eventual or marginal.

Under the Defense Authorization Act, however, the U.S. President is authorized to waive informed consent in military operations "if the President finds that obtaining consent is infeasible or contrary to the best interests of recipients," or if the process of obtaining consent runs contrary to national security interests. In Rempfer v. Sharfstein[17], the court ruled that consent can be waived "only if the President determines, in writing, that obtaining consent is not in the interests of national security."[199] Finally, if informed consent and legal representation is not possible, then informed consent can be waived only if treatment is urgent and there is a low level of risk for the individual.

[17] The US Army administered experimental anthrax vaccines to servicemembers without obtaining explicit consent.

Privacy & Data Ownership

There is ample existing regulation of personal identifiable information (PII) (e.g., name, address, date of birth) and experimental data. For example, in the US, the Federal Privacy Act of 1974 protects PPI from being released without written consent[200], and *Protection of Human Subjects and Adherence to Ethical Standards in DoD-Conducted and Supported Research* Title 32 and DoD Instruction 3216.02 collectively regulate data management for operators. Additionally, data management plans must specify how data "will be stored and protected, who will have access, how PII will be protected, and [how] data will be archived and or destroyed after a study is closed" and must be approved by institutional review boards (IRB) prior to study enrollment.

> *To protect against the inappropriate, or misuse of neural data, data ownership should be clearly defined and understood by all parties. Data ownership involves the possession, protection, and responsibility for information.* (sic)

Of interest, Chile was recently the first country to legislate specific protection for "neurorights," giving brain data the same status as an organ to make it illegal to buy, sell, traffic, or manipulate neural data. The Chilean Senate amended their constitution in 2021 to protect "mental privacy, free will and non-discrimination in citizens' access to neurotechnology." In October of 2022, the United Nations Human Rights Council (UNHCR) adopted by consensus a draft resolution identifying neurorights as an important human rights issue that requires more study.

Responsibility & Accountability

Criminal responsibility is predicated on volition and culpable mental state. With certain neurotechnologies, particularly BCI, culpability may be nuanced and difficult to conclude. Moreover, future integration of neurotechnology and artificial intelligence and big data may "create increasingly networked minds such that the locus of decision making will not always be

clear." Again, legal culpability necessitates that a person's actions were intentional. Determining the locus of agency in implanted neurotechnology and BCI will have significant legal ramifications. Neurotechnologies will need to clarify:

> *Are [they] registering intention at the neurological level? Are they detecting "neuro-correlates" of intention—that is, they are suggestive of (but not in themselves) intention? Or do they represent something else entirely?* (sic)

8.3.5.3 Social Implications

This working group identified the importance of tracking social narratives to understand how enhancement of professional operators, including militarized domestic security forces and police, may impact civilian trust of these personnel. We highlight "the importance of accurate and proactive communication with the public" about the limits and realistic capacities of neurotechnology in order to mitigate the impact of bombastic speculation. We then speculated that "societal tensions between adopters and nonadopters of these technologies" could someday arise, leading to "a stratification of society based on personal decisions around technological enhancement." It was suggested as well that:

> *Neural damage from a directed energy weapon may resemble other neurological syndromes, and may be suspected as either delusional or psychogenic by physicians, which could have the effect of increasing paranoia in the population. ... [And] this fear and paranoia might be further leveraged by adversaries to create social division by encouraging polarizing narratives among a population.*

Militarized neural training could also permeate society as entertainment or "brain-training." Integration of neurotechnology with extended reality (XR) devices, including virtual (VR) and augmented reality (AR), may have a profound an impact on social environments. It was suggested that this could lead "to the erosion of shared realities and truths" and that,

> *Any development of these technologies, much less "war-gaming" with them to identify potential scenarios arising from their deployment, are likely to feed into conspiracy theories, which may have tremendously significant political consequences. … Precedents exist that suggest that public awareness of these "games" will be misunderstood or misportrayed to suggest that the deployment of the harm agent was planned, rather than predicted.* (sic)

In this example, it was noted that "[war]gaming is a tool that policymakers use to evaluate the consequences of policies and strategy, for example, of downstream likelihoods to more widely or narrowly distributed defensive measures against neuroweapons." We also acknowledged that neurotechnology could remap notions of "disability" and "normalcy."

8.3.6 +*Cultural*

8.3.6.1 Statement of Authorship

The IEEE Brain Neuroethics Framework suggested the Cultural considerations within each domain include "cultural differences in acceptance and use," as well as "potential to foster or threaten intra-group culture" (Figure 9.2). The following text is from my section evaluating the ELSCI Cultural implications that is pending publication with the Military Working Group final document[18]. The subcommittee chairs and editors of this working group's final document are Dr. Seth Elkin Frankston PhD, Research Scientist at the US Army CCDC Soldier Center, and Dr. Diane DiEuliis PhD, Senior Research Fellow and Professor at National Defense University.

8.3.6.2 Military Cultural Implications: ELSCI in context

This section explores the characteristics and considerations unique to military culture and their impact on neurotechnology and the enhanced operator. Understanding the cultural landscape of the armed services may suggest features or highlight unique challenges relevant to the design, development, and implementation of neurotechnology.

[18] As of November 30th, 2022

As with any culture, military culture is defined by a system of values, beliefs, attitudes, practices, meanings, and knowledge. Analysis of military culture has identified cultural competencies commonly used by healthcare providers working with military populations.[201,202] This prior work accounts for a range of "beliefs, values, traditions, behaviors, and events" common to military service and society, including organizational structure, social identity, and cultural norms.[201] Militaries are organized around a chain of command, a formal power hierarchical structure of superior and subordinate personnel. In this structure, superiors (e.g., commissioned officers, non-commissioned officers) provide leadership and model appropriate and expected behavior of subordinate personnel. In addition to a strict adherence to the chain of command, military recruits are trained to prioritize the primacy of the group or mission over the self.[201] This early training instills a set of military values and ethics including the value of the group over the individual, meaning near-term comfort or even health of the individual may come at the expense of unit survival and mission success. This aspect of military culture is often identified as a "warrior ethos". The warrior ethos is driven by a constant physical and psychological state of "combat readiness" that can be seen to subsume one's individuality giving greatest salience to the military identity.[201] Warrior culture is not unique to modern western militaries, Riccio et al. (2004) identified seven attributes common across history and region, including ability to set priorities, make tradeoffs, adapt, accept responsibility and dependence for others, motivation by a higher calling.[203] These military cultural norms can lead to "a belief that personal well-being is trivial and seeking care is selfish."[202]

There is a growing awareness of the need to consider the unique landscape of military culture during the design process, development, and implementation of neurotechnology. For example, members of the military can be reluctant to self-report behavioral health concerns due to significant

stigma around mental health and concerns about career consequences, peer perception, and confidentiality. Despite substantial efforts to destigmatize mental health and a trend for increased resources, members of the military are often still reluctant to seek help.[204] Future hesitancy about health disclosure and distrust of civilian medical care are likely to continue which may cause operators to delay seeking medical care when, for example, when a device malfunctions. A design consideration may be to build neurotechnology devices that "tell" on themselves as they begin to malfunction, to obviate the impact of operator reticence about needing personal care or attention.

As military culture supports the primacy of the group or mission over the individual, operators are likely to onboard short-term mission advantages over long-term personal costs. This suggests the importance of the inclusion of long-term costs of neurotechnology "built in" to the initial costs of onboarding of a neurotechnology program (e.g., funding for the Veterans Administration to conduct a longitudinal study of involved operators) with discussion of medical coverage for potential long-term neurological impacts (e.g., dementia, mental illness). Consideration of long-term consequences is of particular concern given a military culture that tends to reward short-term gain despite long-term consequences. A black box warning may not be sufficient for either discussion of risk prior to implantation or operational limits and risks of chronic use. A design consideration may be to include a governor on a device that the level or duration of activation, thus limiting the need for self-regulation.

Finally, operators may find themselves far from modern medical infrastructure as a consequence of military operations. In addition, military culture tends to be high in focal alcohol consumption ("binge") and risky behavior, including activities like high-risk sky-diving and motorcycle driving.[205] As a result, design considerations may include enhanced durability in extreme environments, ease of explant for field medical extraction, means to rapidly turn the device off if

it is not responding or has been damaged, or preparation for unusual infectious exposure or limited access to standard hygienic practices (e.g., no showers or bathing in parasite-infested waters).

Key takeaway: Military culture maintains distinct organizational structure, social identity, and norms that embody a warrior ethos driven by a constant physical and psychological state of "combat readiness". A thoughtful understanding of military culture may suggest design features and unique challenges (e.g., deployment) for neurotechnology developers.

8.4 On Medical Neuroethics

The IEEE Brain Neuroethics – Medical working group focused on neurotechnologies for (1) diagnosis and evaluation of the brain and nervous system, and (2) research on "disorders, syndromes, and injuries of the nervous system caused by abnormalities in electrical, biochemical, and biomechanical signaling, as well as aberrant neurotransmitter systems."[189] For me, one of the intriguing and most complex topics discussed by this group was the application of implanted neurotechnology for regulating mental illness -- concepts of neurodivergence and neurodiversity, identity, consent, autonomy and even medical beneficence take on challenging nuance in the context of mild, moderate, and severe mental derangement. This group also questioned of the permanence of pre-implant informed consent. When working with chronic implants that may provide therapeutic benefit for decades, alongside acute and progressive side-effects, does pre-surgical informed consent need to be revisited? If so, after some duration of time, a physiologic event, a behavioral change? Finally, concepts of responsibility and identity were explored in the context of experimental neurorehabilitation, in which patients may respond exceptionally well to an invasive neurotechnology as therapy but may be forced to explant when the experimental trial

is over. This is a difficult (and heart-wrenching) reality of limited commercial and experimental resources – and is not speculative and has occurred. Neuroethicists struggle to balance the ideal of ongoing support alongside the costs and trade-offs of requiring post-trial support. Within cultural implications, the medical group identified the social bond of illness and the difficulties that may arise for those who are "rehabilitated" and thus ejected from their social support networks. This was a fascinating document on which to serve as moonlighting editor and very, very green neuroethics student. This working group is chaired by Dr. Jacob Robinson PhD, Professor of Bioengineering, Electrical and Computer Engineering at Rice University, and Dr. Rebecca Monteleone PhD, Professor of Disability Studies at the University of Toledo.

8.5 ELSCI APPLIED: VIRTUAL REALITY

This section presents a brief, independent application of the IEEE Neuroethics ELSCI framework for the ethical evaluation of Virtual Reality. The specific context of VR within a VR Brain Computer Interface (VR-BCI) is discussed at specific points, as well.

Ethics

Ethical considerations of VR technology include the safety and risk of headset display, cost and distributed access to VR technology, identity, and the surveilled data that may be collected or uniquely accessible during VR interactions. Information rich data streams unique to VR could include ocular tracking towards virtual world objects alongside more precise understanding of the relationship between self and environment – remember, everything in VR is precisely trackable over space and time. Regarding identity, VR enables unconstrained self-representation, not bound in any sense by reality. One could foresee a dissociation between physical realities (e.g., physical deformity) and a potentially idealized self-representation in VR. This may offer both personal

benefits and challenges as users navigate the "real" fiction of VR. Within the specific context of VR-BCI, ethical considerations also include changes to agency as the VR world itself may become responsive to and an expression of one's personal will and control, beyond the agency one usually has merely over one's physical self. Navigating agential expansion in VR and VR-BCI may become both ethically and socially relevant.

Legality

Considerations of legal security and privacy interact with the ethical discussion of surveillance and privacy. A legal dimension of these concerns may include whether the information reasonably available to others through use of VR may be used in a court of law or whether it may be considered "in the public domain." VR metadata and tracking data may be compared and contrasted with the information that may be gleaned from in-person or traditional electronics communication channels (e.g., cell phones, social media). Metadata that may be gleaned from a VR environment includes precise movements and controller commands, eye and face tracking, LIDAR and camera-based environment tracking, and microphone and room audio recording. It is unclear whether this rich data may be permissible as evidence or under what constraints, and whether this data may be "mined" by public entities. Exactly how these considerations would be evaluated within a legal context is, of course, left for those with sufficient training.

Society

Societal considerations include both the social benefit and disruptions that VR technology may bring. Societal benefits may include increased accessibility to virtual public spaces by a broader segment of society and access to immersive educational and training content that could be otherwise prohibitive by cost or resources required (e.g., expensive or oversized hardware may be rendered with significant functionality and intractability in VR without requiring the material or

financial resources to *actually* manufacture it). On the flipped side of the same coin, however, only those with a sufficiently powerful VR rig may engage these expanded opportunities. The potential abundance of VR may first need to pass through the chokepoint of hardware access and distribution. Broad VR adoption may also effect social change through competing group preferences for virtual versus 'real life' engagement. This may include changes to work-place engagement with demands (or requests) for virtual presence when working-from-home, or, similarly, to educational engagement. It is unclear if the broad adoption of online socialization in youth has had beneficial or detrimental impacts on identity, social confidence, functional development, etc. VR socialization could present similar developmental effects. One detriment to online engagement has been the challenge of predatory anonymity: underaged youths have been targets of manipulation and coercion to produce sexualized content about themselves.[206–209] It is possible that VR may present another space for predation and could, given to the nature of immersive VR and perceptions of embodiment,[210–212] present a particularly dangerous venue for sexual predation. Careful design of VR environments for protected engagement of underaged youths[213] may become crucial.

Culture

Cultural considerations include differences in acceptance and use across cultural and subcultural groups (e.g., gamer culture). The benefits and detriments of VR are likely to distribute unevenly across the globe, driven not only by hardware and resource distribution challenges but also by cultural adoption. One can image that tech-savvy "gamers" would have not only increased access and opportunity to VR hardware, but also increased willingness to adopt virtual realities compared with communities already less integrated with expansive, electronic worlds (be they immersive virtual or 2d). Culturally dependent rates of VR adoption could exacerbate cultural isolation

between these groups. Alternatively, well-designed virtual experiences also have the potential to engage people more profoundly in celebration of cultural uniqueness and differences. Again, the immersive quality of VR offers something closer to a "real, personal experience" than a story, photograph, or documentary. The nuance of "being there" may add weight to the educational and experiential opportunities that VR may uniquely enable.

Chapter 9. Conclusion

9.1 Review of VR Work

To advance neuroscience and brain computer interface (BCI) development, I designed and evaluated a novel virtual reality (VR) experimental platform integrating VR devices with the hardware of in-patient, intracranial neural recording and neural stimulation research (Section 4.4). I then leveraged this platform (1) to collect a rich dataset of human movement for neural decoding (Section 4.4.5.3), (2) to design new sensory percepts using amplitude-modulated continuous direct electrical stimulation (DES) of the cortex (Section 5.2.3), (3) to integrate this novel neural encoding approach with naturalistic human behavior, recoining this 'neurohaptics' (Section 5.2.4), and (4) to explore the behavioral dynamics and efficacy of a novel bidirectional VR-BCI (Section 6.3.4) in which a simple neural trigger elicits a complex, first-person movement sequence in VR and delivers sensory neural feedback during visible interaction. In this case, it was my first bidirectional VR-BCI user who coined a term: 'cerebronaut,' to describe his experience as the first intracranial, bidirectional VR-BCI operator. In parallel with this work, I led a team of two undergraduate researchers in the exploration of embodiment through an advanced implementation of the classic Rubber Hand Illusion experiment (Section 7.4).

At a minimum, my work proved the merit of virtual reality for flexible, functional, and engaging experimental design with invasive neural recording in the EMU patient population. It also demonstrated the interpretability of continuous temporal variation in neural stimulation, provided information-rich sensory S1-DES feedback by amplitude modulation, and introduced a new experimental approach to self-administered, naturalistic neurohaptic integration. The VR tasks I built captured complex naturalistic behavior (reaching, grasping, throwing, etc.) alongside both subjective and objective measures of neurohaptic efficacy.

In the final VR-BCI implementation, my work introduced a custom pipeline for rapid offline identification of BCI control signals to maximize "plug-and-play" BCI functionality for use with our clinical patients and any population with limited time for BCI training. I also demonstrated a low-bandwidth control signal to trigger complex, life-like behavior in VR. While a neural trigger is the "minimum viable" demonstration of a decoding BCI, only a small adjustment in VR is needed to turn the ½ D neural trigger into a continuous 1D control feature: advance or retreat the VR animation step-by-step in time depending on neural trigger state, instead of playing it all the way through when activated. This is, in fact, the next planned step for the VR-BCI work. Additional plans and ideas for future work are described below.

9.2 Review of Intraoperative Work

The initial neural signals analysis studies completed with intraoperative neural recording and stimulation data demonstrated novel approaches to "neural trigger" (or, neural biomarker) detection. This work informs strategies for the identification of spectral and temporal correlation, and evoked potential features of neural signals to guide DBS programming or drive adaptive DBS design in order to improve therapeutic stimulation in patients with PD and essential tremor. It explored both time-frequency and time-amplitude characteristics of recorded dDBS local field potential (LFP) in ways that were novel and agnostic to defined frequency bands.

While I believe temporal correlation and "stability" analysis may prove very useful in the classification of neural states as biomarkers in PD and essential tremor, the relationship between state and behavior (e.g., does temporal desynchronization of neural activity recorded by dDBS in the STN correlation with parkinsonian symptoms?) requires new study design and experimentation. Additionally, the evoked potential analysis suggested a very clear relationship

between directional stimulation and evoked cortical activity that may be useful in dDBS programming and may also serve as a "stimulated" biomarker of dDBS therapeutic efficacy.

This work also set the stage for both the novel spectral noise analysis I later used to verify the preserved quality of intracranial neural recordings after donning a VR headset, and the rapid neural trigger identification pipeline I designed to allow me to implement the VR-BCI task with a reliable list of potential control signals.

9.3 Review of Neuroethics Work

For over a year, I edited and drafted content with the IEEE Brain Neuroethics – Military and Medicine working groups. An author with the Military group, I worked to apply the ELSCI neuroethical framework to the evaluation of existing (and speculative) neurotechnology (Section 8.3) and specifically to the evaluation of military cultural implications given advancing neurotechnology (Section 8.3.6). I believe our framework offers a rational neuroethical assessment and presents useful examples of neurotechnology design considerations in light of the unique ethical, legal, social, and cultural context of global and American militaries. My intent, as stated, was to better understand – and hopefully, respect – neuroethics as a field. I believe I achieved these goals, leaving my PhD with a sense of what (speculative) neuroethics wants to offer and what it is uniquely poised to provide: insightful and ethically versed extrapolation, plucked from the domain of science fiction and critically evaluated for practical insights that may inform current neurotechnological development and design. This is tricky work – and yes, frameworks help.

9.3.1 *Limitations*

Limitations of clinical intracranial neural recording research always include low patient count, lack of control over electrode placement, and difficulty in reproducibility due to unpredictable electrode coverage.

In the intracranial work presented here, a limitation is the lack of behavioral data to evaluate the utility of identified dDBS neural sensing and evoked potential features as biomarkers of PD or ET pathology. Future work may explore the neural features identified by these methods in connection with ongoing motor behavior and side effect evaluation and following various therapeutic DBS stimulation conditions.

Limitations of the VR work include the requirement that the researcher design all tasks and variable tracking scripts. I began work with another team of undergraduates on a "layer" API that would leverage the new universality of the OpenXR SDK to output continuous variables, including kinematics and movement tracking, during *any* Unity-built VR task – including commercial games. This work is still in process and may extend the accessibility of VR to researchers that would like to leverage a professionally designed game but not build their own virtual task.

9.3.2 *Future Work*

9.3.2.1 Neurohaptic Design & Evaluation

The next step for neurohaptic design is to explore more "kinodynamic" encoding strategies. Kinodynamic refers to movement-elicited changes or velocity-dependent feedback. In real life, the brain must integrate the movement of the body with the incoming sensory feedback to understand the world. In virtual reality, with the precision of kinematic tracking, I can encode dynamic stimulation strategies that are dependent on and responsive to the movement of the subject. As a first demonstration of this, I built a task I called "HapticGrating," in which a subject would use a

"magic wand" to explore and distinguish between "invisible structures." These structures were unrendered spatial gratings with distinct spatial frequencies. This task is based on a study of active exploration of spatial grating completed with monkeys by O'Doherty et al. (2019).[214] Given the ready interpretation of "static" temporal variation demonstrated by subjects completing the amplitude-modulated HapticSort work described in this thesis, I predict that subjects will be able to easily and accurately integrate their movements with responsive stimulation to distinguish between HapticGratings of sufficiently different spatial frequency. The limits of spatial grating discriminability and temporal pulse discriminability (reflected in the volitional speed at which a subject completes the task) could be determined by careful data collection.

9.3.2.2 Advanced VR-BCI

The VR-BCI environment lends itself to novel BCI approaches. In a first proposal, Iman Tanumihardja and Vishwas Sathish and I presented an "AI in the Loop" BCI architecture inspired by reinforcement learning (RL). The goal of this architecture was to leverage the availability of environmental information in VR to train an artificial intelligence (AI) agent to use contextual information alongside neural state information to perform the "will" of the BCI user. To describe the intent of this BCI architecture, I likened it to "riding a horse" that has a sense of the world and its action (or policy) space within the world, instead of "driving

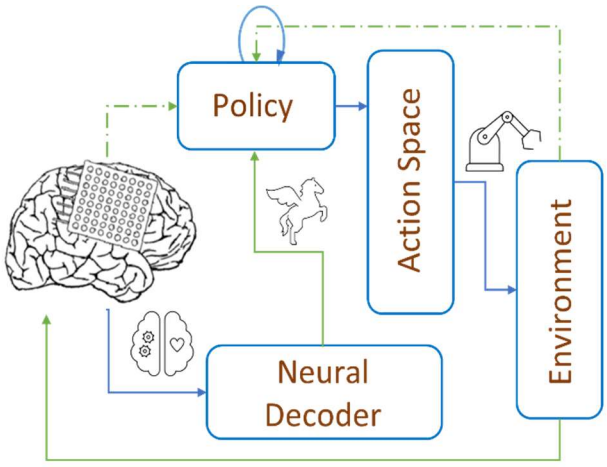

Figure 9.1 Initial "AI-in-the-loop" VR-BCI proposal. This general architecture proposed an AI agent that would be given contextual information about the world (VR scene) and limited neural state decoding information. It would act from a constrained policy space and the action would receive either a negative reward decoded from human "error" signals if the action was incorrect or a nominal reward if correct.

a robot" that can enact only to precise input commands. In this first proposal, we designed a series of tasks designed to use feed-forward "intent" neural triggers to prompt the AI agent action, which could then be modulated by neural feedback "error" signals if the action the AI agent took was incorrect (Figure 9.1). Iman and Vishwas have since refined our initial proposal and are moving forward a refined paradigm.

9.3.2.3 Cognitive Neuroscience

Prior, published work from the GRIDlab demonstrated the ability to induce the Rubber Hand Illusion using concurrent S1-DES in place of actual touch.[119] In this paradigm, the subject saw a rubber hand touched where they felt the percept from direct electrical stimulation of the somatosensory cortex. I hypothesize that we can incorporate S1-DES with the VR-RHI task to demonstrate induction of the illusion in VR using direct neural stimulation in place of physical touch.

9.3.2.4 Neuroethics

A repeated neuroethical concern over BCI development is the potential loss of agency – either real or imagined – on behalf of the BCI user. Already, implanted devices have elicited behavioral changes that are involuntary side effects of stimulation.[215] It has been speculated that this loss of volitional control may be exacerbated in the case motor BCI, in which decoded neural activity in used to move a neuroprosthetic. I propose the development of a volitional BCI architecture that incorporates a separate decoder to determine human intent to use the BCI. I would like to complete a neuroethical evaluation of this architecture alongside Asad Beck and Prof. Timothy Brown.

BIBLIOGRAPHY

1. Paschall, C., Rao, R. P. N., Hauptman, J., G Ojemann, J. & Herron, J. An Immersive Virtual Reality Platform Integrating Human ECOG & sEEG: Implementation & Noise Analysis. (2022).
2. Paschall, C. J. & Hauptmann, L. 1: J. Touching the Void: Intracranial Stimulation for Virtual Reality NeuroHaptic Feedback.
3. Paschall, Courtnie Tanumihardja, Iman Weaver, Kurt Grannan, Ben Ko, Andrew Hauptman, Jason Ojemann, Jeffrey Rao, Rajesh Herron, Jeffrey. Rapid offline identification of neural triggers for a virtual reality brain computer interface (VR-BCI) with intracranial electrodes in humans. Preprint at (2022).
4. O'Doherty, J. E. *et al.* Active tactile exploration using a brain-machine-brain interface. *Nature* **479**, 228–231 (2011).
5. O'Doherty, J. E., Lebedev, M. A., Li, Z. & Nicolelis, M. A. L. Virtual active touch using randomly patterned intracortical microstimulation. *IEEE Trans. Neural Syst. Rehabil. Eng.* **20**, 85–93 (2012).
6. Wen, D. *et al.* Combining brain-computer interface and virtual reality for rehabilitation in neurological diseases: A narrative review. *Ann. Phys. Rehabil. Med.* **64**, 101404 (2021).
7. Camargo-Vargas, D., Callejas-Cuervo, M. & Mazzoleni, S. Brain-Computer Interfaces Systems for Upper and Lower Limb Rehabilitation: A Systematic Review. *Sensors* **21**, (2021).
8. Georgiev, D. D., Georgieva, I., Gong, Z., Nanjappan, V. & Georgiev, G. V. Virtual Reality for Neurorehabilitation and Cognitive Enhancement. *Brain Sci* **11**, (2021).
9. Suhaimi, N. S., Mountstephens, J. & Teo, J. EEG-Based Emotion Recognition: A State-of-the-Art Review of Current Trends and Opportunities. *Comput. Intell. Neurosci.* **2020**, 8875426 (2020).
10. Tauscher, J.-P. *et al.* Immersive EEG: Evaluating Electroencephalography in Virtual Reality. in *2019 IEEE Conference on Virtual Reality and 3D User Interfaces (VR)* 1794–1800 (2019). doi:10.1109/VR.2019.8797858.
11. Juliano, J. M. *et al.* Embodiment Is Related to Better Performance on a Brain-Computer Interface in Immersive Virtual Reality: A Pilot Study. *Sensors* **20**, (2020).
12. Penaloza, C. I., Segado, M. & Debergue, P. BMI-VR based Cognitive Training improves Attention Switching Processing Speed. in *2020 IEEE International Conference on Systems, Man, and Cybernetics (SMC)* 12–17 (2020). doi:10.1109/SMC42975.2020.9283447.
13. Losey, D. M., Stocco, A., Abernethy, J. A. & Rao, R. P. N. Navigating a 2D Virtual World Using Direct Brain Stimulation. *Frontiers in Robotics and AI* **3**, 72 (2016).
14. Topalovic, U. *et al.* Wireless Programmable Recording and Stimulation of Deep Brain Activity in Freely Moving Humans. *Neuron* **108**, 322-334.e9 (2020).
15. Ramirez-Zamora, A. *et al.* Proceedings of the Seventh Annual Deep Brain Stimulation Think Tank: Advances in Neurophysiology, Adaptive DBS, Virtual Reality, Neuroethics and Technology. *Front. Hum. Neurosci.* **14**, 54 (2020).
16. La Vaque, T. J. The history of EEG Hans Berger. *J. Neurother.* **3**, 1–9 (1999).
17. Berger, H. Über das Elektrenkephalogramm des Menschen. *Archiv f. Psychiatrie* **87**, 527–570 (1929).
18. Berger, H. Über das Elektrenkephalogramm des Menschen. *Archiv f. Psychiatrie* **108**, 407–431 (1938).

19. Introduction to the physiological bases of EEG. in *Analyzing Neural Time Series Data* (The MIT Press, 2014). doi:10.7551/mitpress/9609.003.0008.
20. Buzsaki, G. *Rhythms of the brain*. (Oxford University Press, 2011).
21. Varelas, P. N. & Spanaki, M. V. Management of status epilepticus and critical care seizures. in *Seizures in Critical Care* 355–422 (Humana Press, 2010). doi:10.1007/978-1-60327-532-3_15.
22. Cohen, M. X. Time-frequency analysis of analog neural signals. in *Encyclopedia of Computational Neuroscience* 1–3 (Springer New York, 2019). doi:10.1007/978-1-4614-7320-6_421-2.
23. Cronin, J. A. Human psychophysics of direct cortical stimulation of somatosensory cortex. (2018).
24. Preface. in *Analyzing Neural Time Series Data* (The MIT Press, 2014). doi:10.7551/mitpress/9609.003.0001.
25. Wu, J. "james." Neural correlates of human motor planning and visuomotor transformation.
26. Caldwell, D. J., Ojemann, J. G. & Rao, R. P. N. Direct electrical stimulation in electrocorticographic brain–computer interfaces: Enabling technologies for input to cortex. *Front. Neurosci.* (2019).
27. Mégevand, P. & Seeck, M. Electroencephalography, magnetoencephalography and source localization: their value in epilepsy. *Curr. Opin. Neurol.* **31**, 176–183 (2018).
28. Fritsch, G. & Hitzig, E. Electric excitability of the cerebrum (Über die elektrische Erregbarkeit des Grosshirns). *Epilepsy Behav.* **15**, 123–130 (2009).
29. Caton, R. Notes on a case of tumour of the cerebellum. *Lancet* **106**, 620–621 (1875).
30. Cushing, H. A Note upon the Faradaic Stimulation of the Postcentral Gyrus in Conscious Patients. *Brain* **32**, 44–53 (1909).
31. Ojemann, G., Ojemann, J., Lettich, E. & Berger, M. Cortical language localization in left, dominant hemisphere. An electrical stimulation mapping investigation in 117 patients. 1989. *J. Neurosurg.* **108**, 411–421 (2008).
32. Ojemann, G. A. Cortical organization of language. *J. Neurosci.* **11**, 2281–2287 (1991).
33. Gharabaghi, A., Berger, M., Tatagiba, M. & Karnath, H.-O. The role of the right superior temporal gyrus in visual search - insights from intraoperative electrical stimulation. *Neuropsychologia* **44**, 2578–2581 (2006).
34. Flint, A., Jr, Krause, F. & Haubold, H. A. *Surgery of the brain and spinal cord*. (Arkose Press, 2015).
35. Orchers, S., Himmelbach, M., Logothetis, N. & Karnath, H.-O. Direct Electrical Stimulation of Human Cortex -the Gold Standard for Mapping Brain Functions? *Nat. Rev. Neurosci* **13**, 63–70 (2012).
36. Foerster, O. & Altenburger, H. Elektrobiologische Vorgänge an der menschlichen Hirnrinde. *J. Neurol.* **135**, 277–288 (1935).
37. Prochazka, A. Neurophysiology and neural engineering: a review. *J. Neurophysiol.* **118**, 1292–1309 (2017).
38. Djourno, A. & Eyries, C. Auditory prosthesis by means of a distant electrical stimulation of the sensory nerve with the use of an indwelt coiling. *Presse Med.* **65**, 1417 (1957).
39. Chouard, C. H. The early days of the multi channel cochlear implant: efforts and achievement in France. *Hear. Res.* **322**, 47–51 (2015).
40. Chardack, W. M., Gage, A. A. & Greatbatch, W. Treatment of complete heart block with an implantable and selfcontained pacemaker. *Bull. Soc. Int. Chir.* **21**, 411–432 (1962).

41. Shealy, C. N., Mortimer, J. T. & Reswick, J. B. Electrical inhibition of pain by stimulation of the dorsal columns: preliminary clinical report. *Anesth. Analg.* **46**, 489–491 (1967).
42. Anagnostopoulos, C. E. & Glenn, W. W. Electronic pacemakers of the heart, gastrointestinal tract, phrenic nerve, bladder, and carotid sinus: current status. *Surgery* **60**, 480–494 (1966).
43. Nashold, B. S. *et al.* Electromicturition in paraplegia: implantation of a spinal neuroprosthesis. *Proc. Veterans Adm. Spinal Cord Inj. Conf.* **18**, 161–165 (1971).
44. Gardner, J. A history of deep brain stimulation: Technological innovation and the role of clinical assessment tools. *Soc. Stud. Sci.* **43**, 707–728 (2013).
45. Osorio, I. The NeuroPace trial: missing knowledge and insights. *Epilepsia* vol. 55 1469–1470 (2014).
46. Nowak, L. G. & Bullier, J. Axons, but not cell bodies, are activated by electrical stimulation in cortical gray matter. I. Evidence from chronaxie measurements. *Exp. Brain Res.* **118**, 477–488 (1998).
47. Histed, M. H., Bonin, V. & Reid, R. C. Direct activation of sparse, distributed populations of cortical neurons by electrical microstimulation. *Neuron* **63**, 508–522 (2009).
48. Tolias, A. S. *et al.* Mapping cortical activity elicited with electrical microstimulation using FMRI in the macaque. *Neuron* **48**, 901–911 (2005).
49. Matsumoto, R. *et al.* Functional connectivity in the human language system: a cortico-cortical evoked potential study. *Brain* **127**, 2316–2330 (2004).
50. Matsumoto, R. *et al.* Functional connectivity in human cortical motor system: a cortico-cortical evoked potential study. *Brain* **130**, 181–197 (2007).
51. Keller, C. J. *et al.* Mapping human brain networks with cortico-cortical evoked potentials. *Philos. Trans. R. Soc. Lond. B Biol. Sci.* **369**, 20130528 (2014).
52. Keller, C. J. *et al.* Corticocortical evoked potentials reveal projectors and integrators in human brain networks. *J. Neurosci.* **34**, 9152–9163 (2014).
53. Louis, E. D. & Vonsattel, J. P. G. The emerging neuropathology of essential tremor. *Mov. Disord.* **23**, 174–182 (2008).
54. Cabrera, L. Y., Goudreau, J. & Sidiropoulos, C. Critical appraisal of the recent US FDA approval for earlier DBS intervention. *Neurology* **91**, 133–136 (2018).
55. Vingerhoets, F. J. G. *et al.* Subthalamic DBS replaces levodopa in Parkinson's disease: two-year follow-up. *Neurology* **58**, 396–401 (2002).
56. Kandel, E. R., Schwartz, J. H., Jessell, T. M., Siegelbaum, S. A. & Hudspeth, A. J. *Principles of neural science, fifth edition*. (McGraw-Hill Education/Medical, 2012).
57. Dorsey, E. R. & Bloem, B. R. The Parkinson pandemic-A call to action. *JAMA Neurol.* **75**, 9–10 (2018).
58. Oyama, G. *et al.* Deep brain stimulation may improve quality of life in people with Parkinson's disease without affecting caregiver burden. *Neuromodulation* **17**, 126–132 (2014).
59. Herron, J. A. *et al.* Chronic electrocorticography for sensing movement intention and closed-loop deep brain stimulation with wearable sensors in an essential tremor patient. *J. Neurosurg.* **127**, 580–587 (2017).
60. Vissani, M., Isaias, I. U. & Mazzoni, A. Deep brain stimulation: a review of the open neural engineering challenges. *J. Neural Eng.* **17**, 051002 (2020).
61. Levinson, L. H. *et al.* Intraoperative Characterization of Subthalamic Nucleus-to-Cortex Evoked Potentials in Parkinson's Disease Deep Brain Stimulation. *Front. Hum. Neurosci.* **15**, 117 (2021).

62. Hell, F., Palleis, C., Mehrkens, J. H., Koeglsperger, T. & Bötzel, K. Deep Brain Stimulation Programming 2.0: Future Perspectives for Target Identification and Adaptive Closed Loop Stimulation. *Front. Neurol.* **10**, 314 (2019).
63. Wiest, C. *et al.* Local field potential activity dynamics in response to deep brain stimulation of the subthalamic nucleus in Parkinson's disease. *Neurobiol. Dis.* **143**, 105019 (2020).
64. Little, S. *et al.* Adaptive deep brain stimulation in advanced Parkinson disease. *Ann. Neurol.* **74**, 449–457 (2013).
65. Camara, C. *et al.* Resting tremor classification and detection in Parkinson's disease patients. *Biomed. Signal Process. Control* **16**, 88–97 (2015).
66. Flora, E. D., Perera, C. L., Cameron, A. L. & Maddern, G. J. Deep brain stimulation for essential tremor: a systematic review. *Mov. Disord.* **25**, 1550–1559 (2010).
67. Choi, K. S., Riva-Posse, P., Figee, M. & Mayberg, H. Connectome DBS for psychiatric disorders. *Brain Stimul.* **14**, 1735–1736 (2021).
68. Hendriks, S. *et al.* Ethical Challenges of Risk, Informed Consent, and Posttrial Responsibilities in Human Research With Neural Devices: A Review. *JAMA Neurol.* (2019) doi:10.1001/jamaneurol.2019.3523.
69. Schrock, L. E. *et al.* Tourette syndrome deep brain stimulation: a review and updated recommendations. *Mov. Disord.* **30**, 448–471 (2015).
70. Woods, A. J. & Martin, D. M. Clinical research and methodological aspects for tDCS research. in *Transcranial Direct Current Stimulation in Neuropsychiatric Disorders* 265–279 (Springer International Publishing, 2021). doi:10.1007/978-3-030-76136-3_14.
71. Potok, W., Bächinger, M., van der Groen, O., Cretu, A. L. & Wenderoth, N. Transcranial Random Noise Stimulation Acutely Lowers the Response Threshold of Human Motor Circuits. *J. Neurosci.* **41**, 3842–3853 (2021).
72. Franza, M. *TMS-induced control of bodily self-consciousness by combining non-invasive brain stimulation and immersive virtual reality*. https://infoscience.epfl.ch/record/279620 (2020) doi:10.5075/epfl-thesis-7796.
73. Liu, C., Yu, K., Niu, X. & He, B. Transcranial focused ultrasound enhances sensory discrimination capability through somatosensory cortical excitation. *Ultrasound Med. Biol.* **47**, 1356–1366 (2021).
74. Osada, T. *et al.* Distributions of cortical depth of the index finger region in the M1: A representative depth parameter for transcranial ultrasound stimulation. *Brain Stimul.* **15**, 1348–1350 (2022).
75. Quick Statistics About Hearing. *NIDCD* https://www.nidcd.nih.gov/health/statistics/quick-statistics-hearing.
76. Rossi, M. A. & Vitor, S. da S. Restoring vision through retinal implants -- A systematic literature review. *arXiv [q-bio.NC]* (2022).
77. Weiland, J. D. & Humayun, M. S. Retinal prosthesis. *IEEE Trans. Biomed. Eng.* **61**, 1412–1424 (2014).
78. Shim, S., Eom, K., Jeong, J. & Kim, S. J. Retinal Prosthetic Approaches to Enhance Visual Perception for Blind Patients. *Micromachines (Basel)* **11**, (2020).
79. Cronin, J. A. *et al.* Task-Specific Somatosensory Feedback via Cortical Stimulation in Humans. *IEEE Trans. Haptics* **9**, 515–522 (2016).
80. Caldwell, D. J., Cronin, J. A., Levinson, L. H. & P. N. Rao, R. Chapter 14 - Touch restoration through electrical cortical stimulation in humans. in *Somatosensory Feedback for*

Neuroprosthetics (ed. Güçlü, B.) 443–478 (Academic Press, 2021). doi:10.1016/B978-0-12-822828-9.00021-6.
81. Chandrasekaran, S. *et al.* Historical perspectives, challenges, and future directions of implantable brain-computer interfaces for sensorimotor applications. *Bioelectron Med* **7**, 14 (2021).
82. Pandarinath, C. & Bensmaia, S. J. The science and engineering behind sensitized brain-controlled bionic hands. *Physiol. Rev.* **102**, 551–604 (2022).
83. Guclu, B. *Somatosensory Feedback for Neuroprosthetics*. (Elsevier Science, 2021).
84. Orlov, I. V., Stolbkov, Y. K. & Gerasimenko, Y. P. Vestibular prosthetics: Concepts, approaches, results. *Neurosci. Behav. Physiol.* **48**, 711–720 (2018).
85. Strickland, E. A Bionic Nose to Smell. https://spectrum.ieee.org/covid-smell-prosthetic.
86. Rao, R. P. N. Brain co-processors: Using AI to restore and augment brain function. *Handbook of Neuroengineering* (2020).
87. Rao, R. P. Towards neural co-processors for the brain: combining decoding and encoding in brain-computer interfaces. *Curr. Opin. Neurobiol.* **55**, 142–151 (2019).
88. Nishimura, Y., Perlmutter, S. I., Eaton, R. W. & Fetz, E. E. Spike-timing-dependent plasticity in primate corticospinal connections induced during free behavior. *Neuron* **80**, 1301–1309 (2013).
89. Ahlgrim, N. S. & Manns, J. R. Optogenetic Stimulation of the Basolateral Amygdala Increased Theta-Modulated Gamma Oscillations in the Hippocampus. *Front. Behav. Neurosci.* **13**, 87 (2019).
90. Kanta, V., Pare, D. & Headley, D. B. Closed-loop control of gamma oscillations in the amygdala demonstrates their role in spatial memory consolidation. *Nat. Commun.* **10**, 3970 (2019).
91. Jackson, A., Mavoori, J. & Fetz, E. E. Long-term motor cortex plasticity induced by an electronic neural implant. *Nature* **444**, 56–60 (2006).
92. Ni, Z. *et al.* Pallidal deep brain stimulation modulates cortical excitability and plasticity. *Ann. Neurol.* **83**, 352–362 (2018).
93. 2019 David Caldwell Engineering Direct Electrical Stimulation of Human Sensorimotor Cortex.pdf.
94. Zhang, J. J., Bai, Z. & Fong, K. N. K. Priming intermittent theta burst stimulation for hemiparetic upper limb after stroke: A randomized controlled trial. *Stroke* **53**, 2171–2181 (2022).
95. Guggenmos, D. J. *et al.* Restoration of function after brain damage using a neural prosthesis. *Proc. Natl. Acad. Sci. U. S. A.* **110**, 21177–21182 (2013).
96. Shah, P. P., Szaflarski, J. P., Allendorfer, J. & Hamilton, R. H. Induction of neuroplasticity and recovery in post-stroke aphasia by non-invasive brain stimulation. *Front. Hum. Neurosci.* **7**, 888 (2013).
97. Kucewicz, M. T., Worrell, G. A. & Axmacher, N. Direct electrical brain stimulation of human memory: lessons learnt and future perspectives. *Brain* (2022) doi:10.1093/brain/awac435.
98. Vidal, J. J. Toward direct brain-computer communication. *Annu. Rev. Biophys. Bioeng.* **2**, 157–180 (1973).
99. Fetz, E. E. & Finocchio, D. V. Operant conditioning of specific patterns of neural and muscular activity. *Science* **174**, 431–435 (1971).
100. Fetz, E. E. Operant conditioning of cortical unit activity. *Science* **163**, 955–958 (1969).

101. Taylor, D. M., Tillery, S. I. H. & Schwartz, A. B. Direct cortical control of 3D neuroprosthetic devices. *Science* **296**, 1829–1832 (2002).
102. Velliste, M. *et al.* Motor cortical correlates of arm resting in the context of a reaching task and implications for prosthetic control. *J. Neurosci.* **34**, 6011–6022 (2014).
103. Hochberg, L. R. *et al.* Neuronal ensemble control of prosthetic devices by a human with tetraplegia. *Nature* **442**, 164–171 (2006).
104. Bouton, C. "Decoding neural activity from an intracortical implant in humans with tetraplegia." in *2009 First Annual ORNL Biomedical Science & Engineering Conference* (IEEE, 2009). doi:10.1109/bsec.2009.5090450.
105. Collinger, J. L. *et al.* High-performance neuroprosthetic control by an individual with tetraplegia. *Lancet* **381**, 557–564 (2013).
106. Leuthardt, E. C., Miller, K. J., Schalk, G., Rao, R. P. N. & Ojemann, J. G. Electrocorticography-based brain computer interface--the Seattle experience. *IEEE Trans. Neural Syst. Rehabil. Eng.* **14**, 194–198 (2006).
107. Blakely, T., Miller, K. J., Zanos, S. P., Rao, R. P. N. & Ojemann, J. G. Robust, long-term control of an electrocorticographic brain-computer interface with fixed parameters. *Neurosurg. Focus* **27**, E13 (2009).
108. Vadera, S., Marathe, A. R., Gonzalez-Martinez, J. & Taylor, D. M. Stereoelectroencephalography for continuous two-dimensional cursor control in a brain-machine interface. *Neurosurg. Focus* **34**, E3 (2013).
109. Leuthardt, E. C., Schalk, G., Wolpaw, J. R., Ojemann, J. G. & Moran, D. W. A brain-computer interface using electrocorticographic signals in humans. *J. Neural Eng.* **1**, 63–71 (2004).
110. Felton, E. A., Wilson, J. A., Williams, J. C. & Garell, P. C. Electrocorticographically controlled brain-computer interfaces using motor and sensory imagery in patients with temporary subdural electrode implants. Report of four cases. *J. Neurosurg.* **106**, 495–500 (2007).
111. Krusienski, D. J. & Shih, J. J. Control of a brain-computer interface using stereotactic depth electrodes in and adjacent to the hippocampus. *J. Neural Eng.* **8**, 025006 (2011).
112. Ajiboye, A. B. *et al.* Restoration of reaching and grasping movements through brain-controlled muscle stimulation in a person with tetraplegia: a proof-of-concept demonstration. *Lancet* **389**, 1821–1830 (2017).
113. Ethier, C., Oby, E. R., Bauman, M. J. & Miller, L. E. Restoration of grasp following paralysis through brain-controlled stimulation of muscles. *Nature* **485**, 368–371 (2012).
114. Collinger, J. L., Gaunt, R. A. & Schwartz, A. B. Progress towards restoring upper limb movement and sensation through intracortical brain-computer interfaces. *Current Opinion in Biomedical Engineering* **8**, 84–92 (2018).
115. Paralysis statistics. *Reeve Foundation* https://www.christopherreeve.org/living-with-paralysis/stats-about-paralysis.
116. Anderson, K. D. Targeting recovery: priorities of the spinal cord-injured population. *J. Neurotrauma* **21**, 1371–1383 (2004).
117. Bensmaia, S. J. & Miller, L. E. Restoring sensorimotor function through intracortical interfaces: progress and looming challenges. *Nat. Rev. Neurosci.* **15**, 313–325 (2014).
118. Armenta Salas, M. *et al.* Proprioceptive and cutaneous sensations in humans elicited by intracortical microstimulation. *Elife* **7**, (2018).

119. Collins, K. L. *et al.* Ownership of an artificial limb induced by electrical brain stimulation. *Proc. Natl. Acad. Sci. U. S. A.* **114**, 166–171 (2017).
120. Libet, B. *et al.* Production of Threshold Levels of Conscious Sensation by Electrical Stimulation of Human Somatosensory Cortex. *J. Neurophysiol.* **27**, 546–578 (1964).
121. Penfield, W. & Boldrey, E. Somatic Motor and Sensory Representation in the Cerebral Cortex of Man as Studied by Electrical Stimulation. *Brain* **60**, 389–443 (1937).
122. Johnson, L. A. *et al.* Direct electrical stimulation of the somatosensory cortex in humans using electrocorticography electrodes: a qualitative and quantitative report. *J. Neural Eng.* **10**, 036021 (2013).
123. Caldwell, D. J. *et al.* Direct stimulation of somatosensory cortex results in slower reaction times compared to peripheral touch in humans. *Sci. Rep.* **9**, 3292 (2019).
124. Caldwell, D. J. *et al.* Publisher Correction: Direct stimulation of somatosensory cortex results in slower reaction times compared to peripheral touch in humans. *Sci. Rep.* **9**, 20317 (2019).
125. Flesher, S. N. *et al.* A brain-computer interface that evokes tactile sensations improves robotic arm control. *Science* **372**, 831–836 (2021).
126. Mazurek, K. A. & Schieber, M. H. Injecting Information into the Mammalian Cortex: Progress, Challenges, and Promise. *Neuroscientist* **27**, 129–142 (2021).
127. Libet, B. *et al.* Production of Threshold Levels of Conscious Sensation by Electrical Stimulation of Human Somatosensory Cortex. in *Neurophysiology of Consciousness* (ed. Libet, B.) 1–34 (Birkhäuser Boston, 1993). doi:10.1007/978-1-4612-0355-1_1.
128. Hiremath, S. V. *et al.* Human perception of electrical stimulation on the surface of somatosensory cortex. *PLoS One* **12**, e0176020 (2017).
129. Cogan, S. F., Ludwig, K. A., Welle, C. G. & Takmakov, P. Tissue damage thresholds during therapeutic electrical stimulation. *J. Neural Eng.* **13**, 021001 (2016).
130. Unity Technologies. [No title]. https://docs.unity3d.com/Manual/UnityManual.html.
131. Tucker-Davis Technologies. Synapse Manual. https://www.tdt.com/docs/synapse/.
132. Linear ICBM Average Brain (ICBM152) Stereotaxic Registration Model. https://nist.mni.mcgill.ca/icbm-152lin/.
133. Yatagai, T. Discrete Fourier transform and fast Fourier transform. in *Fourier Theory in Optics and Optical Information Processing* 71–84 (CRC Press, 2022). doi:10.1201/9781003121916-5.
134. The discrete time Fourier transform, the FFT, and the convolution theorem. in *Analyzing Neural Time Series Data* (The MIT Press, 2014). doi:10.7551/mitpress/9609.003.0016.
135. Time-frequency power and baseline normalizations. in *Analyzing Neural Time Series Data* (The MIT Press, 2014). doi:10.7551/mitpress/9609.003.0023.
136. Kaplan, J. T. & Iacoboni, M. Listen to my actions! *Behav. Brain Sci.* **28**, 135–136 (2005).
137. Smith, S. T., Fox, R. O. & Raman, V. A quadrature closure for the reaction-source term in conditional-moment closure. *Proc. Combust. Inst.* **31**, 1675–1682 (2007).
138. Velisar, A. *et al.* Dual threshold neural closed loop deep brain stimulation in Parkinson disease patients. *Brain Stimul.* **12**, 868–876 (2019).
139. Steigerwald, F., Müller, L., Johannes, S., Matthies, C. & Volkmann, J. Directional deep brain stimulation of the subthalamic nucleus: A pilot study using a novel neurostimulation device. *Mov. Disord.* **31**, 1240–1243 (2016).
140. Aman, J. E. *et al.* Directional deep brain stimulation leads reveal spatially distinct oscillatory activity in the globus pallidus internus of Parkinson's disease patients. *Neurobiol. Dis.* **139**, 104819 (2020).

141. Tinkhauser, G. *et al.* Directional local field potentials: A tool to optimize deep brain stimulation. *Mov. Disord.* **33**, 159–164 (2018).
142. Ozturk, M. *et al.* Randomized, Double-Blind Assessment of LFP Versus SUA Guidance in STN-DBS Lead Implantation: A Pilot Study. *Front. Neurosci.* **14**, 611 (2020).
143. Horn, A. *et al.* Lead-DBS v2: Towards a comprehensive pipeline for deep brain stimulation imaging. *Neuroimage* **184**, 293–316 (2019).
144. Treu, S. *et al.* Deep brain stimulation: Imaging on a group level. *Neuroimage* **219**, 117018 (2020).
145. Ewert, S. *et al.* Toward defining deep brain stimulation targets in MNI space: A subcortical atlas based on multimodal MRI, histology and structural connectivity. *Neuroimage* **170**, 271–282 (2018).
146. Brain Atlases: Human. *McConnell Brain Imaging Centre* https://www.mcgill.ca/bic/neuroinformatics/brain-atlases-human.
147. Delorme, A. & Makeig, S. EEGLAB: an open source toolbox for analysis of single-trial EEG dynamics including independent component analysis. *J. Neurosci. Methods* **134**, 9–21 (2004).
148. Hellerbach, A. *et al.* DiODe: Directional Orientation Detection of Segmented Deep Brain Stimulation Leads: A Sequential Algorithm Based on CT Imaging. *Stereotact. Funct. Neurosurg.* **96**, 335–341 (2018).
149. Kehnemouyi, Y. M. *et al.* Modulation of beta bursts in subthalamic sensorimotor circuits predicts improvement in bradykinesia. *Brain* **144**, 473–486 (2021).
150. Crowther, L. J. *et al.* A quantitative method for evaluating cortical responses to electrical stimulation. *J. Neurosci. Methods* **311**, 67–75 (2019).
151. *Justin P Barnett*. (Youtube - https://www.youtube.com/@JustinPBarnett, 2021).
152. *Valem Tutorials*. (Youtube - https://www.youtube.com/@ValemTutorials, 2018).
153. *OpenXR-SDK-Source: Sources for OpenXR loader, basic API layers, and example code*. (Github - https://github.com/KhronosGroup/OpenXR-SDK-Source).
154. *ValveVR-OpenVR SDK 1.23.7*. (Github - https://github.com/ValveSoftware, 2022).
155. Open Broadcaster Software. https://obsproject.com/.
156. Moss, J. D. & Muth, E. R. Characteristics of head-mounted displays and their effects on simulator sickness. *Hum. Factors* **53**, 308–319 (2011).
157. Vogels, I. M. L. C. Detection of temporal delays in visual-haptic interfaces. *Hum. Factors* **46**, 118–134 (2004).
158. Zhou, H.-Y., Cheung, E. F. C. & Chan, R. C. K. Audiovisual temporal integration: Cognitive processing, neural mechanisms, developmental trajectory and potential interventions. *Neuropsychologia* **140**, 107396 (2020).
159. Kourtesis, P., Korre, D., Collina, S., Doumas, L. A. A. & MacPherson, S. E. Guidelines for the Development of Immersive Virtual Reality Software for Cognitive Neuroscience and Neuropsychology: The Development of Virtual Reality Everyday Assessment Lab (VR-EAL), a Neuropsychological Test Battery in Immersive Virtual Reality. *Frontiers in Computer Science* **1**, 12 (2020).
160. Wang, W.-E. *et al.* A Novel Method to Understand Neural Oscillations During Full-Body Reaching: A Combined EEG and 3D Virtual Reality Study. *IEEE Trans. Neural Syst. Rehabil. Eng.* **28**, 3074–3082 (2020).
161. Li, G. *et al.* Optimal referencing for stereo-electroencephalographic (SEEG) recordings. *Neuroimage* **183**, 327–335 (2018).

162. Kim, H. K., Park, J., Choi, Y. & Choe, M. Virtual reality sickness questionnaire (VRSQ): Motion sickness measurement index in a virtual reality environment. *Appl. Ergon.* **69**, 66–73 (2018).
163. Lee, B. *et al.* Engineering Artificial Somatosensation Through Cortical Stimulation in Humans. *Front. Syst. Neurosci.* **12**, 24 (2018).
164. Kim, S. *et al.* Behavioral assessment of sensitivity to intracortical microstimulation of primate somatosensory cortex. *Proc. Natl. Acad. Sci. U. S. A.* **112**, 15202–15207 (2015).
165. Get started developing with the HTC VIVE Pro Eye using Tobii XR SDK. https://developer.tobii.com/xr/develop/unity/getting-started/vive-pro-eye/.
166. Matyas, F. *et al.* Motor control by sensory cortex. *Science* **330**, 1240–1243 (2010).
167. Karadimas, S. K. *et al.* Sensory cortical control of movement. *Nat. Neurosci.* **23**, 75–84 (2020).
168. Schneider, D. M. Reflections of action in sensory cortex. *Curr. Opin. Neurobiol.* **64**, 53–59 (2020).
169. Botvinick, M. & Cohen, J. Rubber hands "feel" touch that eyes see. *Nature* **391**, 756 (1998).
170. Dempsey-Jones, H. & Kritikos, A. Handedness modulates proprioceptive drift in the rubber hand illusion. *Exp. Brain Res.* **237**, 351–361 (2019).
171. Kanayama, N., Hara, M. & Kimura, K. Virtual reality alters cortical oscillations related to visuo-tactile integration during rubber hand illusion. *Sci. Rep.* **11**, 1436 (2021).
172. Guterstam, A. *et al.* Direct Electrophysiological Correlates of Body Ownership in Human Cerebral Cortex. *Cereb. Cortex* **29**, 1328–1341 (2019).
173. Q&A with Dr. Joseph J. Fins, Neuroethics Perspectives from a Doctor. https://brain.ieee.org/publications/ieee-brain-talks/qa-with-dr-joseph-j-fins-md-macp-frp-weill-cornell-medical-college-yale-law-school/.
174. Q&A with Dr. James Giordano, Chair, IEEE Brain Neuroethics Subcommittee. https://brain.ieee.org/publications/ieee-brain-talks/qa-with-dr-james-giordano-chair-ieee-brain-neuroethics-subcommittee/.
175. ieee_brain_neuroethics_flyer_OCT2021.pdf.
176. BRAIN Neuroethics Working Group. https://brain.ieee.org/event/brain-neuroethics-working-group/.
177. 20221024_brain_neuroethics_summary_508c.pdf.
178. BRAIN 2025 Report. https://braininitiative.nih.gov/strategic-planning/brain-2025-report.
179. Ethical considerations of neuroscience research and the application of neuroscience research findings for the Presidential Commission for the Study of Bioethical Issues. *J Law Biosci* **1**, 237–242 (2014).
180. Home. https://www.neuroethicssociety.org/.
181. Ramos, K. M., Rommelfanger, K. S., Greely, H. T. & Koroshetz, W. J. Neuroethics and the NIH BRAIN Initiative. *J Responsible Innov* **5**, 122–130 (2018).
182. Chiong, W. Insiders and Outsiders: Lessons for Neuroethics from the History of Bioethics. *AJOB Neurosci.* **11**, 155–166 (2020).
183. Jonsen, A. R. *The Birth of Bioethics*. (Oxford University Press, 2003).
184. MacDuffie, K. E. A "salad bowl" approach to neuroethics collaboration. *AJOB Neurosci.* **11**, 201–203 (2020).
185. Farahany, N. & Ramos, K. M. Neuroethics: Fostering Collaborations to Enable Neuroscientific Discovery. *AJOB Neurosci.* **11**, 148–154 (2020).
186. Roskies, A. Neuroethics for the new millenium. *Neuron* **35**, 21–23 (2002).

187. Roskies, A. Neuroethics. (2021).
188. Greely, H. T. *et al.* Neuroethics Guiding Principles for the NIH BRAIN Initiative. *J. Neurosci.* **38**, 10586–10588 (2018).
189. IEEE Neuroethics Framework. https://brain.ieee.org/publications/neuroethics-framework/addressing-the-ethical-legal-social-cultural-implications-of-neurotechnology/.
190. Rommelfanger, K. S. Reflecting on a Neuroethics Roadmap in a Global Crisis. *AJOB neuroscience* vol. 11 131–134 (2020).
191. Institute of Neuroethics (IoNx). *Institute of Neuroethics (IoNx)* https://instituteofneuroethics.org/our-team.
192. The BRAIN Initiative® and Neuroethics: Enabling and Enhancing Neuroscience Advances for Society. https://braininitiative.nih.gov/strategic-planning/acd-working-groups/brain-initiative%C2%AE-and-neuroethics-enabling-and-enhancing.
193. IEEE Neuroethics Framework. https://brain.ieee.org/publications/neuroethics-framework/addressing-the-ethical-legal-social-cultural-implications-of-neurotechnology/.
194. Beauchamp, T. L. & Childress, J. F. *Principles of Biomedical Ethics*. (Oxford University Press, 1983).
195. Giordano, J. Toward an operational neuroethical risk analysis and mitigation paradigm for emerging neuroscience and technology (neuroS/T). *Exp. Neurol.* **287**, 492–495 (2017).
196. Shook, J. R. & Giordano, J. A principled and cosmopolitan neuroethics: considerations for international relevance. *Philos. Ethics Humanit. Med.* **9**, 1 (2014).
197. Mitscherlich A, M. F. The Nuremberg Code (1947). in *Doctors of infamy: the story of the Nazi medical crimes* xxiii–xxv (New York: Schuman, 1949).
198. Geneva Convention relative to the Treatment of Prisoners of War. *OHCHR* https://www.ohchr.org/en/instruments-mechanisms/instruments/geneva-convention-relative-treatment-prisoners-war.
199. REMPFER v. SHARFSTEIN MD. *Findlaw* https://caselaw.findlaw.com/us-dc-circuit/1422133.html.
200. Implementing, S. A. S. T. Page 53 TITLE 5—GOVERNMENT ORGANIZATION AND EMPLOYEES, 552a. https://www.govinfo.gov/content/pkg/USCODE-2018-title5/pdf/USCODE-2018-title5-partI-chap5-subchapII-sec552a.pdf.
201. Atuel, H. R. & Castro, C. A. Military Cultural Competence. *Clin. Soc. Work J.* **46**, 74–82 (2018).
202. Meyer, E. G. The Importance of Understanding Military Culture. *Acad. Psychiatry* **39**, 416–418 (2015).
203. Riccio, G. *et al. Warrior Ethos: Analysis of the Concept and Initial Development of Applications*. https://apps.dtic.mil/sti/citations/ADA428065 (2004).
204. Born, J. & Frank, C. The relative impact of barriers to care among military health services personnel: exploring differences using context specific scenarios. *BMC Health Serv. Res.* **22**, 607 (2022).
205. Breivik, G., Sand, T. S. & Sookermany, A. M. Risk-Taking and Sensation Seeking in Military Contexts: A Literature Review. *SAGE Open* **9**, 2158244018824498 (2019).
206. Walsh, W. A. & Tener, D. "If you don't send me five other pictures I am going to post the photo online": A qualitative analysis of experiences of survivors of sextortion. *J. Child Sex. Abus.* **31**, 447–465 (2022).

207. Gámez-Guadix, M. *et al.* Assessing image-based sexual abuse: Measurement, prevalence, and temporal stability of sextortion and nonconsensual sexting ("revenge porn") among adolescents. *J. Adolesc.* **94**, 789–799 (2022).
208. Kim, J. G. A study on online sextortion and cyber rape. *Leg. Stud. Inst. Chosun Univ.* **28**, 41–64 (2021).
209. Hendry, N. H. Sextortion. in *The Fourth Industrial Revolution and Its Impact on Ethics* 315–320 (Springer International Publishing, 2021). doi:10.1007/978-3-030-57020-0_23.
210. Matamala-Gomez, M. *et al.* Immersive Virtual Reality and Virtual Embodiment for Pain Relief. *Front. Hum. Neurosci.* **13**, 279 (2019).
211. Arai, K. *et al.* Embodiment of supernumerary robotic limbs in virtual reality. *Sci. Rep.* **12**, 9769 (2022).
212. Casula, E. P. *et al.* Feeling of ownership over an embodied avatar's hand brings about fast changes of fronto-parietal cortical dynamics. *J. Neurosci.* (2021) doi:10.1523/JNEUROSCI.0636-21.2021.
213. Yang, L. K. Protecting youth from dangerous media: Online predators. in *Advancing Responsible Adolescent Development* 75–92 (Springer International Publishing, 2016). doi:10.1007/978-3-319-41535-2_4.
214. O'Doherty, J. E., Shokur, S., Medina, L. E., Lebedev, M. A. & Nicolelis, M. A. L. Creating a neuroprosthesis for active tactile exploration of textures. *Proc. Natl. Acad. Sci. U. S. A.* **116**, 21821–21827 (2019).
215. Zarzycki, M. Z. & Domitrz, I. Stimulation-induced side effects after deep brain stimulation - a systematic review. *Acta Neuropsychiatr.* **32**, 57–64 (2020).

APPENDIX A

Virtual Reality System Questionnaire (VRSQ)

		Very uncomfortable						Very comfortable	N/A
1.	Head gear is	O	O	O	O	O	O	O	O
		Very difficult						Very easy	N/A
2.	Calibrating the system and tracking	O	O	O	O	O	O	O	O
		Very much						Not at all	N/A
3.	Image lags when head is turned slowly	O	O	O	O	O	O	O	O
		Very much						Not at all	N/A
4.	Image lags when head is turned quickly	O	O	O	O	O	O	O	O
		Very much						Not at all	N/A
5.	Image is blurred in some areas	O	O	O	O	O	O	O	O
		Very much						Not at all	N/A
6.	All of the images are blurred	O	O	O	O	O	O	O	O
		Very often						Never	N/A
7.	Image skips or breaks up at times	O	O	O	O	O	O	O	O
		Incomplete						Complete	N/A
8.	Image covers 360 degrees surround	O	O	O	O	O	O	O	O
		Very often						Never	N/A
9.	Auditory glitches	O	O	O	O	O	O	O	O
		Very difficult						Very easy	N/A
10.	Trying to locate source of sounds	O	O	O	O	O	O	O	O

		Very difficult						Very easy	N/A
11.	Trying to aim or point at targets	O	O	O	O	O	O	O	O
		Very difficult						Very easy	N/A
12.	Trying to turn and see what it to the left or right	O	O	O	O	O	O	O	O
		Very difficult						Very easy	N/A
13.	Trying to turn and see what is behind	O	O	O	O	O	O	O	O
		Very difficult						Very easy	N/A
14.	Orienting one's self in the space	O	O	O	O	O	O	O	O
		Confusing						Very clear	N/A
15.	Awareness of body location	O	O	O	O	O	O	O	O
		Very poor						Very good	N/A
16.	Location of hands and arms	O	O	O	O	O	O	O	O
19		Very difficult						Very easy	N/A
17.	Locating buttons on the controller	O	O	O	O	O	O	O	O

[19] Kim et al. (2018). Virtual Reality Sickness Questionnaire (VRSQ). https://dl.uswr.ac.ir/bitstream/Hannan/40901/1/2018%20AppliedErgonomics%20Volume%2069%20May%20%2821%29.pdf

APPENDIX B

Embodiment Questionnaire - Passive

On a scale of -3 to 3, with -3 being "strongly disagree" and 3 being "strongly agree."

I felt as if I was looking at my own hand.

-3 -2 -1 0 1 2 3

I felt as if the virtual arm was my own arm.

-3 -2 -1 0 1 2 3

I felt as if I had three (or four) hands.

-3 -2 -1 0 1 2 3

I felt as if the virtual hand was part of my body.

-3 -2 -1 0 1 2 3

I felt as if my hand was located where I saw the virtual hand.

-3 -2 -1 0 1 2 3

I felt like I could control the movement of the virtual object.

-3 -2 -1 0 1 2 3

I felt like I could have moved the virtual hand.

-3 -2 -1 0 1 2 3

I felt as if my hand could feel the virtual object.

-3 -2 -1 0 1 2 3

I felt a touch (something/feeling) where I saw the hand interact with the virtual object.

-3 -2 -1 0 1 2 3

I felt as if the touch (something/feeling) came from somewhere between my hand and the virtual hand.

-3 -2 -1 0 1 2 3

I felt as if my real hand was turning virtual.

-3 -2 -1 0 1 2 3

During the experiment, the virtual objects felt real.

-3 -2 -1 0 1 2 3

How was the virtual reality experience, overall?

Embodiment Questionnaire - Active

On a scale of -3 to 3, with -3 being "strongly disagree" and 3 being "strongly agree."

I felt as if I was looking at my own hand.

-3	-2	-1	0	1	2	3

I felt as if the virtual arm was my own arm.

-3	-2	-1	0	1	2	3

I felt as if I had three (or four) hands.

-3	-2	-1	0	1	2	3

I felt as if the virtual hand was part of my body.

-3	-2	-1	0	1	2	3

I felt as if my hand was located where I saw the virtual hand.

-3	-2	-1	0	1	2	3

I felt like my hand could interact with (grab/move) the virtual object.

-3	-2	-1	0	1	2	3

I felt like I caused the movement of the virtual hand.

-3	-2	-1	0	1	2	3

I felt as if my hand could feel the virtual object.

-3	-2	-1	0	1	2	3

I felt a touch (something/feeling) where I saw the hand interact with the virtual object.

-3	-2	-1	0	1	2	3

I felt as if the touch (something/feeling) came from somewhere between my hand and the virtual hand.

-3	-2	-1	0	1	2	3

I felt as if my real hand was turning virtual.

-3	-2	-1	0	1	2	3

During the experiment, the virtual objects felt real.

-3	-2	-1	0	1	2	3

How was the virtual reality experience, overall?

APPENDIX C

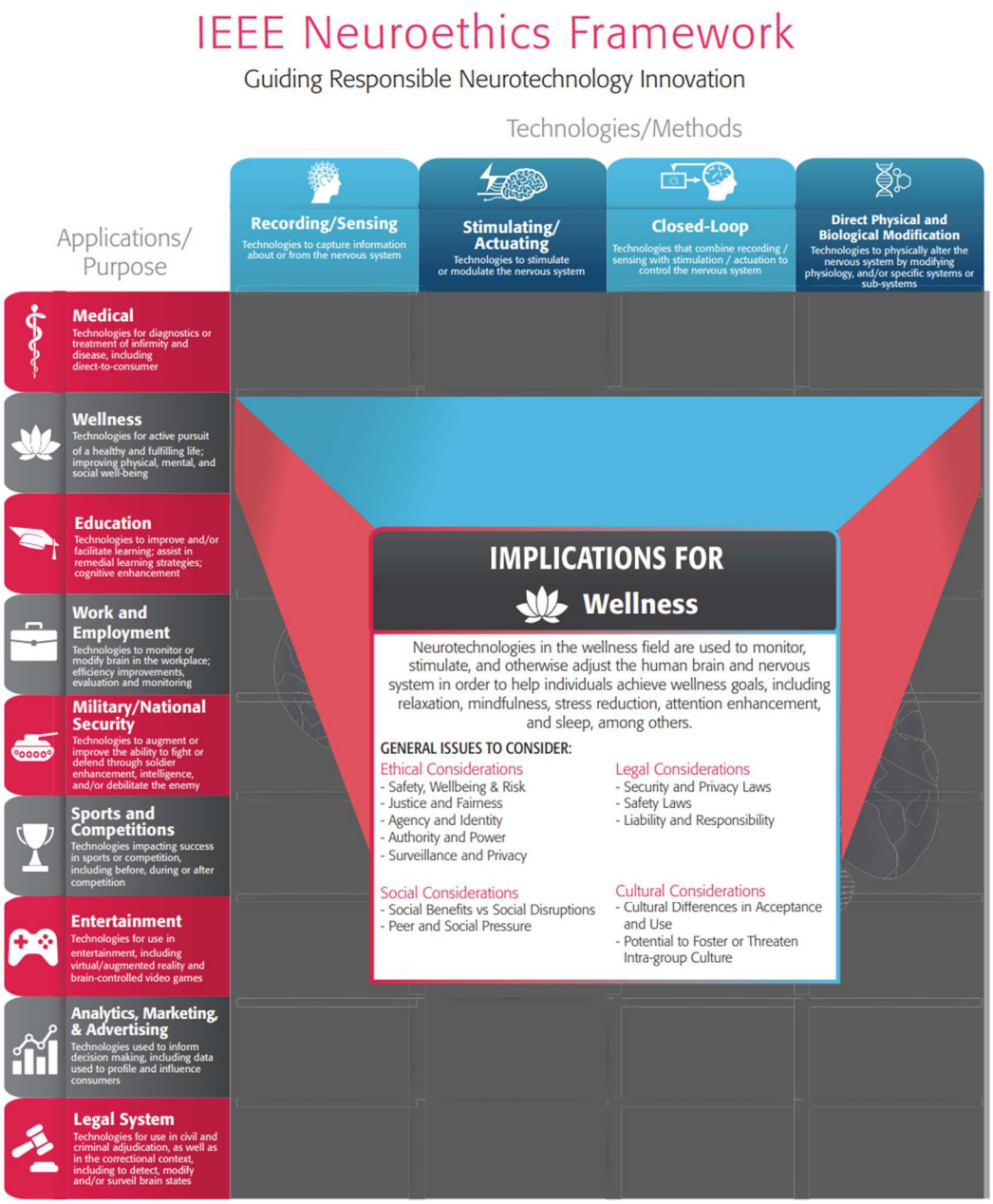

Figure 9.2 Visual Grid of the IEEE Neuroethics Framework. The framework is organized as a matrix of specific types of contemporary neurotechnologies and their current and potential applications. Columns represent different types of neurotechnologies, and the rows represent applications of these technologies. "IEEE Brain is in the process of developing documentation that supports this matrix by providing examples of existing neurotechnologies and exploring the ethical, legal, social, and cultural (ELSCI) issues generated by a particular neurotechnology when used in specific contexts." [193]

APPENDIX D

Dr. Mike X. Cohen's textbook, "Analyzing Neural Time Series Data: Theory and Practice" is *the best* resource for beginner neural signals researchers.[135] Although geared towards EEG-analyses and MATLAB users, the content is highly transferrable to the macro-electrode ECoG and sEEG analyses conducted by most clinical implanted neural devices labs. I am often asked how students may best get started with neural engineering and cognitive neuroelectrophysiology, and my answer is invariably: this textbook (and accompanying YouTube video series).

VITA

As of writing this thesis, Courtnie Jean Paschall was an 6th year MD/PhD candidate with the NIH Medical Scientist Training Program (MSTP) studying neural engineering with the Center for Neurotechnology (CNT) at the University of Washington in Seattle. She was also a Jean B. Viereck ARCS Scholar and UW Reality Lab fellow.

Courtnie was then and remains now a veteran of the US armed forces and military brat who calls Okinawa, Japan and 29 Palms, California home. Prior to this PhD, her academic pursuits had resulted in a 2008 *with merit* B.S. in Applied & Nuclear Physics from the US Naval Academy and a pre-med qualifying 2015 *summa cum laude* B.A. in Neuroscience from the CU Boulder Colorado, with some flight hours in between.

During her time as a graduate student, she was invited to speak about her work at two conferences in beautiful locations. She enjoys public speaking though it makes her nervous every time and she almost never finishes her talk on time. It's not clear if she enjoys being late or it just happens. It is quite clear, however, that she enjoys public science outreach as a volunteer with local schools, on campus, and a Pacific Science Center Science Communication Fellow. Or maybe it's teaching, she might love teaching.

When not in the lab or clinic, Courtnie would occasionally get lost on a good trail, or in a good book, or in the flavors of a great meal. Between such moments, and likely also throughout such moments, she daydreamed. She might tell you daydreaming is her day job.